

TR33795

STELLINGEN

behorende bij het proefschrift

Wave-current interactions

in a

generalized Lagrangian mean formulation

van

Jacco Groeneweg

Delft, 1 oktober 1999

1. De in een golf-stroomgoot waar te nemen golfgeïnduceerde veranderingen in het verticale profiel van de gemiddelde longitudinale snelheid worden veroorzaakt door de golfgedreven gemiddelde verticale flux van longitudinale impuls.
2. Voor de vergelijking van resultaten van golf-stroom experimenten in een goot met 1DV modelresultaten dient rekening gehouden te worden met niet-uniformiteiten in dwarsrichting van de snelheden in de goot.
3. Voor niet-brekende golven wordt in het TELEMAC-3D model (Péchon en Teisson, 1994) de bijdrage aan de impulsbalansvergelijking van de correlatie tussen longitudinale en verticale orbitaalsnelheid ten onrechte verwaarloosd.

Péchon, P. en Teisson, C. (1994). Numerical modelling of three-dimensional wave-driven currents in the surf-zone, 'Proc. 24th Int. Conf. on Coastal Engng, Kobe, Japan', ASCE, New York, pp. 2503-2512.

4. In een oscillerend snelheidsveld kan geen ondubbelzinnige definitie van gemiddelde snelheid worden gegeven in een Eulerse setting.
5. In een numeriek simulatiemodel dient de numerieke nauwkeurigheid van dezelfde orde te zijn als de mate van nauwkeurigheid waarin de fysica wordt weergegeven.

6. De vooruitgang in computertechnologie in ogenschouw nemend is het niet ondenkbaar dat in een zeer nabije toekomst simulatiemodellen aanvullende en vooral nauwkeurige informatie verschaffen van details die nog niet zijn gemeten in het veld en zodoende kunnen bijdragen aan het genereren van nieuwe veld-meetcampagnes.
7. Het is golfonderzoekers gelukt zich de spectrale denkwijze eigen te maken. Het zou eveneens mogelijk moeten zijn te leren denken in termen van GLM.
8. Domeindecompositie is een numerieke oplossingstechniek die uitermate geschikt is voor het oplossen van gekoppelde morfologische en hydrodynamische systemen in de kustzone.
9. Wanneer een krantenkop schreeuwt: "Vredestop in het Midden-Oosten", is het raadzaam het gehele artikel te lezen teneinde er achter te komen uit welke lettergrepen "vredestop" bestaat.
10. De waarde van een grap is omgekeerd evenredig met het aantal decibellen dat de grappenmaker zelf met een lachsalvo voortbrengt.

1. The wave-induced changes of the vertical profile of the longitudinal velocity, which can be observed in a wave-current flume, are due to the wave-driven mean vertical flux of longitudinal momentum.
2. In comparing experimental results from a wave-current flume with 1DV model results, one has to take lateral nonuniformities of the velocities in the flume into account.
3. In the case of nonbreaking waves the contribution of the correlation between the longitudinal and vertical velocity to the momentum balance equation has been neglected unjustifiably in the TELEMAC-3D model (Péchon en Teisson, 1994).

Péchon, P. en Teisson, C. (1994). Numerical modelling of three-dimensional wave-driven currents in the surf-zone, 'Proc. 24th Int. Conf. on Coastal Engng, Kobe, Japan', ASCE, New York, pp. 2503-2512.

4. In an oscillating velocity field the mean velocity cannot be defined unambiguously in a Eulerian setting.
5. In a numerical simulation model the numerical accuracy has to be of the same order as the order of accuracy in which the physics is represented.
6. Considering the progress in computer technology, it is not inconceivable that simulation models will provide complementary and in particular accurate information of details that have not yet been measured in the field. As such they may contribute to the generation of new field measurement campaigns.
7. Wave experts made themselves familiar with the spectral way of thinking. They should also be able to think in terms of GLM.
8. Domain decomposition is a numerical solution technique that is extremely useful to solve coupled morphological and hydrodynamical systems in coastal areas.
9. No translation possible.
10. The value of a joke is inversely proportional to the number of decibels the comedian produces with his own gale of laughter.

TR 3379

7-47/20

7260-52

379

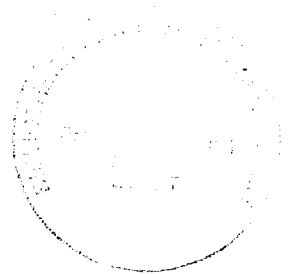
Wave-current interactions  
in a  
generalized Lagrangian mean formulation

*Golf-stroom interacties  
in een  
gegeneraliseerde Lagrangiaans gemiddelde formulering*



Wave-current interactions  
in a  
generalized Lagrangian mean formulation

PROEFSCHRIFT



ter verkrijging van de graad van doctor  
aan de Technische Universiteit Delft,  
op gezag van de Rector Magnificus prof.ir. K.F. Wakker,  
in het openbaar te verdedigen ten overstaan van een commissie,  
door het College voor Promoties aangewezen,  
op vrijdag 1 oktober 1999 te 10.30 uur

door Jacob GROENEWEG  
doctorandus in de wiskunde  
geboren te Marknesse, gemeente Noordoostpolder

Dit proefschrift is goedgekeurd door de promotor:

Prof.dr.ir. J.A. Battjes

Samenstelling promotiecommissie:

Rector Magnificus	voorzitter
Prof.dr.ir. J.A. Battjes	Technische Universiteit Delft, promotor
Prof. D.H. Peregrine	University of Bristol, Groot Britannië
Prof.dr.ir. G.S. Stelling	Technische Universiteit Delft
Prof.dr.ir. M.J.F. Stive	Technische Universiteit Delft
Dr. G.P. Thomas	University College Cork, Ierland
Prof.dr.ir. H.J. de Vriend	Universiteit Twente
Dr.ir. R.E. Uittenbogaard	WL Delft Hydraulics

Ir. G. Klopman heeft als begeleider in belangrijke mate bijgedragen aan het totstandkomen van het proefschrift.

Front cover: Langmuir circulations in Stump Lake, Canada  
photo by Jacco Groeneweg

Copyright © 1999 by Jacco Groeneweg  
Reproduced by PrintPartners Ipskamp B.V., from camera-ready copy supplied  
by the author.

ISBN 90-9013073-X

This thesis is also published in the series 'Communications on Hydraulic and Geotechnical Engineering' of the Faculty of Civil Engineering as Report No. 99-5, ISSN 0169-6548.



## Abstract

The generalized Lagrangian mean (GLM) formulation has been used to describe the interaction of waves and currents. In contrast to the more conventional Eulerian formulation, the GLM description enables splitting of the mean and oscillating motion over the entire depth in an unambiguous and unique way, also in the region between wave crest and trough.

Laboratory experiments by e.g. Kemp & Simons (1982, 1983) and Klopman (1994) showed that the effect of nonbreaking waves on a steady turbulent current over a rigid rough bed is significant. Unexpected wave-induced changes in the profile of the mean horizontal velocity have been observed. For following currents the mean horizontal velocity reaches a maximum and subsequently decreases towards the free surface. Opposing currents show the opposite feature. Compared to the logarithmic profile, the opposing current profile grows more rapidly towards the free surface.

To the authors' knowledge only two theoretical models have been presented to explain the wave-induced changes in the Eulerian-mean horizontal velocity profiles. The model of Nielsen & You (1996) is based on a local force balance in streamwise direction. Lateral variations have been neglected. Dingemans et al. (1996) presented a 2DV lateral model in which secondary circulations in the cross-sectional plane were held responsible for the mean velocity profile changes. The two explanations are in contrast with each other.

The aim of this study has actually been twofold. First, general three-dimensional flow equations have been derived in a GLM setting, in order to obtain a consistent description of the mean motion in an otherwise oscillating field. Secondly, development of a 1DV and a 2DV lateral model and comparison of model results with results obtained from measurements and other models must lead to a better understanding of the mechanisms that cause the changes in the mean horizontal velocity profiles.

Following the concept of the GLM theory, as described by Andrews & McIntyre (1978*a*), general three-dimensional flow equations have been derived in this formulation from the Reynolds-averaged Navier-Stokes equations. This permits the possibility to consider turbulent motion. Extension of Andrews & McIntyre's (1978*a*) original equations with viscous and turbulent stresses lead to equations that are far from comprehensive. Therefore, an alternative derivation has been proposed. The developed models are based on the latter GLM equations.

In this study only regular long-crested nonbreaking waves have been considered, interacting with a turbulent current. In order to develop the 1DV model a WKBJ perturbation series analysis has been applied to the 3D GLM-based flow equations. Assuming slow variation in time and horizontal direction of the amplitude functions of each quantity, a series of ordinary differential equations

has been obtained. This series has been solved successively, resulting in the vertical distributions of the initial current velocity, the current-affected amplitude function of the carrier wave and the wave-induced second-order correction of the mean motion.

By allowing lateral variations, side-wall effects on the orbital and mean motion have been taken into account. The 1DV solution of the orbital motion has been extended with a laterally varying term. The variations in longitudinal direction have been neglected, resulting in a 2DV description of the wave-induced mean motion in a cross section of the flume. A numerical solver for non-hydrostatic flow has been applied to solve the 2DV GLM-based equations.

Measurements in laboratory flumes have been used to validate both models. The wave-induced horizontal drift velocities, which have been obtained for the situation without currents, agreed with Longuet-Higgins' (1953) analytical conduction solution. Agreement with the measurements of Mei et al. (1972) has been obtained for situations in intermediate water depth. For both situations of waves following and opposing the turbulent current the computed profiles agree quantitatively with the measured profiles of Klopman (1994).

The computed cross-sectional distributions of the secondary circulations show qualitative agreement with Klopman's (1997) measurements. However, for following waves the reduction of the horizontal velocity towards the free surface is overpredicted, due to an overestimated downwelling in this region. Comparison of these results with those obtained for a significant wider flume and analysis of the 2DV model results of Dingemans et al. (1996) justify the conclusion that secondary circulations cannot be ruled out in laboratory experiments. However, the velocity profile changes purely due to these circulations are insufficient compared to the total changes of profile. Moreover, following the ideas of Nielsen & You (1996) a local force balance in longitudinal direction proved that the second-order changes are mainly due to a combination of the wave-induced stress and the Stokes correction of the shear stress.

Although only one- and two-dimensional models have been developed to describe the combined motion of a turbulent current and regular nonbreaking waves, the general scheme followed in the development enables extension to three-dimensional modelling. The desired application of the model to coastal areas and analysis of typical three-dimensional features of wave-current interaction in this area seem very well possible.

## Samenvatting

De wisselwerking tussen golven en stroming is hier beschreven met behulp van de zogenaamde generalized Lagrangian mean, kortweg GLM, formulering. In tegenstelling tot de meer conventionele Eulerse beschrijving van de waterbeweging, verschaft de GLM beschrijving de mogelijkheid het gemiddelde deel van het oscillerende deel van de beweging te scheiden, ook in het gebied tussen golfdal en golftop.

Experimenteel onderzoek door onder andere Kemp & Simons (1982, 1983) en Klopman (1994) in een laboratoriumgoot heeft aangetoond dat het effect van niet-brekende golven op een turbulente stroming over een ruwe horizontale bodem significant is. In deze experimenten werden onverwachte veranderingen waargenomen in de verticale verdeling van de gemiddelde horizontale snelheid. Wanneer golven zich voortplanten in de richting van de stroming, bereikt de gemiddelde horizontale snelheid eerst een maximum om vervolgens af te nemen in het bovenste gedeelte van de verticaal. Wanneer golven zich in tegenovergestelde richting voortplanten, wordt het tegenovergestelde waargenomen. Het verticale profiel van de stroomsnelheid groeit harder in de buurt van het vrije oppervlak, vergeleken met de situatie zonder golven.

Voor zover de auteur bekend is, zijn er slechts twee theoretische modellen die een verklaring geven voor de golfgeïnduceerde veranderingen in de Eulers-gemiddelde horizontale snelheidsprofielen. Een model van Nielsen & You (1996) is gebaseerd op een lokale krachtenbalans in de richting van de stroming. Horizontale variaties in de richting loodrecht hierop zijn verwaarloosd. Dingemans et al. (1996) hebben een 2DV lateraal model ontwikkeld, waarin secundaire circulaties in het verticale vlak loodrecht op de stromingsrichting gezien worden als de oorzaak van de veranderingen in de gemiddelde longitudinale snelheid. Deze twee verklaringen zijn in tegenspraak met elkaar.

Het doel van deze studie bestaat uit twee gedeelten. Ten eerste zijn driedimensionale bewegingsvergelijkingen afgeleid in een GLM setting om een consistente beschrijving van de gemiddelde beweging in een oscillerend veld te verkrijgen. Ten tweede dient inzicht te worden verkregen in het mechanisme dat de snelheidsveranderingen veroorzaakt. Hiervoor zijn een 1DV model en een 2DV lateraal model ontwikkeld en zijn de modelresultaten vergeleken met resultaten van gootexperimenten en van andere modellen.

Het concept van de GLM theorie, zoals dat is beschreven door Andrews & McIntyre (1978a), is gevolgd om algemene driedimensionale bewegingsvergelijkingen af te leiden uit de Reynolds-gemiddelde Navier-Stokes vergelijkingen. Dit verschaft de mogelijkheid om turbulente beweging te beschouwen. Uitbreiding van Andrews & McIntyre's (1978a) oorspronkelijke vergelijkingen met viskeuze en turbulente spanningen leidt tot vergelijkingen die verre van

inzichtelijk zijn. Daarom is een alternatieve afleiding gegeven, die leidt tot meer herkenbare vergelijkingen. De ontwikkelde modellen zijn gebaseerd op laatstgenoemde vergelijkingen.

In dit onderzoek is alleen gekeken naar regelmatige langkammige niet-brekende golven, die zijn gesuperponeerd op een turbulente stroming. Om tot een 1DV model te komen is een WKBJ perturbatiereeks ontwikkeling toegepast op de 3D-GLM bewegingsvergelijkingen. Wanneer wordt aangenomen dat de amplitude functies van iedere grootte langzaam in tijd en horizontale richting variëren, wordt een reeks gewone differentiaalvergelijkingen verkregen. De vergelijkingen in deze reeks worden achtereenvolgens opgelost, resulterend in de verticale verdelingen van ten eerste de initiële stroming, ten tweede de amplitude functie van de dragende golf die op zijn beurt wordt beïnvloed door de initiële stroming en tenslotte de golfgeïnduceerde tweede orde correctie van de gemiddelde beweging.

Door variaties in laterale richting toe te laten, zijn zijwand effecten op de gemiddelde en orbitaalbeweging in rekening gebracht. De 1DV oplossing voor de orbitaalbeweging is uitgebreid met een term die afhankelijk is van de laterale richting. In de GLM vergelijkingen zijn alleen de variaties in langsrichting verwaarloosd. Dit leidt tot een 2DV beschrijving van de golfgeïnduceerde beweging in een dwarsdoorsnede van de goot. Een bestaand numeriek model voor het oplossen van niet-hydrostatische stroming is toegepast om de 2DV-GLM vergelijkingen op te lossen.

Metingen in laboratoriumgoten zijn gebruikt om beide modellen te valideren. De golfgeïnduceerde horizontale driftsnelheden, die ontstaan in de situatie zonder golven, komen overeen met Longuet-Higgins' (1953) analytische conductie oplossing. De modelresultaten komen eveneens overeen met metingen van Mei et al. (1972). Zowel voor de situatie dat golven die zich voortplanten in de richting van de stroming, als voor de tegenovergestelde situatie, komen de berekende profielen overeen met de gemeten profielen van Klopman (1994).

Vergeleken met de metingen van Klopman (1997) zijn kwalitatief correcte verdelingen van de secundaire circulaties in het dwarsvlak berekend met het 2DV model. Voor golven in de stromingsrichting wordt de reductie van de gemiddelde horizontale snelheid in de buurt van het vrije oppervlak overschat. Dit is het gevolg van een overschatting van de in het midden van de goot aanwezige 'downwelling'. Uit vergelijking met de resultaten die worden verkregen met het 2DV model voor een significant bredere goot en uit de analyse van de 2DV resultaten van Dingemans et al. (1996) kan worden geconcludeerd dat golfgeïnduceerde secundaire circulaties niet kunnen worden genegeerd in laboratorium experimenten. De louter door secundaire circulaties veroorzaakte veranderingen in de verticale profielen van gemiddelde horizontale snelheid zijn te klein ten opzichte van de totale veranderingen in de horizontale snelheidsprofielen. Tevens is aangetoond dat de tweede-orde veranderingen hoofdzakelijk worden veroorzaakt door een

combinatie van de golfgeïnduceerde schuifspanning en de Stokes correctie van de schuifspanning. Dit zijn de dominante golfgeïnduceerde krachten in de lokale krachtenbalans in longitudinale richting.

De algemene weg waarlangs de 1DV en 2DV modellen zijn ontwikkeld maakt uitbreiding naar een 3D-GLM model mogelijk. De beoogde toepassing van het model op kustzones ligt dan binnen de mogelijkheden. Tevens kunnen typische driedimensionale aspecten van golf-stroom interactie in dit gebied worden geanalyseerd.



# Contents

<b>Abstract</b>	<b>v</b>
<b>Samenvatting</b>	<b>vii</b>
<b>1 Introduction</b>	<b>1</b>
1.1 General . . . . .	1
1.2 Literature review . . . . .	2
1.3 Aim and scope of this study . . . . .	5
1.4 Outline . . . . .	6
<b>2 The generalized Lagrangian mean framework</b>	<b>9</b>
2.1 Introduction of GLM theory . . . . .	9
2.1.1 A new averaging formalism . . . . .	9
2.1.2 Applications of GLM concept . . . . .	11
2.2 Description of GLM formulation . . . . .	13
2.2.1 The GLM operator . . . . .	13
2.2.2 Specification and interpretation of GLM flow . . . . .	14
2.2.3 Basic properties of GLM operator . . . . .	17
<b>3 Derivation of 3D flow equations in GLM formulation</b>	<b>21</b>
3.1 Original derivation of GLM equations . . . . .	21
3.1.1 The pseudomomentum . . . . .	24
3.2 Alternative derivation of GLM equations . . . . .	26
3.2.1 Inclusion of viscous and turbulent effects . . . . .	26
3.2.2 Similarity to radiation stress concept . . . . .	27
3.3 Boundary conditions . . . . .	30
<b>4 1DV model</b>	<b>35</b>
4.1 The $k - \ell$ turbulence model . . . . .	36
4.2 WKBJ perturbation series approach . . . . .	37
4.2.1 Description of WKBJ method . . . . .	37
4.2.2 Application of WKBJ method to the GLM flow equations	38

4.3	Application to wave-current channel problems . . . . .	42
4.3.1	Simplification of present model . . . . .	42
4.3.2	Numerical solution method . . . . .	45
4.4	Comparison with observations . . . . .	46
4.4.1	Mass transport in water waves . . . . .	46
4.4.2	Combined wave-current motion . . . . .	49
4.4.3	Conclusions from numerical experiments . . . . .	55
4.5	Qualitative explanation for profile changes . . . . .	57
<b>5</b>	<b>2DV lateral model</b>	<b>63</b>
5.1	Secondary circulations . . . . .	63
5.2	Formulation of 2DV model in GLM setting . . . . .	66
5.2.1	Derivation of the 2DV-GLM equations in a cross-sectional plane . . . . .	67
5.2.2	Side-wall effects on fluctuating quantities . . . . .	69
5.2.3	Determination of wave-induced driving forces . . . . .	70
5.3	Numerical solution method . . . . .	73
5.3.1	Pressure correction method . . . . .	73
5.3.2	Implementation of 2DV-GLM equations in existing numerical flow model . . . . .	74
5.4	Verification of 2DV model . . . . .	76
5.4.1	Comparison with flume experiments . . . . .	77
5.4.2	Comparison with results 1DV model . . . . .	83
5.5	Evaluation of model results . . . . .	86
<b>6</b>	<b>Generalization to 3D</b>	<b>89</b>
6.1	Existing quasi-3D and fully-3D models . . . . .	89
6.1.1	Quasi-3D models . . . . .	90
6.1.2	3D models . . . . .	92
6.2	Towards a 3D model in GLM formulation . . . . .	94
6.2.1	Modelling of wave motion . . . . .	94
6.2.2	Modelling of 3D wave-induced currents . . . . .	95
6.2.3	Possible applications of 3D GLM-based model . . . . .	97
<b>7</b>	<b>Conclusions and recommendations</b>	<b>99</b>
7.1	Introduction . . . . .	99
7.2	Conclusions . . . . .	99
7.3	Recommendations . . . . .	102
	<b>References</b>	<b>105</b>
<b>A</b>	<b>Derivation of wave-action equation</b>	<b>115</b>



<i>Contents</i>	xiii
<b>B Driving forces at different orders of approximation</b>	<b>117</b>
<b>C Boundary layer affected by orbital motion</b>	<b>121</b>
C.1 Grant & Madsen's formulation of the friction velocity . . . . .	121
C.2 Inclusion of bottom and side wall friction . . . . .	123
<b>List of Figures</b>	<b>126</b>
<b>List of Symbols</b>	<b>129</b>
<b>Acknowledgements</b>	<b>133</b>
<b>Curriculum Vitae</b>	<b>135</b>



# Chapter 1

## Introduction

### 1.1 General

For a good description of water motion in natural systems knowledge of two important factors is unavoidable: surface waves and currents. The waves are usually generated by wind. Density variations, tides, waves, wind or river out-flow may cause a driving mechanism for the current. The importance of their interaction has long been recognized. A good prediction of the vertical structure of the flow field and the resulting morphodynamics in coastal areas can hardly be obtained without taking into account the combined effect of waves and currents.

The subject of wave-current interaction has been studied for decades, both experimentally and theoretically. A large amount of analytical and numerical models have been put forward. Due to the enormous improvements in the field of computer technology more and more physical aspects can be taken into account in these numerical models. Whereas three-dimensional numerical models were utopian ten years ago, the computer capacity no longer hampers the development of these models nowadays. Although numerical results could be obtained within reasonable time, only a few attempts have been made towards the development of a complete three-dimensional numerical model. Nevertheless, the three-dimensional character of the combined motion of waves and currents is of essential importance for the description of transport of sediment, as well as for the understanding and modelling of morphological changes in the coastal region.

The wave-induced driving or influencing of the current can be described by wave-induced fluxes of mass and momentum. In the conventional approach these fluxes are treated in an Eulerian framework, which results in discontinuities in the region between wave trough and wave crest. These difficulties may be prevented by using the hybrid Eulerian-Lagrangian formulation introduced by Andrews & McIntyre (1978a), the so-called *generalized Lagrangian mean* (GLM) method. However, for wave-current interaction purposes little experience with this method

has been gained so far. Application of the GLM method to the combined motion of waves and a current fulfills the need for further development of theories describing wave-current interaction and interpretation and implementation of the physical mechanisms involved.

## 1.2 Literature review

Over the last decades various wave models and models which describe current motion have been developed. However, development of models in which wave characteristics are modified by the existence of a current or, vice versa, current profiles which are modified by wave motion, has always been considered as a tedious task. Soulsby et al. (1993) classified the mechanisms describing the interaction of the wave and current field as follows:

1. Modification of the wave kinematics by the current.
2. Generation of mass transport or streaming by the waves.
3. Enhancement of the bottom friction felt by the currents, due to interaction with the wave boundary layer.
4. Enhancement of the bed shear-stresses and energy dissipation of the waves, due to interaction with the current boundary layer.
5. Refraction of the waves by horizontally sheared currents.
6. Generation of wave-induced radiation stresses acting as a driving force for currents, particularly longshore currents in the surf-zone, i.e. the region in between the breaker line and the coast line.

In fact, two major classes can be distinguished. The first class contains mechanisms 1–4 and describes the combined motion in the vertical plane. The second class is concerned with the mechanisms 5 and 6, acting in the horizontal plane. Major reviews on all of these classes have been presented by Peregrine (1976), Jonsson (1978, 1990), Sleath (1990), Soulsby et al. (1993) and Thomas & Klopman (1997).

The effect of an ambient current on the wave kinematics has received much attention so far. In order to obtain reliable predictions of the wave motion, knowledge of the vertical variation of this current is essential. Moreover, models have to take full account of vorticity in regions where the vorticity is important. This might be either global or restricted to some shear layer. For inviscid fluids the wave modelling is significantly easier. Then, for uniformly distributed currents linear wave theory provides a first order approximation for the wave potential

and free-surface elevation. Higher order solutions for a constant current have been obtained by e.g. Jonsson & Arneborg (1995). These solutions are based on Fenton's (1985) fifth-order expressions derived from Stokes' theory. For non-uniform currents the wave field will be rotational. Only for the linear regime very few solutions exist. The great majority of the literature on wave-current interaction modelling is concerned with the interaction of regular waves with a laminar current under the assumption that the flow is inviscid. Thomas & Klopman (1997) give an extensive overview of models in this class. They differentiated between linear and nonlinear waves interacting with a current having either constant vorticity or an arbitrary velocity distribution.

Field observations clearly illustrate that wave motion, either with or without current, cannot always be described by regular wave theory. Therefore, it is necessary to employ methods which account for the presence of many simultaneous frequencies and possibly directions as well. Huang et al. (1972) were the first to model the effect of a current on irregular deep-water waves. A major review on irregular wave theory was presented by Borgman (1990) and Jonsson (1990).

The impact of waves on the mean motion depends strongly on the wave regime. Modelling of currents that are generated or modified by nonbreaking waves require a different treatment than those induced by breaking waves. In coastal areas strong currents are generated in the surf zone. In the surf zone longshore currents and wave set-up were recognized in field experiments but could not be explained properly until the theoretical formalism of the radiation stress was discovered by Longuet-Higgins & Stewart (1960, 1961). Since then so many contributions have been made towards the understanding of the surf zone phenomena that mentioning them all would be an impossible task. Therefore only the pioneering papers on longshore currents and wave set-up of Longuet-Higgins (1970), Bowen (1969), Bowen et al. (1968) and Thornton (1970) are touched upon, as well as the overviews on coastal zone phenomena in the books of Phillips (1977) and Mei (1989) and the review papers of Peregrine (1983), Battjes (1988), Battjes et al. (1990) and Svendsen & Putrevu (1996). This theory was the basis of a range of numerical models such as

- cross-shore profile models, which give the longshore current distribution ignoring longshore variation, by e.g. Southgate (1989).
- two-dimensional coastal area models, in which the depth-averaged current is considered, proposed by Ebersole & Dalrymple (1980), Wu & Liu (1985), Wind & Vreugdenhil (1986), among others. Recently, a description and intercomparison of seven models in this class were presented by P  chon et al. (1997).
- quasi-three-dimensional and three-dimensional coastal area models developed by e.g. De Vriend & Stive (1987), S  nchez-Arcilla et al. (1992), Van

Dongeren & Svendsen (1997) and Péchon & Teisson (1994).

Outside the surf-zone the wave-induced driving mechanism for the mean motion is different. For regular waves on otherwise still water Stokes (1880) introduced the mean Lagrangian, or mass-transport, velocity. Longuet-Higgins (1953), indicated that fluid-friction effects dominate the wave-induced changes in the mean flow. He was the first to recognize that the inclusion not only significantly modifies the mean motion in the bottom and free surface boundary layer, but in the core region of the fluid as well. Later on, Craik (1982a) extended this theory for both the Eulerian-mean and the Lagrangian-mean motion by taking into account spatial and temporal wave attenuation. Russell & Osorio (1957) and Mei et al. (1972) measured drift velocities in a wave flume. Mei et al. (1972, pp.151-152) state that they obtain quantitative agreement (for a certain range of wave slopes  $kh$ ) with Longuet-Higgins' conduction solution. More recently, Iskandarani & Liu (1991a, 1991b, 1993) reported on experiments on two- and three dimensional mass transport velocity profiles.

In many models on wave-current interaction there is a separation of the flow domain into three layers: the surface shear layer, the main region and the bottom boundary layer. Such a division is based on the influence of viscosity and turbulence. The bottom boundary layer has been studied elaborately due to its importance for sediment transport purposes. Soulsby et al. (1993) compared a large amount of bottom shear stress predictions with experimental and field data for the combined motion of waves and currents over a rough bed. Among others, the theoretical models used in that paper have been described in the review paper by Davies & Villaret (1997). The models of e.g. Grant & Madsen (1979), Christoffersen & Jonsson (1985), and Sleath (1991) are based on the idea that the current profile is logarithmic above the wave boundary layer. In these models the wave effects are only taken into account in the wave boundary layer and little attention was paid to the current velocity distribution near the free surface. As a result the models above are not suitable for determining the wave-induced current profile over the entire depth.

In contrast to the large number of theoretical solutions, the amount of experimental data is very limited. The available data tend to concentrate on flow features in the near-bed region. At greater heights above the beds some experimental data on Eulerian-mean velocities under regular, nonbreaking waves in a laboratory flume have been reported by Bakker & Van Doorn (1978) (more extensively reported in Van Doorn 1981), Kemp & Simons (1982, 1983) and Supharatid et al. (1992). In the papers by Kemp & Simons and Supharatid et al. the two situations of waves following and opposing a turbulent current were considered. Swan (1990) observed the modification of the wave motion in the presence of a strongly-sheared current velocity throughout the depth of the flow field and compared these data with existing theoretical solutions. Klopman

(1994) measured orbital and mean velocities over the whole depth of a channel in experiments concerning waves following and opposing a turbulent current.

In all experimental studies mentioned above the authors found that the Eulerian-mean velocities have completely different distributions than those which are the result of linear addition of the separately obtained current and wave velocities. For currents following a regular wave field the Eulerian-mean horizontal velocity reaches a maximum value at a level between bottom boundary layer and wave trough and decreases towards the free surface. In contrast, for waves opposing the current the Eulerian-mean horizontal velocity increases more rapidly towards the free surface than in absence of waves. The deviation from the logarithmic profile is obvious. Only few attempts have been made towards numerical modelling of the phenomena observed in the experimental data. You (1996) developed a model to give a quantitative description of the current profile near the mean water surface employing the effect of the wave-induced stress. Based on the same principle Nielsen & You (1996) presented a model describing the wave-induced changes of the current profile over the entire depth qualitatively. These two models neglect all variations in spanwise direction, in contrast to the model developed by Dingemans et al. (1996). They considered wave-induced secondary circulations in the cross-sectional plane as the main mechanism causing the changes in the current profile.

An intriguing point is that the model of Nielsen & You (1996) confirms the theory that changes of the mean horizontal velocity profile are purely caused by phenomena in longitudinal direction, whereas Dingemans et al. (1996) suppose the secondary lateral circulations to be the reason for changes in the mean horizontal velocity profile in streamwise direction. Their prediction of the existence of lateral circulations is supported by laboratory measurements of Klopman (1997).

### 1.3 Aim and scope of this study

The problems of understanding the mechanism of wave current interactions have mostly been tackled via the Eulerian equations of mean motion. A major difficulty with the Eulerian representation of the flow field is the unique and unambiguous identification of the mean motion in an otherwise oscillating field, since at a fixed position between wave trough and wave crest there is water only part of the time. A consistent way to split the mean and oscillating motion is through the *generalized Lagrangian-mean* (GLM) method as proposed by Andrews & McIntyre (1978a). This is a hybrid Eulerian-Lagrangian description of motion, in which the Lagrangian-mean flow is described by means of equations in Eulerian form.

The purpose of this work is to apply the GLM theory to the combined motion

of regular nonbreaking waves on an arbitrarily distributed current. Irregular as well as breaking waves are out of the scope of this study. The wave-induced changes in the vertical profiles of the mean motion and the effect of the current on the orbital motion, which have been observed in the experimental flume data mentioned in section 1.2, are of main interest.

In order to achieve the goal just mentioned two types of models have been developed. Firstly, a 1DV model is presented based on the WKBJ perturbation series approach. The model not only predicts the nonlinear changes in the vertical profile of the mean velocity due to the presence of waves, but determines the modifications of the orbital velocity profiles caused by the current as well. Secondly, a 2DV model has been developed, in which the changes in lateral direction are taken into account as well, in order to provide more insight in the effect of the secondary circulations on the mean horizontal velocity profile.

Comparison of the results of both models must lead to a better understanding of the mechanisms that cause the changes in the mean horizontal velocity profiles. The most significant contribution may be based on phenomena acting in longitudinal direction (as in Nielsen & You 1996) or in spanwise direction (as in Dingemans et al. 1996) or even in both directions. In the latter, three-dimensional case phenomena in longitudinal as well as lateral direction are significant. In the present study we investigate which contribution or set of contributions is dominant.

In the present study, we do not aim at developing a complete three-dimensional model in the GLM formulation that is suitable to describe the three-dimensional character of the combined motion of waves and currents in the coastal area. Instead experience has been gained in dealing with the GLM theory, applying the theory to water wave-current problems and interpreting results so that they can be compared to existing experimental and theoretical results. As such this study must be considered as a step towards a more consistent way of modelling wave-current interaction.

## 1.4 Outline

The arrangement of this thesis is as follows. The formalism of the GLM theory as well as its applications are outlined in chapter 2. Furthermore, a description and an interpretation of the GLM averaging procedure is given.

In chapter 3 the derivation of the three-dimensional flow equations in a GLM formulation is given. Firstly, the main features in the original derivation of Andrews & McIntyre (1978a) are pointed out. Special attention has been given to the pseudomomentum, which is generally regarded as an important quantity in the driving mechanism for the mean motion. Secondly, an alternative approach



of the GLM formulation is outlined, along with proper boundary conditions at the bottom and the free surface.

In chapter 4 the development of the 1DV model is described. The GLM equations are solved using a WKBJ type perturbation series approach. The resulting boundary-value problem, with only the vertical spatial coordinate as independent variable, is solved numerically. The model is applied to wave-current channel problems and the results of the 1DV model are compared with both theoretical solutions and experimental data.

The 2DV model is described in chapter 5. For the evaluation of the wave-induced driving force the oscillating quantities obtained with the 1DV model are modified in lateral direction to account for the side-wall effects. The resulting set of time-dependent 2DV flow equations is solved using an existing numerical model for non-hydrostatic flow. The results of the 2DV model are compared with experimental data both in the cross-sectional plane of the flume and in longitudinal direction. Finally, the 1DV and 2DV results are compared with each other leading to a conclusion about the dominant mechanism responsible for the mean horizontal velocity profile changes.

In chapter 6 suggestions for generalization of the GLM-based model to three dimensions are discussed. Comparison is made with some of the few existing quasi-3D and fully-3D models describing wave-current interactions. Finally, conclusions and recommendations are listed in chapter 7.



## Chapter 2

# The generalized Lagrangian mean framework

### 2.1 Introduction of GLM theory

As already mentioned in chapter 1, the interaction of waves and currents is of great importance for a good prediction of the vertical structure of the mean flow field. In particular, a clear description of the driving forces is essential for the prediction of wave-induced currents. These driving forces are expressed in terms of mean wave momentum fluxes. For depth-averaged currents the excess momentum flux or radiation stress introduced by Longuet-Higgins & Stewart (1960) reflects the influence of the waves in mean momentum equations in a conventional Eulerian framework. Mean motion and wave motion are usually separated by averaging over the wave phases (see e.g. Phillips 1977, Mei 1989). For depth-varying currents considered in an Eulerian formulation, Dingemans (1997, p.228) noticed the difficulty in identifying the mean motion in an otherwise oscillating field.

#### 2.1.1 A new averaging formalism

Finding a unique and unambiguous separation of the mean and oscillating motion is difficult in the Eulerian representation of the flow field, because at a fixed position at a level between the wave trough and the wave crest there is water only part of the time. This difficulty can be avoided by considering the Lagrangian representation of the flow field. The simplest idea is Stokes' classical idea of Lagrangian averaging by taking the time mean following a single particle. This idea has its limitations. The formulation cannot apply in any exact sense if we wish to speak of the Lagrangian-mean velocity at a given point in space. This is due to the fact that the particle to be followed will generally wander away from

this point. Therefore, the expression "Lagrangian-mean velocity field" does not make sense in the classical concept of the mean following a single particle.

An important step towards a more general concept, in which the Lagrangian-mean velocity is a true field variable, was provided by the transformation theory of the Lagrangian equations of motion, given by Eckart (1963). Its application to problems of mean-flow evolution has been developed by Dewar (1970), Bretherton (1971) and Soward (1972). The derivations of the first two authors depend on various asymptotic approximations. Soward's derivations were exact in principle but did not lead to exact theorems on mean-flow evolution due to finite-amplitude waves. Eventually Andrews & McIntyre (1978a) presented the *Generalized Lagrangian mean* theory, or simply GLM, in their pioneering paper. They not only generalized the classical notion of Lagrangian-mean flow, but also described an exact theory on mean-flow evolution due to finite-amplitude waves, which does not depend on any asymptotic approximation. However, in the general case of finite-amplitude disturbances the equations for the mean motion are rather complicated and difficult to interpret physically.

As will be outlined in section 2.2 the GLM description is a *hybrid* Eulerian-Lagrangian description of motion, since it describes the Lagrangian-mean flow by means of equations in Eulerian form with position  $\mathbf{x}$  and time  $t$  as independent variables. Apart from the basic idea of getting a precise distinction between mean motion and wave motion, from which an exact definition of wave momentum (also called pseudomomentum) can be obtained, Andrews & McIntyre (1978a, p.612) listed some other advantages of the GLM approach. They pointed out that an Eulerian description of Lagrangian-mean flow is desirable to express ideas like steady mean flow, steadiness of the wave field and spatial homogeneity in some specific direction. McIntyre (1980b, p.131) remarks that the GLM theory provides a precise analytical structure which not only explains what is involved in generalizing the classical notions of Lagrangian-mean and Stokes drift, but also makes available certain analytical tools, the use of which might prove helpful in the search for an improved understanding of the physics involved.

Closely related to the above is the fact that the GLM approach explicitly represents the effect of wave forcing upon mean flow evolution. De Vriend & Kitou (1990) mentioned the difficulties in formulating forces induced by surface waves in an Eulerian framework in a three-dimensional hydrostatic mean current model. Formulation of the vertical distribution of wave forces in this framework will lead to singularities at the mean free surface, due to wave dissipation and wind-input, and at the bottom, due to bottom friction. However, by using a Lagrangian formulation the derived wave forces are not likely to contain singularities and vary smoothly over depth. Finally, Grimshaw (1984, p.11) claimed the GLM formulation to be very natural by writing that, despite the fact that the equations of fluid mechanics have originally been developed in an Eulerian frame-

work, wave characteristics like wave action are more obvious in its Lagrangian counterpart.

Before the Lagrangian-mean flow equations can be solved, knowledge of wave quantities is required. Andrews & McIntyre (1978*b*) derived an equation for the wave action in a simple but very general form, which does not depend on the approximations of slow amplitude modulation or linearization. The wave-action equation found by Bretherton & Garrett (1968) for slowly varying, linear waves was shown to be a corollary of this general equation, due to the fact that the part of the total momentum that depends on wave motion itself, the pseudomomentum, can be linked to the wave action for slowly varying waves. A different approach is given by Uittenbogaard (1992). He rewrote the terms in the mean flow equations, given in a Lagrangian formulation, in terms of easily identifiable quantities which can be evaluated by an existing wave model. This approach was also followed by Grimshaw (1981), who studied drift velocities of water waves in a GLM setting. The situation of no ambient current is in fact a limit of all situations concerning the combined wave-current motion. The approach in the present study touches upon those of Uittenbogaard (1992) and Grimshaw (1981).

### 2.1.2 Applications of GLM concept

In most papers mentioned above the authors tried to verify their statements by applying the GLM theory to realistic flow problems. According to the following outline the GLM theory is applicable to a great variety of flow problems. Andrews & McIntyre (1978*a*) derived a complete set of equations for the mean flow for the case of a stratified, rotating fluid under external and self-gravity forces. For the important case of 'longitudinally symmetric' mean flow, which is appropriate to astrophysical examples (see Andrews & McIntyre 1976), the role of wave phenomena, in particular wave dissipation, in mean flow evolution was discussed. Here mean denotes a Cartesian space average. Rather than giving a catalogue of all the contexts in fluid mechanics where wave problems have been invoked, Grimshaw (1984) gave a brief account of the influence of internal gravity waves on an ensemble-averaged stratified shear flow. Under simplifying assumptions, like incompressibility, constant gravity acceleration, no frictional forces and Boussinesq's assumption with respect to density variations, the very general case considered by Andrews & McIntyre (1978*a*) was repeated by Uittenbogaard (1992) and Dingemans (1997, note 2.6) for application to water wave problems. Uittenbogaard (1992) considered wave-induced changes of the ensemble-averaged velocity, whereas Dingemans (1997) confined himself to inviscid flow while emphasizing several types of averaging such as time and ensemble averaging. By applying the GLM theory to an inertio-gravity problem McIntyre (1980*a*, p.164)

mentioned the Lagrangian zonal-mean flow problem to be simpler compared to its corresponding Eulerian zonal-mean flow problem in several respects. In the first place, there is no Lagrangian-mean flow across any of the (rippled) closed boundaries. Secondly, a more direct description of momentum transport can be given, compared to the Eulerian description using Reynolds stress. Without going into detail reference is made to an application given by Lighthill (1992), which is both surprising and interesting. He described acoustic streaming in the ear. Both Lagrangian-mean and Eulerian-mean motion of inner-ear fluids induced by sound waves were considered.

A fluid-flow phenomenon that has been investigated thoroughly is the occurrence of Langmuir circulations. These are organized convective motions that form in the surface layer of open bodies of water. When the wind blows over a water surface and generates waves, numerous streaks parallel to the wind direction may be observed. Langmuir (1938) related these streaks to convergence lines between counter rotating vortices below the surface. Different mechanisms for generating Langmuir circulations have been proposed in literature. Craik & Leibovich (1976), Craik (1977) and Leibovich (1977) presented models in which the vortices are induced by the interactions between the waves, via the so-called Stokes drift, and a weak wind-induced shear flow. These models have been divided into two classes, CL1 and CL2. Leibovich (1983) reviewed the subject and discussed the two mechanisms in terms of 'vortex forces'. Before that, Leibovich (1980) rederived the CL theories by applying the GLM theory. However, in contrast to the CL theories the GLM method did not require any assumption regarding the wave motion and the current profile. From that moment the GLM method has been considered as a powerful tool to understand e.g. the (instability) mechanism behind the generation of secondary flows.

Many applications of the CL theory followed, only a few are mentioned here. Craik (1982b, 1982c) applied the GLM theory in an investigation of hydrodynamic stability of parallel shear flow. Magnaudet (1989) made a thorough analysis of wavy stratified duct flow and investigated also the interaction between waves and turbulence. Furthermore, Nordsveen & Bertelsen (1997) applied the GLM theory to study the wave-induced secondary motions that were observed in the fully developed turbulent gas-liquid stratified flow in near horizontal ducts. Finally, reference is made to a paper of Phillips (1998) in which he reviews several years' work on the nonlinear interaction of growing finite-amplitude rotational waves with unidirectional viscous shear flows of various strengths. The wave-mean interaction is described using the GLM formulation.

## 2.2 Description of GLM formulation

The GLM theory establishes a definition of the GLM velocity  $\bar{\mathbf{u}}^L$  at the outset and then derives general equations for its evolution from the equations of motion. As outlined in subsection 2.1.2 the formalism of the theory applies for different forms of averaging, such as time, zonal and ensemble averaging. The physical interpretation of  $\bar{\mathbf{u}}^L$  depends on the particular choice of averaging. Before specifying the type of flow problem with corresponding averaging procedure that is considered in this study and giving an interpretation of  $\bar{\mathbf{u}}^L$  in that situation, the general description of the GLM theory is given.

### 2.2.1 The GLM operator

The description of the basic formalism of the GLM theory is outlined here in a somewhat abstract way. In the GLM theory GLM operators are related to Eulerian-mean operators. Let  $\overline{(\ )}$  be a general averaging operator (time, space, ensemble, etc.) taking a scalar, vector or tensor field  $\varphi(\mathbf{x}, t)$  into a corresponding (Eulerian-mean) field  $\overline{\varphi}(\mathbf{x}, t) = \overline{\varphi(\mathbf{x}, t)} = \langle \varphi(\mathbf{x}, t) \rangle$  at position  $\mathbf{x}$  and time  $t$ . The notation  $\langle (\ ) \rangle$  is also used for the same averaging operator, for the sake of convenience. Whether the operator denotes time, space or ensemble averaging is not relevant for the general outline of the GLM theory at this stage. Only when the type of flow problem and splitting in mean and oscillating parts has to be defined, the averaging operation has to be specified. This is carried out in the next subsection.

To overcome the problems mentioned in subsection 2.1.1, arising in the Eulerian and pure Lagrangian framework, Andrews & McIntyre (1978a) generalized the classical Lagrangian-mean description such that the expression "Lagrangian-mean velocity field" makes sense. An essential part in the GLM theory is the definition of the particle displacement  $\boldsymbol{\xi}$  associated with the disturbed motion. Like all quantities in the GLM formulation, it is defined as a function of the position  $\mathbf{x}$  and time  $t$  and no longer primarily as a function of the individual particle label as in a purely Lagrangian description. In fact, the generalized Lagrangian flow is described by means of equations in Eulerian form.

After having described the disturbance-associated particle displacement field  $\boldsymbol{\xi}(\mathbf{x}, t)$ , the exact GLM operator  $\overline{(\ )}^L$ , corresponding to any given Eulerian-mean operator  $\langle (\ ) \rangle$ , is defined as,

$$\overline{\varphi(\mathbf{x}, t)}^L = \langle \varphi(\mathbf{x} + \boldsymbol{\xi}(\mathbf{x}, t), t) \rangle. \quad (2.1)$$

Definition (2.1) implies that the average is taken with respect to the values of  $\varphi$  at the disturbed particle positions, which are denoted by  $\boldsymbol{\Xi}(\mathbf{x}, t) = \mathbf{x} + \boldsymbol{\xi}(\mathbf{x}, t)$ . For convenience, the notation  $\varphi^\xi(\mathbf{x}, t)$  is used instead of  $\varphi(\mathbf{x} + \boldsymbol{\xi}(\mathbf{x}, t), t)$  as well.

By assuming that the mapping  $\mathbf{x} \rightarrow \mathbf{x} + \boldsymbol{\xi}(\mathbf{x}, t)$  is invertible, Andrews & McIntyre (1978a, p.615) stated that for any given  $\mathbf{u}(\mathbf{x}, t)$  there is a unique 'reference velocity field'  $\mathbf{v}(\mathbf{x}, t)$ , such that, when the point  $\mathbf{x}$  moves with the velocity  $\mathbf{v}$  the point  $\mathbf{x} + \boldsymbol{\xi}$  moves with the actual velocity  $\mathbf{u}^\xi$ , i.e.

$$(\partial/\partial t + v_j \partial/\partial x_j) \boldsymbol{\xi} = \mathbf{u}^\xi. \quad (2.2)$$

They obtained the GLM description by requiring that

$$\overline{\boldsymbol{\xi}(\mathbf{x}, t)} = 0, \quad (2.3)$$

i.e.  $\boldsymbol{\xi}$  is a true disturbance quantity and that the reference  $\mathbf{v}$  is a mean quantity,

$$\mathbf{v}(\mathbf{x}, t) = \overline{\mathbf{v}(\mathbf{x}, t)}, \quad (2.4)$$

which immediately yields  $\mathbf{v} = \overline{\mathbf{u}}^L$ . By introducing the Lagrangian disturbance velocity  $\mathbf{u}^\ell$  in a natural way as,

$$\mathbf{u}^\ell(\mathbf{x}, t) = \mathbf{u}^\xi(\mathbf{x}, t) - \overline{\mathbf{u}(\mathbf{x}, t)}^L, \quad (2.5)$$

relation (2.2) yields

$$\overline{D}^L \boldsymbol{\xi} = \mathbf{u}^\ell, \quad (2.6)$$

with  $\overline{D}^L = \partial/\partial t + \overline{\mathbf{u}}_j^L \partial/\partial x_j$  the Generalized Lagrangian-mean material derivative, denoting the rate of change following the GLM flow. Relation (2.6) between the disturbance-associated fields  $\boldsymbol{\xi}$  and  $\mathbf{u}^\ell$  not only defines  $\boldsymbol{\xi}$  but also validates the claim to regard  $\boldsymbol{\xi}$  as a disturbance-associated particle displacement. Summarizing, the basic equations of the GLM theory are (2.1), (2.3), (2.5) and (2.6).

Eulerian-mean and generalized Lagrangian-mean quantities are related to each other by the generalized 'Stokes correction'  $\overline{\varphi}^S$ , which is defined as

$$\overline{\varphi(\mathbf{x}, t)}^S = \overline{\varphi(\mathbf{x}, t)}^L - \overline{\varphi(\mathbf{x}, t)}. \quad (2.7)$$

When  $\varphi$  denotes velocity  $\mathbf{u}$ , the Stokes correction  $\overline{\mathbf{u}}^S$  is often referred to as Stokes drift. The Stokes correction is a disturbance-related quantity. In subsection 2.2.3 an expression for the Stokes correction in terms of Lagrangian disturbance quantities is given.

## 2.2.2 Specification and interpretation of GLM flow

In general the combined motion of currents and free-surface waves can be divided in a mean part, an oscillating part and a turbulent part. In the present study the motion has been assumed to be averaged over the turbulent motion. The resulting ensemble-averaged quantities are deterministic and assumed to consist



of a mean part and a part representing the wave motion. In this study only periodic, nonbreaking waves are considered. By denoting  $T$  as the short-wave period, the mean value of an ensemble-averaged quantity  $\varphi$  is defined as the time average,

$$\overline{\varphi}(\mathbf{x}, t) = \frac{1}{T} \int_{-T/2}^{T/2} \varphi(\mathbf{x}, t + t') dt' . \quad (2.8)$$

This approach implies that interactions between turbulence and wave quantities have been neglected.

Now that the averaging procedure has been specified, an interpretation of the GLM flow can be given. In their description of wave-mean flow interactions in the atmosphere or oceans, Bühler & McIntyre (1998) gave a physical interpretation for the slow-modulation average over the rapidly varying wave phase. In fact a similar situation is considered here. Furthermore, Uittenbogaard (1992) presented a clear outline for the ensemble-average whereas Andrews & McIntyre (1978a) considered the zonal average.

In the special case of a slow-modulation average, or more specifically a time average (2.8), the physical interpretation of the GLM framework is straightforward. Consider the trajectory of a fluid particle starting at point  $\mathbf{x}_0$  in figure 2.1, i.e. the solution of  $d\mathbf{x}/dt = \mathbf{u}(\mathbf{x}, t)$ . Since  $\mathbf{u}$  is assumed to be averaged over the turbulent motion, the trajectory is actually an ensemble-averaged trajectory. In a pure Lagrangian setting the Lagrangian velocity  $\mathbf{u}^L$  is defined implicitly as

$$\mathbf{u}^L(\mathbf{x}_0, t) = \mathbf{u}(\mathbf{x}_0 + \int_{t_0}^t \mathbf{u}^L(\mathbf{x}_0, t') dt', t) , \quad (2.9)$$

(see e.g. Phillips, 1977, equation (3.3.2)), where the velocity of a particle is actually evaluated along its trajectory and assigned to its initial position. The time-averaging process associates two different trajectories with each particle: firstly its actual, rapidly varying trajectory (dashed line in figure 2.1) and secondly its mean, slowly varying trajectory (drawn line in figure 2.1). The GLM theory claims the existence of a disturbance-associated particle displacement field  $\boldsymbol{\xi}(\mathbf{x}, t)$ , that links both trajectories (dashed arrow in figure 2.1). In the ensemble-averaged setting  $\boldsymbol{\xi}$  is fully determined by the wave motion. In the GLM setting a position  $\mathbf{x}$  at time  $t$  is considered as a mean position corresponding one to one to an actual particle position  $\mathbf{x} + \boldsymbol{\xi}(\mathbf{x}, t)$ . The actual or generalized Lagrangian velocity is again evaluated at the actual position, but it is now assigned to the mean position,

$$\mathbf{u}^\xi(\mathbf{x}, t) = \mathbf{u}(\mathbf{x} + \boldsymbol{\xi}(\mathbf{x}, t), t) . \quad (2.10)$$

The GLM velocity is defined by taking the time average of (2.10), according to (2.1). The trajectories of points moving with velocity  $\overline{\mathbf{u}}^L$  are exactly the mean particle trajectories sought. The analogy between (2.9) and (2.10) reveals the

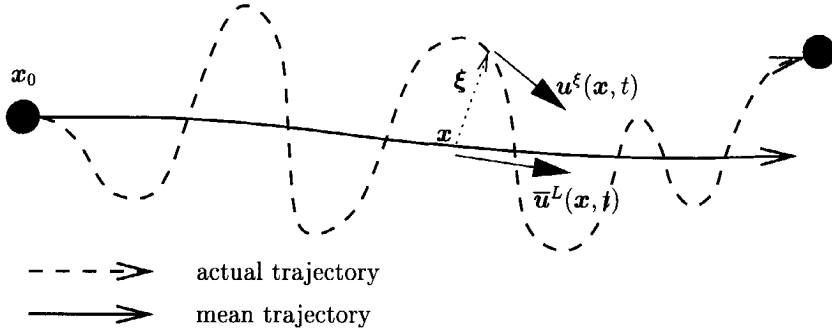


Figure 2.1: Mean and actual particle trajectories (this figure is identical to figure 3 in Bühler & McIntyre 1998)

Lagrangian aspects in the GLM method. However, the field  $\xi$  depends on the position  $\mathbf{x}$  and time  $t$ , and is thus no longer primarily a function of the individual particle label, as in a purely Lagrangian description.

In a GLM setting the frame of reference is determined by the positions  $\mathbf{x}$ . Since these positions can be considered as mean particle positions, a separation between the mean and oscillating motion is obtained in an elegant way. Relation (2.10) shows that if there are no waves, the Eulerian and generalized Lagrangian velocities are equal, because then  $\xi = 0$ .

On the other hand, in a pure Lagrangian setting the particles are fixed compared to their reference frame by definition. Consequently, the free surface is a coordinate line. Likewise, the free surface elevation in a GLM setting is not given by the instantaneous elevation, but by the GLM elevation. The problems in an Eulerian setting with the identification of the mean motion in the region between wave crest and wave trough do not arise in a GLM setting. In wave-current flow particles drift from minus infinity to plus infinity, so mean particle or initial particle positions are not useful. This rules out the use of a pure Lagrangian description of the wave-current flow.

The description of the GLM theory in terms of mean trajectories is only useful for its interpretation. For conceptual purposes the motion is split up into a mean (GLM) part and oscillatory deviations from this mean part. In the GLM method the mean oscillatory excursion equals zero. So the GLM velocities can be attached to the GLM coordinates in a meaningful way (see subsection 2.2.1). Obviously, the advantages of the Eulerian and Lagrangian description are combined.

In essence, the GLM theory treats all the points  $\mathbf{x}$  in the domain as a time-

dependent reference space for both mean and actual trajectories. Bühler & McIntyre (1998) explained this by introducing a dual reference frame. The first reference is established by the trivial mapping  $\mathbf{x} \rightarrow \mathbf{x}$ , which associates with a fixed position  $\mathbf{x}$  the mean trajectory of a particle passing through  $\mathbf{x}$  at time  $t$ . Hence, the time-dependent aspect has now been introduced. The second reference is established by  $\mathbf{x} \rightarrow \mathbf{x} + \boldsymbol{\xi}(\mathbf{x}, t)$ , which associates with  $\mathbf{x}$  the actual particle trajectory of the same particle. This dual reference frame avoids the use of the classical Lagrangian particle labels as a reference space.

Bühler & McIntyre (1998) state that for the present interpretation to work properly, one has to assume that exactly one mean trajectory passes through each point  $\mathbf{x}$  at a given time  $t$ . Otherwise  $\boldsymbol{\xi}(\mathbf{x}, t)$  would not be unique. In other words, mean particle trajectories must not cross each other. It is not a priori clear whether or not this will occur. Distinct fluid particles may share the same mean position. Nevertheless, the mean trajectories are assumed not to cross. Andrews & McIntyre (1978a, p.615) translate this assumption in mathematical terms by requiring that the mapping  $\mathbf{x} \rightarrow \mathbf{x} + \boldsymbol{\xi}(\mathbf{x}, t)$  is invertible.

### 2.2.3 Basic properties of GLM operator

Before the GLM theory is applied to the flow equations for the combined motion of water waves and currents, some basic properties of the GLM operator are derived. For that purpose, we use the following notation. Latin indices  $i, j$  or  $k$  take the value 1, 2 or 3. It is sometimes convenient in the subsequent analysis to distinguish between horizontal coordinates  $x_\alpha$  ( $\alpha = 1, 2$ ) and the vertical coordinates  $z = x_3$  by employing Greek indices for horizontal variables and Latin variables for all three coordinates. Similarly,  $u_\alpha$  denotes a horizontal velocity component and  $w = u_3$  the vertical velocity. A different notation has been used for vectors operating in all three directions,  $\mathbf{u} = (u_1, u_2, u_3)$  and those involving the horizontal direction,  $\mathbf{u}_h = (u_1, u_2)$ . Furthermore, Einstein's summation convention is used, i.e.  $u_j v_j = u_1 v_1 + u_2 v_2 + u_3 v_3$ .

The disturbance related quantities, like  $\boldsymbol{\xi}$  and  $\mathbf{u}^\ell$ , scale with the wave motion, which has amplitude  $a$ . This wave amplitude is supposed to be small with respect to both depth and wavelength. Despite the fact that  $a$  is not dimensionless, the order of approximation is denoted by  $O(a^n)$ . Since the equations of motion are not non-dimensionalized,  $O(a)$  is used for convenience instead of  $O(\varepsilon)$  with  $\varepsilon = ka$  or  $\varepsilon = a/h$ .

In order to deal properly with the transformation from Eulerian to GLM formulation and vice versa via the mapping  $\mathbf{x} \rightarrow \mathbf{x} + \boldsymbol{\xi}$ , some important consequences of the chainrule are outlined. Although the properties of the latter mapping have been given by Andrews & McIntyre (1978a, appendix A1), or in a more fundamental way by Dingemans (1997, p.239–241), they are repeated

here for their relevance in the derivation of the GLM flow equations. First, the chainrule itself yields

$$\frac{\partial \varphi^\xi}{\partial x_i} = \frac{\partial \varphi}{\partial \Xi_j} \frac{\partial \Xi_j}{\partial x_i} \quad , \quad \left( \frac{\partial \varphi}{\partial x_i} \right)^\xi \equiv \frac{\partial \varphi}{\partial \Xi_i} = \frac{\partial \varphi^\xi}{\partial x_j} \frac{\partial \Xi_j}{\partial \Xi_i} . \quad (2.11)$$

The latter factor  $\partial x_j / \partial \Xi_i$  in (2.11) can be expressed in terms of  $\partial \Xi_j / \partial x_i \equiv \delta_{ij} + \partial \xi_j / \partial x_i$  by introducing  $K_{ij}$  as the cofactors of the Jacobian  $J$  of the mapping  $\mathbf{x} \rightarrow \mathbf{x} + \boldsymbol{\xi}$ , i.e.  $J = \det(\partial \Xi_j / \partial x_i)$ . Here  $\delta_{ij}$  denotes Kronecker's delta. By definition  $K_{ij} = (-1)^{i+j} \det B_{ij}$  with  $B_{ij}$  the matrix that is obtained after deleting the  $i$ -th row and  $j$ -th column from the matrix  $\partial \Xi_j / \partial x_i$ . By expressing the inverse of latter matrix in terms of its cofactors, the following relation can be derived,

$$\frac{\partial \Xi_i}{\partial x_k} K_{ij} = J \delta_{kj} = \frac{\partial \Xi_k}{\partial x_i} K_{ji} . \quad (2.12)$$

For small disturbances  $|\boldsymbol{\xi}|$  the following approximate expression for the cofactor  $K_{ij}$  can be derived from the first relation in (2.12),

$$K_{ij} = J \left( \delta_{ij} - \frac{\partial \xi_j}{\partial x_i} + \frac{\partial \xi_k}{\partial x_i} \frac{\partial \xi_j}{\partial x_k} \right) + O(a^3) . \quad (2.13)$$

Application of (2.12) yields for the second relation in (2.11) that

$$\left( \frac{\partial \varphi}{\partial x_i} \right)^\xi = \frac{K_{ij}}{J} \frac{\partial \varphi^\xi}{\partial x_j} . \quad (2.14)$$

Let  $\Xi_{i,j} = \partial \Xi_i / \partial x_j$ . Now upon using relation (2.12), an expression for the variation of the Jacobian  $J$  has been obtained,

$$\frac{\partial J}{\partial \psi} = \frac{\partial J}{\partial \Xi_{i,j}} \frac{\partial \Xi_{i,j}}{\partial \psi} = K_{ij} \frac{\partial \Xi_{i,j}}{\partial \psi} , \quad (2.15)$$

where  $\partial / \partial \psi$  denotes  $\partial / \partial t$  or  $\partial / \partial x_k$ . This property will be employed in the derivation of the mass conservation equation in section 3.1. In that derivation the material derivative of  $J$  is required. From relation (2.12) and property (2.14) the following relation can be derived

$$\begin{aligned} \overline{D}^L J &= K_{ij} \overline{D}^L \left( \frac{\partial \Xi_i}{\partial x_j} \right) \\ &= K_{ij} \left\{ \frac{\partial}{\partial x_j} \left( \overline{D}^L \Xi_i \right) - \frac{\partial \overline{u}_k^L}{\partial x_j} \frac{\partial \Xi_i}{\partial x_k} \right\} = \frac{\partial u_i^\xi}{\partial x_j} K_{ij} - \frac{\partial \overline{u}_k^L}{\partial x_j} \delta_{kj} J . \end{aligned} \quad (2.16)$$

Relation (2.14) yields that  $K_{ij} (\partial u_i^\xi / \partial x_j) = J (\partial u_i / \partial x_i)^\xi$ . Therefore, (2.16) reduces to

$$\bar{D}^L J = J \left\{ \left( \frac{\partial u_j}{\partial x_j} \right)^\xi - \frac{\partial \bar{u}_j^L}{\partial x_j} \right\}. \quad (2.17)$$

A direct consequence of relation (2.2) and the chainrule (2.11) is that

$$\left( \frac{D\varphi}{Dt} \right)^\xi = \bar{D}^L (\varphi^\xi), \quad (2.18)$$

where  $D/Dt = \partial/\partial t + \mathbf{u} \cdot \nabla$  denotes the material derivative with respect to the total velocity  $\mathbf{u}$ . Transformation from an Eulerian setting to its GLM counterpart yields the application of the 'dual' mapping that associates with a fixed point  $\mathbf{x}$  the actual particle position  $\Xi$ . A relation between an Eulerian and a GLM quantity can be derived directly by Taylor series expansion around the actual particle position  $\Xi$ . For some quantity  $\varphi(\mathbf{x}, t)$  this yields,

$$\begin{aligned} \varphi(\mathbf{x}, t) &= \varphi(\Xi - \boldsymbol{\xi}, t) \\ &= \varphi(\Xi, t) + \sum_{n=1}^{\infty} \frac{(-1)^n}{n!} \xi_{j_1} \cdots \xi_{j_n} \frac{\partial^n \varphi(\Xi, t)}{\partial \Xi_{j_1} \cdots \partial \Xi_{j_n}}. \end{aligned} \quad (2.19)$$

By applying the chainrule (2.14) to the partial derivatives occurring in the summation in the right-hand side of relation (2.19), the partial derivatives with respect to  $\Xi_j$  can be replaced by partial derivatives with respect to  $x_j$ . By defining for some quantity  $\phi = \phi(\mathbf{x}, t)$  the operator

$$\mathcal{T}(\phi, \boldsymbol{\xi}, \mathbf{x}, t) \quad (2.20)$$

$$= \sum_{n=1}^{\infty} \frac{(-1)^{n+1}}{n!} \xi_{j_1} \xi_{j_2} \cdots \xi_{j_n} \frac{1}{J} K_{j_1 m_1} \frac{\partial}{\partial x_{m_1}} \left( \frac{1}{J} K_{j_2 m_2} \frac{\partial}{\partial x_{m_2}} \left[ \cdots \frac{1}{J} K_{j_n m_n} \frac{\partial \phi}{\partial x_{m_n}} \right] \right),$$

relation (2.19) can be written as,

$$\varphi(\mathbf{x}, t) = \varphi^\xi(\mathbf{x}, t) - \mathcal{T}(\varphi^\xi, \boldsymbol{\xi}, \mathbf{x}, t). \quad (2.21)$$

According to definition (2.7) of the Stokes correction, relation (2.21) shows that an expression for the Stokes correction in terms of GLM quantities can be obtained by averaging the operator  $\mathcal{T}(\varphi^\xi, \boldsymbol{\xi}, \mathbf{x}, t)$ . By substituting (2.13) into (2.21) and (2.20) a second-order approximation for the Stokes correction is obtained,

$$\begin{aligned} \bar{\varphi}^S(\mathbf{x}, t) &\equiv \bar{\varphi}^L(\mathbf{x}, t) - \bar{\varphi}(\mathbf{x}, t) \\ &= \left\langle \xi_j \left( \frac{\partial \varphi^\xi}{\partial x_j} - \frac{\partial \xi_k}{\partial x_j} \frac{\partial \varphi^\xi}{\partial x_k} \right) \right\rangle - \left\langle \frac{1}{2} \xi_j \xi_k \frac{\partial^2 \varphi^\xi}{\partial x_j \partial x_k} \right\rangle + O(a^3). \end{aligned} \quad (2.22)$$

The operator  $\mathcal{T}$  will be exploited in section 3.2 to derive a set of GLM flow equations that differs from the original derivation of the GLM flow equations given by Andrews & McIntyre (1978*a*).

## Chapter 3

# Derivation of 3D flow equations in GLM formulation

The derivation of the GLM equations of motion is based on the Reynolds-averaged equations of motion for an incompressible homogeneous fluid in an Eulerian formulation, which are given by the mass-conservation equation,

$$\frac{\partial u_j}{\partial x_j} = 0 , \quad (3.1)$$

and the momentum equations,

$$\frac{Du_i}{Dt} + \frac{1}{\rho} \frac{\partial p}{\partial x_i} - X_i = F_i . \quad (3.2)$$

The density  $\rho$  is assumed to be constant.  $\mathbf{X}$  is a function which allows for contributions that can be ascribed to viscosity and/or turbulence. In subsection 3.2.1 the function  $\mathbf{X}$  will be specified.  $\mathbf{F}$  represents large-scale driving forces for the mean flow in horizontal direction and equals the gravitational acceleration in vertical direction. These equations are completed with boundary conditions at the bottom and free surface, which are derived in section 3.3.

### 3.1 Original derivation of GLM equations

Andrews & McIntyre (1978*a*) derived the exact GLM equations of motion from the compressible Navier–Stokes equations. Nevertheless, the GLM theory can also be applied to incompressible flow problems. For an extensive derivation of the GLM flow equations reference is made to Andrews & McIntyre (1978*a*) and Dingemans (1997, § 2.10.6). Once again, the main steps in that derivation are repeated here.

The general idea is to consider the quantities in (3.1), (3.2) at their displaced positions, multiplying the momentum equations by  $\partial \Xi_j / \partial x_i$  and taking the mean of the resulting equations. Following Andrews & McIntyre (1978a) the mass conservation equation for a compressible fluid is considered,

$$\frac{D\rho}{Dt} + \rho \frac{\partial u_j}{\partial x_j} = 0. \quad (3.3)$$

In order to obtain a mass conservation equation of a similar form as (3.3) for the GLM flow, Eckart (1963) introduced the density

$$\tilde{\rho} = \rho^\xi J. \quad (3.4)$$

Using relation (2.17), which expresses the material derivative of  $J$  in terms of velocity gradients, the following relation for the material derivative of the modified density (3.4) is derived,

$$\begin{aligned} \bar{D}^L \tilde{\rho} &\equiv \bar{D}^L (\rho^\xi J) = J (D\rho/Dt)^\xi + \rho^\xi J \left\{ \left( \frac{\partial u_j}{\partial x_j} \right)^\xi - \frac{\partial \bar{u}_j^L}{\partial x_j} \right\} \\ &= J \left\{ \left( D\rho/Dt + \rho \frac{\partial u_j}{\partial x_j} \right)^\xi - \rho^\xi \frac{\partial \bar{u}_j^L}{\partial x_j} \right\}. \end{aligned} \quad (3.5)$$

Now the mass conservation equation in GLM framework follows directly by applying its Eulerian counterpart (3.3). Hence,

$$\bar{D}^L \tilde{\rho} + \tilde{\rho} \frac{\partial \bar{u}_j^L}{\partial x_j} = 0. \quad (3.6)$$

For an incompressible fluid the density  $\rho$  is constant. The mass conservation equation for GLM flow then reduces to

$$\frac{\partial \bar{u}_j^L}{\partial x_j} = -\bar{D}^L (\log J). \quad (3.7)$$

Obviously, the GLM velocity field  $\bar{\mathbf{u}}^L$  is no longer divergence-free in the presence of waves.

For the derivation of the momentum equations in a GLM framework the Eulerian counterpart (3.2) is considered in a disturbed position. Application of relation (2.18) to the resulting equation leads to

$$\bar{D}^L u_j^\xi + \frac{1}{\rho} \left( \frac{\partial p}{\partial x_j} \right)^\xi - X_j^\xi = F_j^\xi. \quad (3.8)$$



Multiplication of (3.8) by the matrix  $\partial \Xi_j / \partial x_i$  and application of the chainrule (2.11, first part) results in

$$\frac{\partial \Xi_j}{\partial x_i} \bar{D}^L u_j^\xi + \frac{1}{\rho} \frac{\partial p^\xi}{\partial x_j} - \frac{\partial \Xi_j}{\partial x_i} X_j^\xi = \frac{\partial \Xi_j}{\partial x_i} F_j^\xi. \quad (3.9)$$

The first term on the left-hand side of equation (3.9) can be rewritten by putting  $\partial \Xi_j / \partial x_i$  under the material derivative  $\bar{D}^L$  and using relation (2.2),

$$\begin{aligned} \frac{\partial \Xi_j}{\partial x_i} \bar{D}^L u_j^\xi &= \bar{D}^L \left( \frac{\partial \Xi_j}{\partial x_i} u_j^\xi \right) - u_j^\xi \bar{D}^L \left( \frac{\partial \Xi_j}{\partial x_i} \right) \\ &= \bar{D}^L u_i^\xi + \bar{D}^L \left( \frac{\partial \xi_j}{\partial x_i} u_j^\xi \right) - u_j^\xi \frac{\partial}{\partial x_i} (\bar{D}^L \Xi_j) + u_j^\xi \frac{\partial \Xi_j}{\partial x_k} \frac{\partial \bar{u}_k^L}{\partial x_i} \\ &= \bar{D}^L u_i^\xi + \bar{D}^L \left( \frac{\partial \xi_j}{\partial x_i} u_j^\xi \right) - u_j^\xi \frac{\partial u_j^\xi}{\partial x_i} + u_j^\xi \frac{\partial \bar{u}_j^L}{\partial x_i} + u_j^\xi \frac{\partial \xi_j}{\partial x_k} \frac{\partial \bar{u}_k^L}{\partial x_i}. \end{aligned} \quad (3.10)$$

An important quantity that will appear after averaging is the so-called pseudo-momentum per unit of mass  $\bar{P}^L$ , which is given by

$$\bar{P}_i^L = - \overline{\frac{\partial \xi_j}{\partial x_i} u_j^\xi} = - \frac{\partial \xi_j}{\partial x_i} u_j^\xi. \quad (3.11)$$

Substituting (3.10) into (3.9) and averaging the resulting equation finally leads to the GLM momentum equation, which was originally derived by Andrews & McIntyre (1978*a*, appendix B),

$$\begin{aligned} \bar{D}^L \bar{u}_i^L + \frac{1}{\rho} \frac{\partial \bar{p}^L}{\partial x_i} - \bar{X}_i^L - \bar{F}_i^L \\ = \left\langle \frac{\partial \xi_j}{\partial x_i} X_j^\xi \right\rangle + \left\langle \frac{\partial \xi_j}{\partial x_i} F_j^\xi \right\rangle + \bar{D}^L \bar{P}_i^L + \frac{\partial}{\partial x_i} \left( \frac{1}{2} (\bar{u}_j^\xi \bar{u}_j^\xi) \right) + \bar{P}_j^L \frac{\partial \bar{u}_j^L}{\partial x_i}. \end{aligned} \quad (3.12)$$

The averaged momentum equation (3.12), which is completely written in terms of Lagrangian quantities, contains the fluctuating quantities on the right-hand side. In order to quantify the wave-induced force on the mean motion the pseudomomentum seems an important quantity. For the physical and conceptual meaning of the pseudomomentum one is referred to e.g. Andrews & McIntyre (1978*b*), Craik (1982*b*) or Grimshaw (1984). In subsection 3.1.1 a brief description of this quantity will be given.

The GLM equations of motions are exact equations in the sense that no asymptotic analysis is required as long as viscous or turbulence effects are not

fully specified and left as general as in (3.12). As Andrews & McIntyre (1978a) mentioned throughout their derivation of the GLM equations, these equations also hold for finite amplitude waves. Incorporation of viscous effects unavoidably requires some asymptotic analysis. A correct formulation of the viscous part in terms of GLM quantities leads to lengthy expressions for the function  $\overline{X}_i^L$ . As to be expected the situation is worse for turbulent motion. Therefore, the derivation of the GLM equations by Andrews & McIntyre (1978a) is adapted in section 3.2.

### 3.1.1 The pseudomomentum

Like the Stokes drift  $\overline{\mathbf{u}}^S$  the pseudomomentum  $\overline{\mathbf{P}}^L$  is a wave property in the sense that it can be consistently computed from wave quantities alone. It turns out that  $\overline{\mathbf{P}}^L$  plays an essential role in mean-flow forcing if the GLM momentum equations (3.12) are considered. Andrews & McIntyre (1978a, corollary II) showed this by taking the curl of (3.12). The vortical part of  $\overline{\mathbf{u}}^L$  is being forced by the curl of  $\overline{\mathbf{P}}^L$ .

Andrews & McIntyre (1978b) interpreted the pseudomomentum in terms of wave action. They considered  $\overline{(\ )}$  to be an ensemble average and obtained the wave-action equation

$$\overline{\mathbf{D}}^L \mathbf{A} + \frac{1}{\bar{\rho}} \frac{\partial \mathbf{B}_j}{\partial x_j} = \mathcal{F}, \quad (3.13)$$

by scalar multiplication of the shifted momentum equation by  $\partial \xi_j / \partial \chi$ . In that analysis each field is assumed to depend on the ensemble label  $\chi$ . If the average operator  $\overline{(\ )}$  reflects time averaging instead of ensemble averaging, a similar approach as above will lead to a wave-action equation like (3.14). Its derivation is given in appendix A. The wave action  $\mathbf{A}$  is defined by

$$\mathbf{A} \equiv \overline{\frac{\partial \xi_j}{\partial t} u_j^\ell}, \quad (3.14)$$

and the non-advective flux of wave action  $\mathbf{B}$  by

$$\mathbf{B}_i \equiv \overline{p^\ell \frac{\partial \xi_j}{\partial t} K_{ji}}. \quad (3.15)$$

The right-hand side of (3.13) is given by

$$\mathcal{F} \equiv \overline{\frac{\partial \xi_j}{\partial t} X_j^\ell} + \overline{\frac{\partial \xi_j}{\partial t} F_j^\ell}, \quad (3.16)$$

a wave property representing the generation or dissipation of wave action. For conservative motion  $\mathcal{F} = 0$ .

The physical interpretation of  $\bar{\mathbf{P}}^L$  depends on the type of averaging. For cases in which the mean is taken as the spatial average in  $x$ -direction, Andrews & McIntyre (1978*b*, section 2) proved that the  $x$ -component of the pseudomomentum  $\bar{P}_1^L$  equals the generalized wave action (3.14) with  $\partial/\partial t$  replaced by  $-\partial/\partial x$ . They also considered the special situation of slowly varying waves, assuming that

$$\xi \propto \exp [i(\mathbf{k} \cdot \mathbf{x} - \omega t - \chi)] . \quad (3.17)$$

Here  $\mathbf{k}$  and  $\omega$  denote the wave number and wave frequency. Then, correct to  $O(a)$ ,

$$\frac{\partial \xi}{\partial \chi} = \omega^{-1} \frac{\partial \xi}{\partial t} = -k_i^{-1} \frac{\partial \xi}{\partial x_i} = \omega_0^{-1} \bar{D}^L \xi , \quad (3.18)$$

with  $\omega_0 = \omega - \mathbf{k} \cdot \bar{\mathbf{u}}^L$  the intrinsic wave frequency. Note that in the third term there is no sum over index  $i$ . Consequently, for slowly varying waves the pseudomomentum  $\bar{\mathbf{P}}^L$  and the wave action  $A$ , given by (3.14), are related as

$$\bar{\mathbf{P}}^L = \frac{\mathbf{k}}{\omega} A . \quad (3.19)$$

One should be aware that  $\bar{(\quad)}$  denotes the time-average operator. Substitution of (2.5) into (3.18) yields to leading order that  $\partial \xi / \partial t = (\omega / \omega_0) \mathbf{u}^\ell$ . Substitution of this result into (3.14), (3.19) leads to

$$\bar{\mathbf{P}}^L = \bar{\rho}^{-1} \frac{\mathbf{k}}{\omega_0} E , \quad (3.20)$$

with  $E = \bar{\rho} \overline{u_j^\ell u_j^\ell}$  the density of wave energy. In fact, to leading order the pseudomomentum per unit of mass reduces to Bretherton & Garrett's (1968) wave action density  $E/\omega_0$  times the wave number  $\mathbf{k}$  in case of slowly varying waves.

After having rewritten  $\mathbf{A}$  and  $\mathbf{B}$  Andrews & McIntyre (1978*b*, section 4) showed that the generalized wave-action equation (3.13) reduces, in the conservative case  $\mathcal{F} = 0$ , to

$$\bar{D}^L \left( \bar{\rho}^{-1} \frac{E}{\omega_0} \right) + \bar{\rho}^{-1} \nabla \cdot \left( \mathbf{c}_{g0} \frac{E}{\omega_0} \right) = 0 , \quad (3.21)$$

with  $\mathbf{c}_{g0}$  the intrinsic group velocity. After approximating  $\bar{\rho}$  by  $\rho$ ,  $\bar{\mathbf{u}}^L$  by  $\bar{\mathbf{u}}$  and defining  $\mathbf{c}_g = \mathbf{c}_{g0} + \bar{\mathbf{u}}$  as the absolute group velocity, (3.21) reduces to Bretherton & Garrett's (1968) approximate form of the wave-action conservation law

$$\frac{\partial}{\partial t} \left( \frac{E}{\omega_0} \right) + \nabla \cdot \left( \mathbf{c}_g \frac{E}{\omega_0} \right) = 0 . \quad (3.22)$$

Here use was made of the continuity equation (3.6). The foregoing analysis provides a simple and general derivation of Bretherton & Garrett's equation, which

does not depend on a variational principle. This was emphasized by McIntyre (1980a, p. 168).

Finally, the relation between pseudomomentum and Stokes drift is highlighted. Andrews & McIntyre (1978a, p. 632) proved that if the Eulerian mean velocity is of second order in wave-amplitude, the difference between the pseudomomentum  $\bar{\mathbf{P}}^L$  and the Stokes drift  $\bar{\mathbf{u}}^L$  is of third order if and only if the waves are irrotational. Weak currents that are wave-induced and occur in boundary-layer streaming problems have a second-order mean velocity. After an extensive derivation Uittenbogaard (1992) concluded that for a steady wave-induced displacement  $\boldsymbol{\xi}$  and uniform Eulerian mean flow the pseudomomentum equals the Stokes drift if the wave field is irrotational. This property of the pseudomomentum is important in the derivation of the CL vortex force, which appears as wave-induced driving force in the CL equations. As already mentioned in subsection 2.1.2 these equations can be derived from the GLM equations (see Leibovich 1980).

## 3.2 Alternative derivation of GLM equations

### 3.2.1 Inclusion of viscous and turbulent effects

Before proceeding with the alternative derivation of the GLM equations of motion, the function  $\mathbf{X}$  is specified in order to deal with viscosity or turbulence effects. When the flow is considered viscous and non-turbulent, the function  $\mathbf{X}$  can be expressed using the stress tensor,

$$X_i = \frac{1}{\rho} \frac{\partial \tau_{ij}}{\partial x_j} \quad , \quad \frac{\tau_{ij}}{\rho} = \nu \left( \frac{\partial u_i}{\partial x_j} + \frac{\partial u_j}{\partial x_i} \right) \quad , \quad (3.23)$$

where  $\nu$  equals the kinematic viscosity  $\nu_0$ . The same representation can be used in the turbulent regime as well. The shear stresses are directly related to the strain-rate tensor by using Boussinesq's hypothesis. A turbulence model has to be implemented to determine the eddy viscosity  $\nu$  and provide a proper closure of the model equations.

A review of turbulence models and their use in hydrodynamic problems can be found in Rodi (1980). As will be discussed in chapter 4, a one-equation  $k - \ell$  turbulence model has been implemented in the 1DV model to determine the distribution of the eddy viscosity over the entire depth. A two-equation  $k - \varepsilon$  turbulence model has been implemented in the 2DV model. This will be outlined in chapter 5.

### 3.2.2 Similarity to radiation stress concept

The GLM counterpart  $\overline{\mathbf{X}}^L$  can be expressed in terms of GLM quantities by averaging (3.23) at disturbed positions. Second-order partial derivatives of the velocities cause very lengthy expressions. Another option is to split the transformation of  $\mathbf{X}$  into two steps in which the shear stress tensor  $\tau_{ij}$  is maintained as dependent variable. However, evaluation at the disturbed positions still requires a lot of effort. In order to obtain lucid expressions for  $\overline{\mathbf{X}}^L$ , the equations are no longer evaluated at the actual positions, but at the fixed positions  $\mathbf{x}$ , which are related with mean particle positions. Andrews & McIntyre (1978a, § 8) used this approach as well to show the general limitations of the 'radiation stress' concept.

For the alternative derivation of the GLM equations of motion the momentum equations in Eulerian formulation are transformed by applying the definition of the total Stokes correction, which is defined as  $\varphi^S = \mathcal{T}(\varphi^\xi, \xi, \mathbf{x}, t)$  according to (2.21). The only difficulty concerns the treatment of the acceleration term. However, relation (2.22) can also be exploited to express  $Du_i/Dt$  entirely in terms of GLM quantities. Substitution of relation (2.18) into the expression that is obtained after expanding the acceleration term in Taylor series around  $\Xi$ , yields

$$\begin{aligned} \frac{Du_i}{Dt}(\mathbf{x}, t) = & \overline{D}^L u_i^\xi - \xi_j \frac{\partial}{\partial x_j} (\overline{D}^L u_i^\xi) \\ & + \xi_j \frac{\partial \xi_k}{\partial x_j} \frac{\partial}{\partial x_k} (\overline{D}^L u_i^\xi) + \frac{1}{2} \xi_j \xi_k \frac{\partial^2}{\partial x_j \partial x_k} (\overline{D}^L u_i^\xi) + O(a^3). \end{aligned} \quad (3.24)$$

Extra attention is paid to the second term on the right-hand side of relation (3.24), which upon using (2.5), can be written as

$$\xi_j \frac{\partial}{\partial x_j} (\overline{D}^L u_i^\xi) = \frac{\partial}{\partial x_j} (\overline{D}^L (\xi_j u_i^\xi)) - \frac{\partial}{\partial x_j} (u_j^\xi u_i^\xi) - \frac{\partial \xi_j}{\partial x_j} \overline{D}^L u_i^\xi. \quad (3.25)$$

Substitution of the definition for the Stokes correction and the acceleration term (3.24) into the momentum equation in Eulerian formulation results in a momentum equation in terms of Lagrangian quantities,

$$\begin{aligned} \overline{D}^L u_i^\xi + \frac{1}{\rho} \frac{\partial p^\xi}{\partial x_i} - \frac{1}{\rho} \frac{\partial \tau_{ij}^\xi}{\partial x_j} - F_i^\xi \\ = \frac{1}{\rho} \frac{\partial p^S}{\partial x_i} - \frac{1}{\rho} \frac{\partial \tau_{ij}^S}{\partial x_j} - F_i^S + \frac{\partial}{\partial x_j} (\overline{D}^L (\xi_j u_i^\xi)) - \frac{\partial}{\partial x_j} (u_j^\xi u_i^\xi) - \frac{\partial \xi_j}{\partial x_j} \overline{D}^L u_i^\xi \\ - \xi_j \frac{\partial \xi_k}{\partial x_j} \frac{\partial}{\partial x_k} (\overline{D}^L u_i^\xi) - \frac{1}{2} \xi_j \xi_k \frac{\partial^2}{\partial x_j \partial x_k} (\overline{D}^L u_i^\xi) + O(a^3). \end{aligned} \quad (3.26)$$

Note that the total velocity is considered in (3.26), so no averaging has been carried out so far. Furthermore, in the right-hand side the divergence of the disturbance displacement appears. As long as the Eulerian disturbance velocity field  $\mathbf{u}' = \mathbf{u} - \bar{\mathbf{u}}$  is divergence-free, i.e.  $\partial u'_j / \partial x_j = 0$ , the divergence of the disturbance displacement is of second order,

$$\frac{\partial \xi_j}{\partial x_j} = O(a^2). \quad (3.27)$$

For the GLM motion the following equation can be derived by averaging equation (3.26) and using (3.27),

$$\begin{aligned} \bar{D}^L \bar{u}_i^L + \frac{1}{\rho} \frac{\partial \bar{p}^L}{\partial x_i} - \frac{1}{\rho} \frac{\partial \bar{\tau}_{ij}^L}{\partial x_j} - \bar{F}_i^L \\ = \frac{1}{\rho} \frac{\partial \bar{p}^S}{\partial x_i} - \frac{1}{\rho} \frac{\partial \bar{\tau}_{ij}^S}{\partial x_j} - \bar{F}_i^S + \frac{\partial}{\partial x_j} \left( \bar{D}^L (\xi_j \bar{u}_i^L) \right) - \frac{\partial}{\partial x_j} (\bar{u}_j^L \bar{u}_i^L) \\ - \left\langle \xi_j \frac{\partial \xi_k}{\partial x_j} \right\rangle \frac{\partial}{\partial x_k} (\bar{D}^L \bar{u}_i^L) - \frac{1}{2} \overline{\xi_j \xi_k} \frac{\partial^2}{\partial x_j \partial x_k} (\bar{D}^L \bar{u}_i^L) + O(a^3). \end{aligned} \quad (3.28)$$

Subtracting equation (3.28) from (3.26) provides the momentum equations for the disturbed Lagrangian motion. Substitution of the fluctuating part of the total Stokes correction into the resulting equation then leads to

$$\bar{D}^L u_i^\ell + \frac{1}{\rho} \frac{\partial}{\partial x_i} \left( p^\ell - \xi_j \frac{\partial \bar{p}^L}{\partial x_j} \right) - \frac{\partial}{\partial x_j} \left( \tau_{ij}^\ell - \xi_k \frac{\partial \bar{\tau}_{ij}^L}{\partial x_k} \right) = \xi_j \frac{\partial}{\partial x_j} (\bar{D}^L \bar{u}_i^L) + O(a^2). \quad (3.29)$$

The wave-induced driving force for the mean motion  $\bar{S}_i^L$  can be written as,

$$\bar{S}_i^L = \frac{1}{\rho} \frac{\partial \bar{p}^S}{\partial x_i} - \frac{1}{\rho} \frac{\partial \bar{\tau}_{ij}^S}{\partial x_j} - \bar{F}_i^S + \bar{R}_i^L, \quad (3.30)$$

where

$$\bar{R}_i^L = -\frac{\partial r_{ij}}{\partial x_j} - \left\langle \xi_j \frac{\partial \xi_k}{\partial x_j} \right\rangle \frac{\partial}{\partial x_k} (\bar{D}^L \bar{u}_i^L) - \frac{1}{2} \overline{\xi_j \xi_k} \frac{\partial^2}{\partial x_j \partial x_k} (\bar{D}^L \bar{u}_i^L) + O(a^3), \quad (3.31)$$

and

$$r_{ij} = \overline{u_i^\ell u_j^\ell} - \bar{D}^L (\bar{u}_i^\ell \bar{u}_j^\ell). \quad (3.32)$$

The tensor  $r_{ij}$  is closely related to the radiation-stress tensors defined, amongst others, by Longuet-Higgins & Stewart (1960). Andrews & McIntyre (1978a, p.634), who derived a tensor which depends on the pressure part of the driving

force  $\bar{S}_i^L$  in (3.30), stated that in order to be called a radiation stress,  $r_{ij}$  must represent the sole effect of the waves on the mean flow. Although  $\bar{R}_i^L$  will be dominated by  $r_{ij}$ , for turbulent motion the effect of the Stokes correction of the shear stress  $\bar{\tau}_{ij}^S$  on the wave-induced driving force  $\bar{S}_i^L$  will be significant. In case of inviscid motion, Andrews and McIntyre concluded that  $r_{ij}$  represents the sole effect of the waves and thus can be called a radiation stress.

When viscous and/or turbulence effects are neglected, the GLM equations consisting of the mass conservation equation (3.7) and the momentum equation (3.28) are not exact, i.e. third and higher order wave-induced terms have been omitted. In contrast to the original GLM momentum equation (3.12) the alternative GLM equations have to be modified if more accurate solutions are required. Therefore, the alternative GLM equations do not seem to be convenient for inviscid flows. However, if the shear stresses have to be included, asymptotic analysis will lead to descriptions which are more lucid in the alternative approach. Moreover, the function  $X_i$  is written as a divergence of the shear stresses in order to obtain a system of first-order differential equations. Furthermore, in the form presented in this section the GLM equations have a similar form as the Eulerian equations. By evaluating the right-hand side of equations (3.7) and (3.28) the GLM quantities can be computed by existing numerical models which solve the Eulerian equations (3.1), (3.2).

For completeness expressions are given which relate the mean and fluctuating shear stresses  $\bar{\tau}_{ij}^L$  and  $\tau_{ij}^\ell$  to the GLM and disturbed Lagrangian velocities for arbitrary distributions of the eddy viscosity  $\nu$ . For the derivation of the GLM shear stresses in terms of GLM velocities, definition (3.23) is used. By definition the shear stresses have to be evaluated at disturbed positions. According to the chain-rule (2.14) the following expression for the shear stresses is obtained,

$$\frac{\tau_{ij}^\ell}{\rho} = \frac{\nu^\ell}{J} \left( K_{jk} \frac{\partial u_i^\ell}{\partial x_k} + K_{ik} \frac{\partial u_j^\ell}{\partial x_k} \right). \quad (3.33)$$

By averaging (3.33) and applying relation (2.12) a second-order approximation for the mean shear stresses is obtained,

$$\begin{aligned} \frac{\bar{\tau}_{ij}^L}{\rho} = & \frac{\bar{\nu}^L}{J} \left\{ \frac{\partial \bar{u}_i^L}{\partial x_j} - \left\langle \frac{\partial \xi_k}{\partial x_j} \frac{\partial u_i^\ell}{\partial x_k} \right\rangle + \left\langle \frac{\partial \xi_m}{\partial x_j} \frac{\partial \xi_k}{\partial x_m} \right\rangle \frac{\partial \bar{u}_i^L}{\partial x_k} \right. \\ & \left. + \frac{\partial \bar{u}_j^L}{\partial x_i} - \left\langle \frac{\partial \xi_k}{\partial x_i} \frac{\partial u_j^\ell}{\partial x_k} \right\rangle + \left\langle \frac{\partial \xi_m}{\partial x_i} \frac{\partial \xi_k}{\partial x_m} \right\rangle \frac{\partial \bar{u}_j^L}{\partial x_k} \right\} \\ & + \frac{1}{J} \left\{ \left\langle \nu^\ell \frac{\partial u_i^\ell}{\partial x_i} \right\rangle - \left\langle \nu^\ell \frac{\partial \xi_k}{\partial x_i} \right\rangle \frac{\partial \bar{u}_j^L}{\partial x_k} + \left\langle \nu^\ell \frac{\partial u_i^\ell}{\partial x_j} \right\rangle - \left\langle \nu^\ell \frac{\partial \xi_k}{\partial x_j} \right\rangle \frac{\partial \bar{u}_i^L}{\partial x_k} \right\} + O(a^3). \end{aligned} \quad (3.34)$$

Subtracting equation (3.34) from (3.33) results in

$$\begin{aligned} \frac{\tau_{ij}^\ell}{\rho} = & \frac{\bar{\nu}^L}{J} \left\{ \frac{\partial u_i^\ell}{\partial x_j} - \frac{\partial \xi_k}{\partial x_j} \frac{\partial \bar{u}_i^L}{\partial x_k} + \frac{\partial u_j^\ell}{\partial x_i} - \frac{\partial \xi_k}{\partial x_i} \frac{\partial \bar{u}_j^L}{\partial x_k} \right\} \\ & + \frac{\nu^\ell}{J} \left\{ \frac{\partial \bar{u}_j^L}{\partial x_i} + \frac{\partial \bar{u}_i^L}{\partial x_j} \right\} + O(a^2). \end{aligned} \quad (3.35)$$

As already mentioned in subsection 3.2.1 the GLM and disturbed eddy viscosity  $\bar{\nu}^L$  and  $\nu^\ell$  have to be determined by a turbulence model. Under specific circumstances the general expressions (3.34), (3.35) will reduce significantly. E.g. when the flow is viscous and non-turbulent,  $\bar{\nu}^L$  equals the kinematic viscosity and  $\nu^\ell = 0$ . Another advantage of considering the stresses  $\tau_{ij}$  as dependent variables is related to the formulation of boundary conditions. At the free-surface boundary these are often expressed in terms of normal and tangential stresses. Furthermore, near solid walls partial-slip conditions can be imposed. This means that shear stresses are prescribed in terms of the friction velocity at this wall. In the next section formulations of the boundary conditions in a GLM frame will be worked out. In that section no-slip conditions, implying that tangential velocities vanish at the wall, are considered instead of partial-slip conditions.

### 3.3 Boundary conditions

An important aspect in the GLM theory is the derivation of the boundary conditions, especially at the free surface. The bottom is assumed to be impermeable, resulting in a vanishing vertical velocity at the bottom. Furthermore, the bottom is a so-called no-slip boundary, causing the horizontal velocity to vanish. Therefore the following conditions hold at  $z = -h(\mathbf{x}_h)$ ,

$$u_i = 0. \quad (3.36)$$

Andrews & McIntyre (1978a) already mentioned that at an impermeable boundary the component of the GLM velocity normal to the bottom boundary equals the velocity of the boundary itself. Moreover, since a particle at the bottom will stick to its position the disturbance displacement as well as the GLM velocity will vanish at the bottom,

$$\xi_i = 0 \quad , \quad \bar{u}_i^L = 0. \quad (3.37)$$

At the free surface, which is unknown beforehand, two types of boundary conditions are imposed. The kinematic boundary condition states that the normal velocity component of the free surface equals the normal velocity component



of the flow,

$$\frac{D\zeta}{Dt} = w. \quad (3.38)$$

The dynamic boundary condition denotes a balance between the normal and shear stresses on both sides of the free surface,

$$n_i \tau_{ij} n_j - p = -p_F, \quad (3.39a)$$

$$n_i \tau_{ij} \tau_j = \tau_{Fr}, \quad (3.39b)$$

$$n_i \tau_{ij} s_j = \tau_{Fs}, \quad (3.39c)$$

where  $\mathbf{n}, \mathbf{r}, \mathbf{s}$  form an orthonormal set of vectors, such that the  $\mathbf{n}$ -direction is normal to the free surface and the  $\mathbf{r}$  and  $\mathbf{s}$ -directions are tangential to the free surface. In (4.5) surface tension effects are neglected. Moreover,  $p_F$  denotes the pressure and  $\tau_{Fr}, \tau_{Fs}$  equal the wind shear-stress components just above the free surface.

The free-surface boundary conditions are transformed into a GLM formulation without special effort, if the assumption that the mapping  $\mathbf{x} \rightarrow \mathbf{x} + \boldsymbol{\xi}(\mathbf{x}, t)$  is invertible, is accepted. Then, if the fluid particles are assumed to be in their disturbed positions  $\Xi$ , one can always split these positions as  $\Xi = \mathbf{x} + \boldsymbol{\xi}(\mathbf{x}, t)$ . Hence, if the free surface in Eulerian coordinates is given by

$$z - \zeta(\mathbf{x}_h, t) = 0, \quad (3.40)$$

with  $\zeta$  the deviation of the free surface from the still-water level  $z = 0$ , and a point on the free surface is considered to be in a disturbed position, then by splitting the disturbed position, one finds

$$z + \xi_3(\mathbf{x}_h, z, t) - \zeta(\mathbf{x}_h + \boldsymbol{\xi}_h(\mathbf{x}_h, z, t), t) = 0. \quad (3.41)$$

According to definitions (2.3) and (2.1) averaging relation (3.41) results in a description of the free surface in GLM coordinates,

$$z = \bar{\zeta}^L(\mathbf{x}_h, t). \quad (3.42)$$

This result is one of the strong points of the GLM formulation. The free surface varies slowly in time, in contrast to the corresponding rapidly varying level in the Eulerian setting. At the free surface the vertical displacement equals the oscillating part of the GLM free-surface elevation, i.e.

$$\eta(\mathbf{x}_h, z, t) \equiv \xi_3(\mathbf{x}_h, z, t) = \zeta^l(\mathbf{x}_h, t) \quad \text{for} \quad z = \bar{\zeta}^L(\mathbf{x}_h, t). \quad (3.43)$$

This approach was followed by Grimshaw (1981) as well. By applying relations (3.41) and (3.42) the following identity can be derived,

$$\begin{aligned} & \varphi^\xi(\mathbf{x}_h, \bar{\zeta}^L(\mathbf{x}_h, t), t) \\ & \equiv \varphi \left\{ \mathbf{x}_h + \boldsymbol{\xi}_h \left[ \mathbf{x}_h, \bar{\zeta}^L(\mathbf{x}_h, t), t \right], \bar{\zeta}^L(\mathbf{x}_h, t) + \eta \left[ \mathbf{x}_h, \bar{\zeta}^L(\mathbf{x}_h, t), t \right], t \right\} \\ & = \varphi \left\{ \mathbf{x}_h + \boldsymbol{\xi}_h \left[ \mathbf{x}_h, \bar{\zeta}^L(\mathbf{x}_h, t), t \right], \zeta \left( \mathbf{x}_h + \boldsymbol{\xi}_h \left[ \mathbf{x}_h, \bar{\zeta}^L(\mathbf{x}_h, t), t \right], t \right), t \right\} \end{aligned} \quad (3.44)$$

which implies that generalized Lagrangian arguments are attached to the free surface in a GLM formulation if Eulerian arguments are evaluated at the free surface in an Eulerian framework.

By applying relation (3.44) the kinematic boundary condition (3.38) is transformed directly to

$$\bar{D}^L \zeta^\xi = w^\xi \quad \text{for } z = \bar{\zeta}^L(\mathbf{x}_h, t). \quad (3.45)$$

If the pressure and the wind shear stresses just above the free surface are neglected, the dynamic boundary conditions (4.5) are equivalent to,

$$-pn_i + \tau_{ij}n_j = 0 \quad \text{for } z = \zeta(\mathbf{x}_h, t), \quad (3.46)$$

with  $n_\alpha = -\partial\zeta/\partial x_\alpha$ ,  $n_3 = 1$ . Application of relation (3.44) immediately yields

$$-p^\xi n_i^\xi + \tau_{ij}^\xi n_j^\xi = 0 \quad \text{for } z = \bar{\zeta}^L(\mathbf{x}_h, t), \quad (3.47)$$

with

$$n_\alpha^\xi = - \left( \frac{\partial \zeta^\xi}{\partial x_\alpha} - \frac{\partial \xi_\beta}{\partial x_\alpha} \frac{\partial \zeta^\xi}{\partial x_\beta} \right) + O(a^3), \quad n_3^\xi = 1. \quad (3.48)$$

After averaging, proper boundary conditions at the free surface  $z = \bar{\zeta}^L(\mathbf{x}, t)$  are obtained. For the GLM flow they read up to second order as,

$$\begin{aligned} \bar{\tau}_{\alpha 3}^L = & - \left\langle p^\ell \frac{\partial \zeta^\ell}{\partial x_\alpha} \right\rangle - \bar{p}^L \left( \frac{\partial \bar{\zeta}^L}{\partial x_\alpha} - \left\langle \frac{\partial \xi_\beta}{\partial x_\alpha} \frac{\partial \zeta^\ell}{\partial x_\beta} \right\rangle \right) \\ & + \left\langle \tau_{\alpha\beta}^\ell \frac{\partial \zeta^\ell}{\partial x_\beta} \right\rangle + \bar{\tau}_{\alpha\beta}^L \left( \frac{\partial \bar{\zeta}^L}{\partial x_\beta} - \left\langle \frac{\partial \xi_\gamma}{\partial x_\beta} \frac{\partial \zeta^\ell}{\partial x_\gamma} \right\rangle \right) + O(a^3), \end{aligned} \quad (3.49a)$$

$$-\bar{p}^L + \bar{\tau}_{33}^L = \left\langle \tau_{3\beta}^\ell \frac{\partial \zeta^\ell}{\partial x_\beta} \right\rangle + \bar{\tau}_{3\beta}^L \left( \frac{\partial \bar{\zeta}^L}{\partial x_\beta} - \left\langle \frac{\partial \xi_\gamma}{\partial x_\beta} \frac{\partial \zeta^\ell}{\partial x_\gamma} \right\rangle \right) + O(a^3), \quad (3.49b)$$

and for the fluctuating motion up to first order,

$$\tau_{\alpha 3}^{\ell} = -\bar{p}^L \frac{\partial \zeta^{\ell}}{\partial x_{\alpha}} + \bar{\tau}_{\alpha \beta}^L \frac{\partial \zeta^{\ell}}{\partial x_{\beta}} + O(a^2) , \quad (3.50a)$$

$$-p^{\ell} + \tau_{33}^{\ell} = \bar{\tau}_{3\beta}^L \frac{\partial \zeta^{\ell}}{\partial x_{\beta}} + O(a^2) . \quad (3.50b)$$

Equations (3.49) and (3.50) look extremely implicit. However, the terms in the right-hand side of equations (3.49) are of second order, assuming that the horizontal variation of the mean free-surface elevation,  $\partial \bar{\zeta}^L / \partial x_{\alpha}$ , is of second order. The present form of these boundary conditions is sufficient for implementation in the numerical models which are described in chapters 4 and 5.



# Chapter 4

## 1DV model

In this chapter a 1DV model is developed in order to obtain more insight in wave-induced changes in the mean horizontal velocity profiles. Application of a WKBJ perturbation series approach to the general three-dimensional GLM flow equations derived in chapter 3 results in a series of ordinary differential equations which have to be solved successively. The only dependent variable is the vertical coordinate, which explains the abbreviation 1DV. In this model the vertical distribution of current-affected orbital velocities is computed. Vice versa, the vertical profiles of the mean velocities, which are influenced by the wave motion, are determined.

In this chapter we restrict ourselves to the combined wave-current motion over a horizontal bottom. The viscous or turbulent initial current is driven by a vertically uniform body force. In case of a turbulent current, a one-equation  $k - \ell$  turbulence model has been implemented in order to obtain the vertical distribution of the eddy viscosity.

The WKBJ approach is valid for irregular waves with narrow-banded spectra. However, as already mentioned only regular nonbreaking waves are considered. The waves are taken to be dissipative in spatial direction. In the WKBJ approach this is represented by a complex-valued wave number, see subsection 4.2.1. In general, waves are allowed to propagate under an arbitrary angle with the current. Since the model has been validated with laboratory flume data, only the situations of waves following and opposing the current have been considered. An important aspect of this model is the omission of flow variations in the direction perpendicular to the flow direction. In order to make a valid comparison between the model results and the measurements, the latter have to be considered at locations where the lateral velocity component vanishes. Due to symmetry, the laboratory flume measurements in the flume center are considered.

Before proceeding to a description of the 1DV model by means of the WKBJ perturbation series approach the  $k - \ell$  turbulence model will be outlined in the

next section.

## 4.1 The $k - \ell$ turbulence model

In his review Rodi (1980) summed up a number of turbulence models with applications in hydrodynamics. One of these models is the so-called  $k - \ell$  turbulence model. Since  $k$  already denotes the wave number, the turbulence kinetic energy per unit of mass is denoted by  $q$ . The evolution equation of  $q$  has been modelled as,

$$\frac{Dq}{Dt} - \mathcal{P} + \mathcal{D} - \frac{\partial f_j}{\partial x_j} = 0, \quad (4.1)$$

with

$$\mathcal{P} \equiv \nu \left( \frac{\partial u_m}{\partial x_k} + \frac{\partial u_k}{\partial x_m} \right) \frac{\partial u_k}{\partial x_m}, \quad (4.2)$$

$$\mathcal{D} \equiv c_D \frac{q^{\frac{3}{2}}}{\ell}, \quad (4.3)$$

$$f_i \equiv \left( \nu_0 + \frac{\nu}{\sigma_k} \right) \frac{\partial q}{\partial x_i}. \quad (4.4)$$

Here  $\mathcal{P}, \mathcal{D}, f_i$  denote the turbulence kinetic energy production, dissipation and flux in  $x_i$ -direction respectively. Furthermore,  $\ell$  is the prescribed turbulence lengthscale and  $c_D$  and  $\sigma_k$  are empirical constants. The eddy viscosity is related to  $q$  and  $\ell$  by

$$\nu = c'_\mu q^{\frac{1}{2}} \ell, \quad (4.5)$$

with  $c'_\mu$  another constant.

Following Rodi (1980) the rate of change and the convective and diffusive transport of turbulent kinetic energy are neglected at the bottom. Consequently, the production of turbulence kinetic energy is in balance with the dissipation of turbulence kinetic energy at the bottom. This results in the following boundary condition,

$$q - \frac{\nu}{(c'_\mu)^2} \left[ \left( \frac{\partial u_k}{\partial x_m} + \frac{\partial u_m}{\partial x_k} \right) \frac{\partial u_k}{\partial x_m} \right]^{\frac{1}{2}} = 0. \quad (4.6)$$

The boundary condition for the turbulence kinetic energy is assumed to be a symmetry condition,

$$\frac{\partial q}{\partial \mathbf{n}} = \frac{\partial q}{\partial x_j} n_j = f_j n_j = 0. \quad (4.7)$$

In subsection 4.2.2 the implementation of this turbulence model in the 1DV-GLM model will be outlined in more detail. In that subsection an expression for the mixing-length will be given as well. Values for the empirical constants will be listed in subsection 4.3.

## 4.2 WKBJ perturbation series approach

As already pointed out above the equations for the mean and fluctuating motion show that the wave motion has an impact on the mean motion and vice versa. The equations describing both types of motion can be solved simultaneously but this would be very inefficient due to nonlinearities. Therefore, a WKBJ type expansion into perturbation series is carried out to distinguish between the slow modulation of the current profile in time and horizontal direction and the fast varying wave components.

### 4.2.1 Description of WKBJ method

The essence of the WKBJ-expansion method is to suppose that the amplitude function  $\Psi$  of a quantity  $\varphi(\mathbf{x}, t)$  varies much more slowly in time and horizontal space than the phase function  $S$ . We suppose that  $\varphi$  can be represented as

$$\varphi(\mathbf{x}, t) = \varphi(\mathbf{x}_h, z, t) = \Psi(\mathbf{x}_h, z, t) \exp(iS(\mathbf{x}_h, z, t)) , \quad (4.8)$$

with  $i = \sqrt{-1}$ . Let  $\delta$  be a small modulation parameter, indicating the slight relative variation in the mean motion on the scale of the characteristic wavelength. By introducing slowly varying temporal and horizontal spatial coordinates

$$\mathbf{X}_h = \delta \mathbf{x}_h , \quad T = \delta t , \quad (4.9)$$

the function  $\varphi$  in (4.8) can be rewritten as,

$$\varphi(\mathbf{x}, t) = \Psi(\mathbf{X}_h, z, T) \exp(iS(\mathbf{X}_h, z, T)/\delta) . \quad (4.10)$$

More details on the WKBJ expansion method can be found e.g. in Olver (1974, ch.6).

A variation on the WKBJ method is given by Chu & Mei (1970). They introduced the characteristic wave slope  $\varepsilon = ka$ , with  $k$  and  $a$  characteristic values of the wave number and the wave amplitude, as a nonlinearity parameter and assumed  $\varepsilon$  to be of the same order as the modulation parameter  $\delta$ . By expanding to both nonlinearity and rate of modulation the following expansions of WKBJ type were assumed

$$\varphi(\mathbf{x}, t) = \sum_{n=0}^{\infty} \varepsilon^n \sum_{m=-n}^{+n} \hat{\varphi}^{(n,m)}(\mathbf{X}_h, z, T) E^m , \quad (4.11)$$

where

$$E = \exp(i(k_\beta X_\beta - \omega T)/\varepsilon) . \quad (4.12)$$

with  $\hat{\varphi}^{(n,-m)}$  complex conjugates of the amplitude functions  $\hat{\varphi}^{(n,m)}$ . Chu & Mei (1970) expanded  $\mathbf{k}$  and  $\omega$  to nonlinearity as well, which is omitted here. The approach of expanding each quantity, except the wave number and frequency, into the perturbation series given by (4.11), has been used before by Lo & Mei (1985). Both approaches have been described by Liu & Dingemans (1989). Due to the presence of dissipation, the waves will decay, either in time or in the horizontal direction or both. Therefore  $\mathbf{k}$  and  $\omega$  can be complex. The imaginary part describes the wave attenuation. Since only periodic waves are considered,  $\omega$  is real. The wave number is allowed to be complex.

### 4.2.2 Application of WKBJ method to the GLM flow equations

Due to the introduction of slow horizontal and temporal coordinates, substitution of variables as perturbation series into the GLM equations of motion (3.7), (3.28) results in a cascade of problems at the different orders of approximation, which can be solved successively. These problems are systems of ordinary differential equations (ODEs) with the vertical coordinate  $z$  as the only independent variable. Except for the (0,0)-problem, these ODEs are linear. In the obtained hierarchical system the (0,0)-solution is the basic solution, describing a uniform steady current. Slow variations are described by the (1,0)-solution. The (1,1)-solution is the wave part, describing the motion of the waves according to the linear theory including the effect of mean velocity shear. Finally, the (2,0)-solution describes the second-order changes in the mean velocity profile due to the presence of waves.

The WKBJ-type expansion (4.11) considered here concerns the total flow, i.e. the sum of the mean ( $m = 0$ ) and fluctuating ( $m \neq 0$ ) part. Due to that clear distinction, in the following analysis reference is made to equations and conditions concerning the total motion for one moment and the mean and fluctuating parts of that motion for the other. Substitution of the expanded forms into the governing equations (3.7), (3.28) and boundary conditions at the bottom boundary (3.37) and at the free surface (3.45), (3.47), results in the following set of ODEs for each index  $(n, m)$ ,

$$imk_{\beta}\hat{u}_{\beta}^{(n,m)} + \frac{\partial\hat{w}^{(n,m)}}{\partial z} = \hat{F}^{(n,m)}, \quad (4.13)$$



$$\begin{aligned}
& -im\omega_0 \hat{u}_\alpha^{(n,m)} + \hat{w}^{(0,0)} \frac{\partial \hat{u}_\alpha^{(n,m)}}{\partial z} + imk_\alpha \frac{1}{\rho} \left( \hat{p}^{(n,m)} - \hat{\eta}^{(n,m)} \frac{\partial \hat{p}^{(0,0)}}{\partial z} \right) + \\
& - imk_\beta \frac{1}{\rho} \left( \hat{\tau}_{\alpha\beta}^{(n,m)} - \hat{\eta}^{(n,m)} \frac{\partial \hat{\tau}_{\alpha\beta}^{(0,0)}}{\partial z} \right) - \frac{1}{\rho} \frac{\partial}{\partial z} \left( \hat{\tau}_{\alpha 3}^{(n,m)} - \hat{\eta}^{(n,m)} \frac{\partial \hat{\tau}_{\alpha 3}^{(0,0)}}{\partial z} \right) = \hat{G}_\alpha^{(n,m)},
\end{aligned} \tag{4.14a}$$

$$\begin{aligned}
& -im\omega_0 \hat{w}^{(n,m)} + \hat{w}^{(0,0)} \frac{\partial \hat{w}^{(n,m)}}{\partial z} + \frac{1}{\rho} \frac{\partial}{\partial z} \left( \hat{p}^{(n,m)} - \hat{\eta}^{(n,m)} \frac{\partial \hat{p}^{(0,0)}}{\partial z} \right) + \\
& - imk_\beta \frac{1}{\rho} \left( \hat{\tau}_{3\beta}^{(n,m)} - \hat{\eta}^{(n,m)} \frac{\partial \hat{\tau}_{3\beta}^{(0,0)}}{\partial z} \right) - \frac{1}{\rho} \frac{\partial}{\partial z} \left( \hat{\tau}_{33}^{(n,m)} - \hat{\eta}^{(n,m)} \frac{\partial \hat{\tau}_{33}^{(0,0)}}{\partial z} \right) = \hat{G}_3^{(n,m)}.
\end{aligned} \tag{4.14b}$$

Here  $\omega_0 = \omega - k_\beta \hat{u}_\beta^{(0,0)}$  is the intrinsic frequency. The forcing functions  $\hat{F}^{(n,m)}$ ,  $\hat{G}_i^{(n,m)}$  are in terms of amplitude functions of order lower than  $n$ . This also holds for the right-hand sides  $\hat{D}_i^{(n,m)}$ ,  $\hat{H}_i^{(n,m)}$ ,  $\hat{K}_i^{(n,m)}$ ,  $\hat{L}^{(n,m)}$ ,  $\hat{T}_{ij}^{(n,m)}$  of the equations (4.17), (4.20), (4.22), (4.23). For convenience, expressions for these functions are given up to second order in appendix B. Since  $\overline{\eta(\mathbf{x}, t)} = 0$  due to restriction (2.3), the zeroth harmonic ( $m = 0$ ) of  $\eta$  equals zero

$$\hat{\eta}^{(n,0)} = 0 \quad \text{for } n \geq 0, \tag{4.15}$$

and because the still-water level is described by  $z = 0$  not only in an Eulerian framework but in a GLM formulation as well, the zeroth-order free-surface elevation vanishes,

$$\hat{\zeta}^{(0,0)} = 0. \tag{4.16}$$

The amplitude function of the disturbance displacement  $\xi$  satisfies upon (2.5),

$$-im\omega_0 \hat{\xi}_i^{(n,m)} + \hat{w}^{(0,0)} \frac{\partial \hat{\xi}_i^{(n,m)}}{\partial z} = \hat{u}_i^{(n,m)} + \hat{D}_i^{(n,m)} \quad \text{for } n \geq 1, m \neq 0, \tag{4.17}$$

with the bottom boundary condition

$$\hat{\xi}_i^{(n,m)} = 0 \quad \text{for } z = -h \quad \text{and } n \geq 1, m \neq 0. \tag{4.18}$$

Furthermore, at the free surface the vertical disturbance displacement equals the fluctuating part of the surface elevation, according to (3.43),

$$\hat{\eta}^{(n,m)} = \hat{\zeta}^{(n,m)} \quad \text{for } z = \bar{\zeta}^L \quad \text{and } n \geq 1, m \neq 0. \tag{4.19}$$

The boundary conditions at the bottom boundary are given by

$$\hat{u}_i^{(n,m)} = \hat{H}_i^{(n,m)}. \quad (4.20)$$

The boundary conditions at the free surface (3.45), (3.47) may be expanded into Taylor's series about  $z = 0$ ,

$$\sum_{k=0}^{\infty} \frac{(\bar{\zeta}^L)^k}{k!} \frac{\partial^k}{\partial z^k} \{w^\xi - \bar{D}^L \zeta^\xi\} = 0, \quad (4.21a)$$

$$\sum_{k=0}^{\infty} \frac{(\bar{\zeta}^L)^k}{k!} \frac{\partial^k}{\partial z^k} \{-p^\xi n_i^\xi + \tau_{ij}^\xi n_j^\xi\} = 0, \quad (4.21b)$$

resulting in the following conditions at  $z = 0$  for each index  $(n, m)$ ,

$$im\omega_0 \hat{\zeta}^{(n,m)} + \hat{w}^{(n,m)} = \hat{L}^{(n,m)}, \quad (4.22a)$$

$$\hat{\tau}_{\alpha 3}^{(n,m)} + \hat{\zeta}^{(n,m)} \left( imk_\alpha \hat{p}^{(0,0)} - imk_\beta \hat{\tau}_{\alpha\beta}^{(0,0)} \right) + \delta(m) \hat{\zeta}^{(n,0)} \frac{\partial \hat{\tau}_{\alpha 3}^{(0,0)}}{\partial z} = \hat{K}_\alpha^{(n,m)}, \quad (4.22b)$$

$$\begin{aligned} & -\hat{p}^{(n,m)} + \hat{\tau}_{33}^{(n,m)} - imk_\beta \hat{\zeta}^{(n,m)} \hat{\tau}_{3\beta}^{(0,0)} \\ & + \delta(m) \hat{\zeta}^{(n,0)} \left( -\frac{\partial \hat{p}^{(0,0)}}{\partial z} + \frac{\partial \hat{\tau}_{33}^{(0,0)}}{\partial z} \right) = \hat{K}_3^{(n,m)}, \end{aligned} \quad (4.22c)$$

where  $\delta(m) = 1$  for  $m = 0$ , otherwise  $\delta(m) = 0$ .

For the shear stresses the following expressions have been derived from relation (3.33),

$$\frac{\hat{\tau}_{\alpha\beta}^{(n,m)}}{\rho} = \hat{\nu}^{(0,0)} \left( imk_\beta \hat{u}_\alpha^{(n,m)} + imk_\alpha \hat{u}_\beta^{(n,m)} \right) + \hat{T}_{\alpha\beta}^{(n,m)}, \quad (4.23a)$$

$$\frac{\hat{\tau}_{\alpha 3}^{(n,m)}}{\rho} = \hat{\nu}^{(0,0)} \left( \frac{\partial \hat{u}_\alpha^{(n,m)}}{\partial z} + imk_\alpha \hat{w}^{(n,m)} \right) + \hat{T}_{\alpha 3}^{(n,m)}, \quad (4.23b)$$

$$\frac{\hat{\tau}_{33}^{(n,m)}}{\rho} = 2 \hat{\nu}^{(0,0)} \frac{\partial \hat{w}^{(n,m)}}{\partial z} + \hat{T}_{33}^{(n,m)}. \quad (4.23c)$$

The determination of the eddy viscosity  $\nu$  has been simplified. The distribution of  $\nu$  is assumed to consist only of the basic component  $\hat{\nu}^{(0,0)}$ . This means that  $\nu$  is independent of both time and wave motion and thus determined only by the steady current. Hence, after substituting the WKBJ-type expansions into equations (4.1)-(4.5) and corresponding boundary conditions (4.6), (4.7), which

describe the  $k - \ell$  turbulence model, only the resulting zeroth-order equations have to be considered. These nonlinear ODEs are given by

$$\hat{w}^{(0,0)} \frac{\partial \hat{q}^{(0,0)}}{\partial z} - \hat{\mathcal{P}}^{(0,0)} + \hat{\mathcal{D}}^{(0,0)} - \frac{\partial \hat{f}_3^{(0,0)}}{\partial z} = 0, \quad (4.24)$$

with

$$\hat{\mathcal{P}}^{(0,0)} \equiv \hat{\nu}^{(0,0)} \frac{\partial \hat{u}_\beta^{(0,0)}}{\partial z} \frac{\partial \hat{u}_\beta^{(0,0)}}{\partial z}, \quad (4.25a)$$

$$\hat{\mathcal{D}}^{(0,0)} \equiv c_D \frac{\left(\hat{q}^{(0,0)}\right)^{\frac{3}{2}}}{\ell}, \quad (4.25b)$$

$$\hat{f}_3^{(0,0)} \equiv \left( \nu_0 + \frac{\hat{\nu}^{(0,0)}}{\sigma_k} \right) \frac{\partial \hat{q}^{(0,0)}}{\partial z}, \quad (4.25c)$$

$$\hat{\nu}^{(0,0)} = c'_\mu \left(\hat{q}^{(0,0)}\right)^{\frac{1}{2}} \ell, \quad (4.25d)$$

and

$$\hat{q}^{(0,0)} = \frac{\hat{\nu}^{(0,0)}}{(c'_\mu)^2} \left( \frac{\partial \hat{u}_\beta^{(0,0)}}{\partial z} \frac{\partial \hat{u}_\beta^{(0,0)}}{\partial z} \right)^{\frac{1}{2}} \quad \text{for } z = -h, \quad (4.26a)$$

$$\hat{f}_3^{(0,0)} = 0 \quad \text{for } z = 0. \quad (4.26b)$$

In these equations the mixing length has to be specified. According to Rodi (1980) the turbulence length scale profile should be linear close to the bottom, i.e.  $\ell(s) = \kappa s$ , with  $s$  the distance to the bed and  $\kappa = 0.41$  the Von Kármán constant. The following choice for the mixing length  $\ell$ , which is prescribed as function of the flow geometry only,

$$\ell(z) = \kappa (z + h + z_0) \left( \frac{-z + z_a}{h + z_a} \right)^{\frac{1}{2}} \quad \text{for } -h \leq z \leq 0, \quad (4.27)$$

was proposed by Bakhmetev (1932) for  $z_a = 0$ . If  $z_a = 0$  the mixing length and thus the eddy viscosity would be zero at the free surface, causing near-singular behavior. The parameter  $z_a > 0$  is introduced to assure that the mixing length is strictly positive. The present form of the mixing length induces a parabolically shaped vertical profile for the eddy viscosity. The parameter  $z_0$  is related to the roughness of the bed and denotes the zero-intercept level of a log velocity profile for the situation without waves.

Now all ingredients have been delivered to describe the vertical distributions of both mean and oscillating motion. Since the flow equations involved cannot be solved analytically, numerical techniques must provide solutions for the problems at different orders. The numerical solution methods that have been used will be discussed in subsection 4.3.2.

### 4.3 Application to wave-current channel problems

#### 4.3.1 Simplification of present model

For model verification two test problems are considered, which both concern wave and current motion in a laboratory flume with a horizontal bed. Since a comparison with measurements in the center of the flume has been made and influences from the side walls are not taken into account, lateral variations (in horizontal direction perpendicular to the propagation direction, or  $y$ -direction) have been neglected. Furthermore, in all experiments the mass transport through all cross-sectional planes is assumed constant, or even zero if no initial current is present, in a local area around the measuring point.

In a GLM setting the mass transport in the direction along the flume per unit of channel width is given by

$$Q = \left\langle \int_{-h}^{\bar{\zeta}^L} u^{\epsilon} dz \right\rangle = \left\langle \int_{-h}^{\bar{\zeta}^L} \bar{u}^L + u^{\epsilon} dz \right\rangle = \int_{-h}^{\bar{\zeta}^L} \bar{u}^L dz, \quad (4.28)$$

(see e.g. Grimshaw, 1981, p.336). As in the pure Lagrangian setting, the lower and upper boundaries of the integral (4.28) are mean values. Consequently, the GLM of the depth-averaged velocity equals the depth-averaged GLM velocity. For the situation without waves (4.28) reduces to the discharge per unit of channel width and equals the Eulerian equivalent,

$$Q_E = \int_{-h}^{\bar{\zeta}} \bar{u} dz. \quad (4.29)$$

The discharges  $Q$  and  $Q_E$  are no longer equal in the presence of waves. As already mentioned in section 2.2, the Stokes drift is responsible. Here we restrict ourselves to closed wave tanks. Without an ambient current it is appropriate to choose  $Q$  equal to zero in a steady situation, see Grimshaw (1981, p.336) after Longuet-Higgins (1953, p. 571). In order to be consistent with the latter, the total mass transport should be equal to the mass transport observed without waves, if  $\bar{u}^L$  also contains a contribution from an ambient current. In fact, the latter equals the measured discharge through the recirculation pipes.

A major advantage of the GLM method is outlined here. If waves are superposed on a current with a discharge  $Q$ , the total mass transport still equals  $Q$  and is given by (4.28). In an Eulerian description of the mean flow two parts of the mass flux are being distinguished, i.e.  $Q_E$  and a wave-induced mass flux. The latter is related to the Stokes drift. In numerous papers these two components have been given, see e.g. Mei (1989, section 10.2) and Battjes (1988, section 5).

Since the measurements have been carried out in only one cross-section of the flume and we are interested only in the local solution of flow field, information about the free-surface elevation has to be specified. Therefore the mean free surface elevation has been chosen equal to zero,  $\hat{\zeta}^{(1,0)} = \hat{\zeta}^{(2,0)} = 0$  and the amplitude function of the fluctuating part of the free surface is set equal to the measured wave amplitude,  $\hat{\zeta}^{(1,1)} = a$ .

The zeroth-order solution is supposed to be steady and uniform in horizontal direction, thus only dependent of the vertical coordinate  $z$ . According to (3.2) the turbulent shear current is driven by a body force  $\mathbf{F}$ . This vertically uniform body force is directly expressed in terms of the bed shear stress  $\hat{\tau}_b^{(0,0)}$  for the uniform current, because the horizontal momentum equation (4.14a) yields a linear shear stress distribution in the current direction, or  $x$ -direction,

$$\hat{\tau}_{13}^{(0,0)} = \hat{\tau}_b^{(0,0)} \left( \frac{-z}{h} \right). \quad (4.30)$$

The constant  $\hat{\tau}_b^{(0,0)}$  is chosen such that for a given mass transport  $\hat{Q}^{(0,0)}$  per unit of channel width, the horizontal zeroth-order velocity  $\hat{u}^{(0,0)}$  satisfies,

$$\hat{Q}^{(0,0)} = \int_{-h}^0 \hat{u}^{(0,0)} dz. \quad (4.31)$$

The hydrostatic pressure distribution is found from the vertical momentum equation,

$$\hat{p}^{(0,0)} = -\rho g z. \quad (4.32)$$

The nonlinear equations (4.24)–(4.26) together with the relations (4.30)–(4.32) are solved numerically.

Since at first order ( $n = 1, -1 \leq m \leq 1$ ) all forcing terms are zero, the solution for the mean motion at first order is completely determined by the mean free surface elevation  $\hat{\zeta}^{(1,0)}$  in a sense that the amplitude variables can be written as,

$$\hat{\varphi}^{(1,0)}(X, T, z) = \Phi(z) \hat{\zeta}^{(1,0)}(X, T). \quad (4.33)$$

For an arbitrary value of  $\hat{\zeta}^{(1,0)}$  the shape function  $\Phi(z)$  of each variable  $\hat{\varphi}^{(1,0)}$  is determined numerically. Although  $\hat{\zeta}^{(1,0)} = 0$  and thus  $\hat{\varphi}^{(1,0)} = 0$ , their temporal and spatial derivatives in horizontal direction are not necessarily equal to zero.

The first-order first-harmonic solution represents the carrier wave solution. This problem is solved most easily by introducing related variables

$$\check{\varphi}^{(1,1)} = \hat{\varphi}^{(1,1)} - \hat{\eta}^{(1,1)} \frac{\partial \hat{\varphi}^{(1,1)}}{\partial z}, \quad (4.34)$$

which up to first order can be seen as the Eulerian counterpart of the amplitude function of the generalized Lagrangian variable  $\hat{\varphi}^{(1,1)}$ . For laminar flow ( $\nu =$

$\nu_0$ ) the equations for the carrier wave reduce to the so-called Orr–Sommerfeld equation, which is often used in the study of hydrodynamic stability, see e.g. Drazin & Reid (1981). The derivation of the Orr–Sommerfeld equation in terms of Eulerian type quantities  $\tilde{\varphi}^{(1,1)}$  is similar as the original derivation in a true Eulerian setting. This can be found e.g. in Drazin & Reid (1981, chapter 25) and Thomas & Klopman (1997, section 7.2) and will not be repeated here. The carrier wave solution will show thin wave boundary layers near the bottom and the free surface. Outside the boundary layers the velocities will be close to the velocities obtained with the potential-flow theory. For a given frequency  $\omega$ , the unknown complex-valued wave number  $k$  ( $\mathbf{k} = (k, 0)^T$ ) is determined from the boundary conditions at the free surface. This is described in more detail in subsection 4.3.2.

Our main interest concerns the second-order mean motion ( $n = 2, m = 0$ ). The forcing terms are no longer equal to zero, but contain temporal and (horizontal) spatial derivatives of first-order zeroth-harmonic variables ( $n = 1, m = 0$ ) as well as correlations of wave-related variables ( $n = 1, m = \pm 1$ ). For second and higher order problems ( $n \geq 2$ ) the homogeneous problem is similar to the zeroth and first-order problem. Because the forcing terms are nonzero, a constraint must be imposed to avoid secular behavior of the particular solution. For  $m = 0$  this so-called solvability condition reads as

$$\int_{-h}^0 \hat{F}^{(2,0)} dz = \hat{L}^{(2,0)} - \hat{H}_3^{(2,0)}. \quad (4.35)$$

By substituting (B.5a), (B.5d), (B.5e) into (4.35) and writing  $\hat{u}^{(1,0)} = \hat{U}^{(1)} \hat{\zeta}^{(1,0)}$ , the solvability condition reduces to a relation between the temporal and horizontal derivatives of the first-order mean surface elevation,

$$\begin{aligned} \frac{\partial \hat{\zeta}^{(1,0)}}{\partial T} + \hat{u}^{(0,0)} \Big|_{(z=0)} \frac{\partial \hat{\zeta}^{(1,0)}}{\partial X} + \left( \int_{-h}^0 \hat{U}^{(1)} dz \right) \frac{\partial \hat{\zeta}^{(1,0)}}{\partial X} = \\ = i \left( k - \bar{k} \right) \int_{-h}^0 \tilde{u}^{(2,0)} dz + \tilde{w}^{(2,0)} \Big|_{(z=0)}. \end{aligned} \quad (4.36)$$

Here  $\tilde{u}^{(2,0)}$  and  $\tilde{w}^{(2,0)}$  denote the second-order approximation of the Stokes correction, given in appendix B by relation (B.4). By writing each temporal or spatial gradient of a first-order dependent variable as a product of its shape function and the gradient of the first-order mean surface elevation, as in (4.33), and substituting (4.36) to remove the temporal gradients from the expressions for the forcing functions, an extra dependent variable  $\partial \hat{\zeta}^{(1,0)} / \partial X_\alpha$  is introduced. Therefore, an additional constraint has to be imposed. As for the situation of currents without waves, the gradient of the mean free-surface elevation is chosen such that relation (4.28) still holds at second order. Because the mean free surface elevation

is assumed to be zero, this results in

$$\int_{-h}^0 \hat{u}^{(2,0)} dz = 0. \quad (4.37)$$

After evaluation of the driving force, the linear non-homogeneous system of ODEs is solved numerically.

### 4.3.2 Numerical solution method

In the previous subsection all ingredients have been delivered that describe the vertical distributions of both mean and oscillating motion. Since these equations cannot be solved analytically, numerical techniques must provide solutions for the problems at different orders.

Due to the existence of boundary layers near the bottom and the free surface, grid refinement (in vertical direction) has been carried out in these regions. This refinement is based on a one-dimensional two-sided stretching function as proposed by Vinokur (1983, section 3). All systems of equations at different orders are solved on the same grid. As a consequence results obtained at one order of approximation can be used in the solution method at a higher order without requiring interpolation techniques.

The nonlinear system of ODEs describing the (0,0)-problem, has been solved iteratively using a relaxation method described in Press et al. (1992, section 17.3). It is primarily based on ideas, which amongst others can be found in Keller (1968, chapter 3). The system of ODEs, which in general form can be written as  $df/dz = g(f)$ , is replaced by a system of finite difference equations on a grid  $-h = z_1 < z_2 < \dots < z_M = 0$ ,

$$f_k - f_{k-1} - (z_k - z_{k-1}) g\left(\frac{1}{2}(f_k + f_{k-1})\right) = 0, \quad (4.38)$$

so that  $f_k \approx f(z_k)$ . This set is completed with boundary conditions for  $f_1$  and  $f_M$ . Since  $g$  is a nonlinear function, Newton's iteration method is applied to solve (4.38). Each iteration a system of linear equations,  $B\mathbf{f} = \mathbf{b}$  with  $\mathbf{f} \approx (f_1, \dots, f_M)^T$  and  $B$  a bi-diagonal block matrix, has to be solved. The form of this matrix is given in figure 17.3.1 in Press et al. (1992). The solution  $\mathbf{f}$  can simply be obtained by means of Gaussian elimination.

For higher order problems ( $n \geq 1$ ) the numerical solution method is simpler, because the problems to be solved are linear. For the (1,1)-problem not only the quantities  $\hat{u}^{(1,1)}$ ,  $\hat{w}^{(1,1)}$ ,  $\hat{p}^{(1,1)}$  and  $\hat{\tau}_{13}^{(1,1)}$  have to be determined, but the wave number  $k$  is unknown as well. The former four unknowns satisfy four ODEs and five boundary conditions, two at the bottom given by (4.20) and three at the free surface given by (4.22). The extra boundary condition determines the

value of  $k$  for a given wave frequency  $\omega$ . The wave number is obtained by Newton iteration. More specifically, each iteration the four ODEs with the four boundary conditions (4.20), (4.22b,c) are solved, using the wave number  $k$  at the previous iteration level. A Newton step is applied to the kinematic boundary condition at the free surface (4.22a) in order to update  $k$ .

The set of linear ODEs is solved with the trapezoidal rule, which is of second-order accuracy. The resulting system of linear equations consists of a bi-diagonal block matrix once again. Notice that this matrix is different than the block matrix  $B$  obtained for the (0,0)-problem. This system is also solved by applying Gaussian elimination. For the solution of the (2,0)-problem the wave number is not a dependent variable. Now  $\hat{Q}^{(2,0)} = 0$  is an extra restriction in order to satisfy (4.37). Apart from that the numerical solution method is the same as for the (1,1)-problem.

## 4.4 Comparison with observations

Two different types of laboratory wave current channel measurements have been used to verify the present model. Firstly, the drift flow generated by a uniform regular wave train has been studied and secondly, the combined motion of a regular wave field imposed on an ambient current has been considered.

### 4.4.1 Mass transport in water waves

For the situation of no ambient current both the analytical conduction solution presented by Longuet-Higgins (1953) for the horizontal drift, or mass transport for waves, in a viscous fluid, and experimental observations of the drift velocities in a closed wave channel by Mei et al. (1972) are taken as a reference. Although these references are based on pure Lagrangian averaging, i.e. averaging by following a single fluid particle, it is nevertheless legitimate to compare the results with the GLM results obtained by the present model. This is due to the fact that the present model provides GLM velocities which are of second order, and if there is no initial current, the difference between a pure Lagrangian mean velocity and a GLM velocity can be proven to be of third order.

Note that the 1DV model computes the solution over the whole depth at once, whereas Longuet-Higgins used a three layer approach. He first solved the equations for the mean flow in the boundary layers in order to obtain boundary conditions for the interior problem. The solution for a progressive wave was referred to as 'conduction solution' (p. 571) and given by

$$\bar{u}^L = \frac{\omega a^2 \cotanh(kh)}{h^2} (z+h) \left[ \frac{3}{4} \left( \frac{z}{h} - 1 \right) + \frac{1}{2} k^2 h^2 \left( \frac{3z}{h} + 1 \right) \right]$$



$$+ \frac{\omega a^2 k}{2 \sinh^2(kh)} \left[ \frac{9}{4} \left( \frac{z}{h} \right)^2 - \frac{3}{4} + \cosh(2k(z+h)) \right]. \quad (4.39)$$

Furthermore, Longuet-Higgins (1953) neglected the effect of wave decay. In the present model this effect is taken into account. The wave decay, which is assumed to be spatial and not temporal, is ruled by the imaginary part of the wave number  $k$ .

Mei et al. (1972) generated a regular wave field in a closed 12 m long, 0.76 m wide tank with a smooth bed. The still-water depth  $h = 13$  cm. For waves in a closed channel a constant horizontal pressure gradient is imposed which is chosen to yield zero mass transport  $Q = 0 \text{ m}^3 \text{ s}^{-1}$ . Two sets of measurements from a station 3.5 m from the wave maker are considered, viz.  $a = 1.1$  cm,  $T = 0.81$  s ( $\text{Re}(kh) = 1.02$ ) and  $a = 0.76$  cm,  $T = 0.56$  s ( $\text{Re}(kh) = 1.81$ ).

For these boundary layer streaming problems the eddy-viscosity distribution has been assumed constant over the vertical and chosen equal to the kinematic viscosity,  $\nu = \nu_0 = 10^{-6} \text{ m}^2 \text{ s}^{-1}$ . This means that the second-order GLM velocity should be equal to Longuet-Higgins' conduction solution, if dissipative effects such as wave decay would have been neglected. In figure 4.1 the results from our model are compared with the conduction solution and the observations by Mei et al. (1972, figures 4.1a and 4.1l in their report). The differences with the conduction solution are too small to be seen in this figure.

In view of the agreement between the computed solution and the conduction solution, the conclusion is justified that the wave decay has little influence when the flow is viscous and non-turbulent. Craik (1982a, p.201) remarked that significant departures from the conduction solution can be expected when the magnitude of the imaginary part of  $k$  becomes comparable with (or greater than)  $h^{-1}$ . However, in both test problems this is not the case, since  $\text{Im}(kh) = O(10^{-3})$ .

Comparison with the experimental results shows good agreement for the first case ( $\text{Re}(kh) = 1.02$ ). However, the velocity gradient in the upper part of the water column is clearly overpredicted for the second case. Mei et al. (1972, p.152) remarked that for  $0.9 \leq \text{Re}(kh) \leq 1.5$  the measurements agreed with the conduction solution. The model results confirm this statement. Furthermore, Longuet-Higgins (1953, p.580) pointed out that observations in deep water do not seem to be greatly different from those predicted by irrotational wave theory. The latter theory provides a velocity gradient at the free surface being half of the one predicted by the conduction solution (4.39), see e.g. Longuet-Higgins (1953, p.536). This can be seen in figure 4.1b.

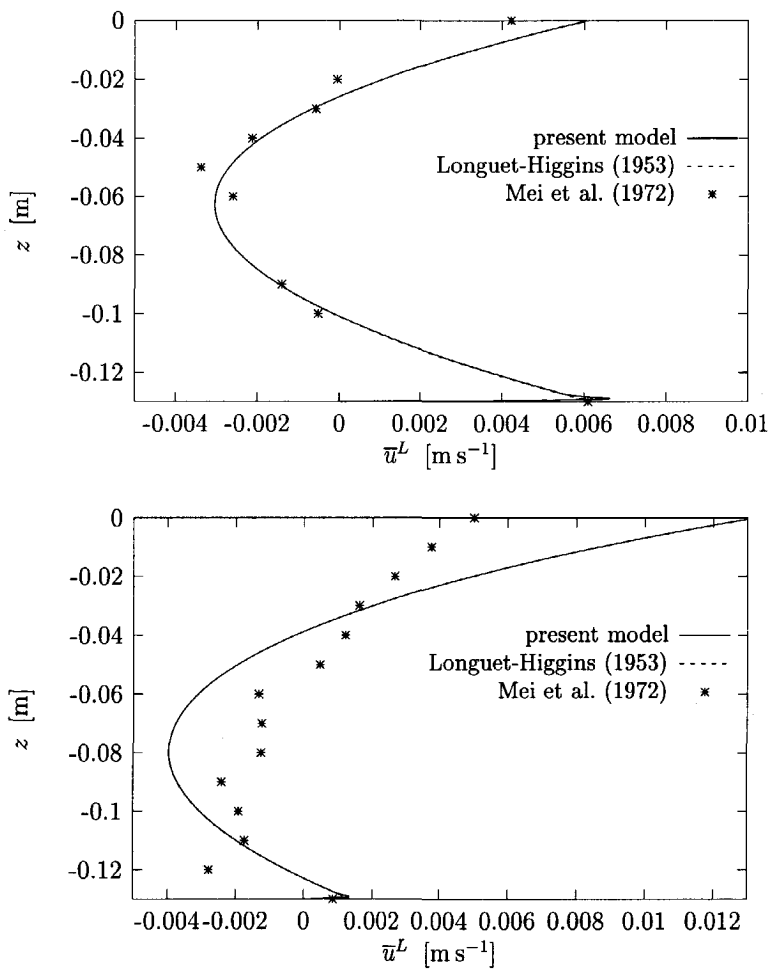


Figure 4.1: Second-order drift velocities: (a)  $\text{Re}(kh) = 1.02$ , (b)  $\text{Re}(kh) = 1.81$ .

### 4.4.2 Combined wave-current motion

In this subsection wave-induced changes in an initial turbulent current are considered. Model results are compared with measurements, obtained by Klopman (1994), in a wave-current laboratory flume. The channel is 45 m long and 1 m wide. The bed was roughened using coarse sand, with a grain size of about 2 mm. Klopman (1994) used Laser Doppler velocimetry (LDV) flow meters to measure horizontal and vertical velocities of the total turbulent flow at a measuring section 22.5 m away from the wave boards. Since the bed is neither smooth nor rough, the flow is in the intermediate turbulent regime. A flow-circulation circuit provided a turbulent current with a constant discharge  $Q = 0.08 \text{ m}^3 \text{ s}^{-1}$  in a flume with a still-water depth  $h = 0.50 \text{ m}$ . A monochromatic wave field with a wave period  $T = 1.44 \text{ s}$  and wave amplitude  $a = 0.060 \text{ m}$  is imposed on the current. The following values for the empirical constants in the turbulent model have been used,  $\sigma_k = 1$ ,  $C_D = 0.156$ ,  $C'_\mu = 0.54$ . These values are normally used for these type of problems, see Rodi (1980, section 2.5). From the measurements the bed roughness parameter  $z_0 = 0.037 \text{ mm}$ , confirming the intermediate turbulence regime. The choice  $z_a = 1 \text{ mm}$  results in a length scale  $\ell_0 = 0.01 \text{ m}$  at the still-water level.

#### Uniform current: (0,0)-solution

The 1DV-model provides a (0,0)-solution for which the initial current profile is almost logarithmic. Only in the upper part the current profile deviates from a log-profile. In figure 4.2 the model results are compared with Klopman's (1994, test serie SP) velocity profile for the initial current. In that same figure the corresponding computed eddy-viscosity profile is given. Due to the choice of the mixing length (4.27) the profile is almost parabolic. For this run the 1DV model predicts a bottom shear stress  $\hat{\tau}_b^{(0,0)} = 5.4 \cdot 10^{-2} \text{ Nm}^{-2}$ .

#### Carrier wave: (1,1)-solution

The solution for the first order first harmonic problem consists of complex-valued amplitude functions. For the situation of a following current both real and imaginary parts of the amplitude functions of the horizontal and vertical velocities,  $\tilde{u}^{(1,1)}$  and  $\tilde{w}^{(1,1)}$ , the pressure  $\tilde{p}^{(1,1)}$  and the shear stress  $\tilde{\tau}_{13}^{(1,1)}$  are given in figure 4.3 – 4.6. Outside the predicted boundary layers near the bottom and the free surface these profiles are similar to those obtained with potential wave theory. In the boundary layers the imaginary parts of  $\tilde{u}^{(1,1)}$  and  $\tilde{\tau}_{13}^{(1,1)}$  deviate significantly from the characteristic values in the interior. The boundary layer thickness is determined by the magnitude of the eddy viscosity. Since  $\hat{\nu}^{(0,0)}$  is assumed to be valid for the wave motion as well, a boundary layer thickness  $\delta_w$  of a few centimeter may be expected,  $\delta_w = O(2\nu/\omega)$ ,  $\nu = O(10^{-4}) \text{ m}^2 \text{ s}^{-1}$ .

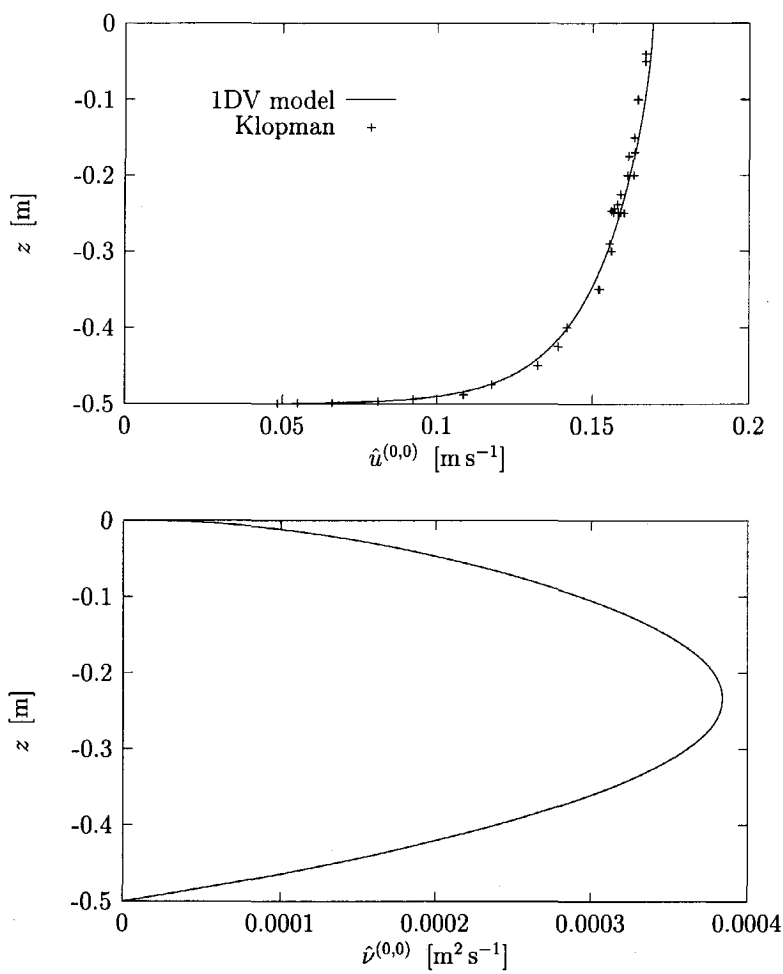


Figure 4.2: (0,0)-solution: (a) mean horizontal velocity, (b) eddy viscosity.

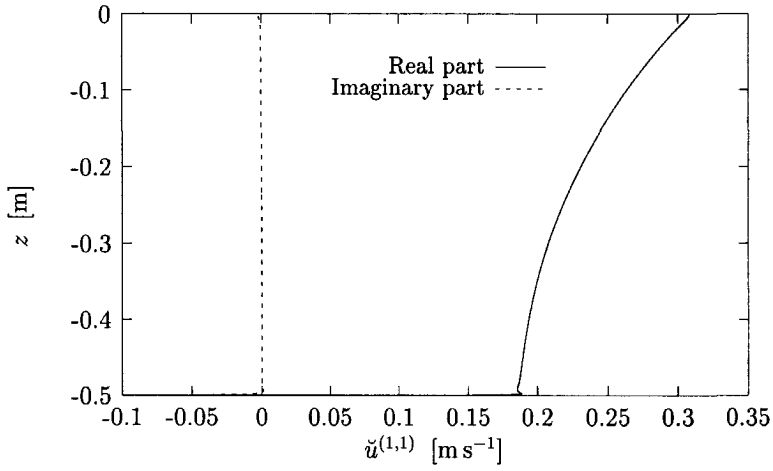


Figure 4.3: (1,1)-solution for following waves: horizontal velocity.

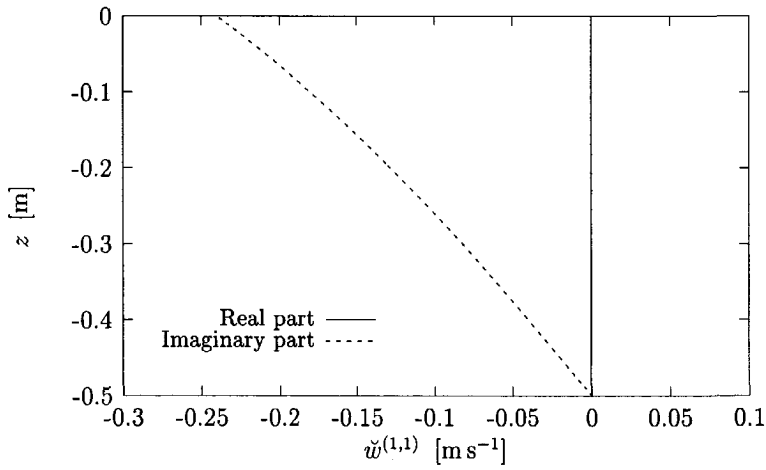


Figure 4.4: (1,1)-solution for following waves: vertical velocity.

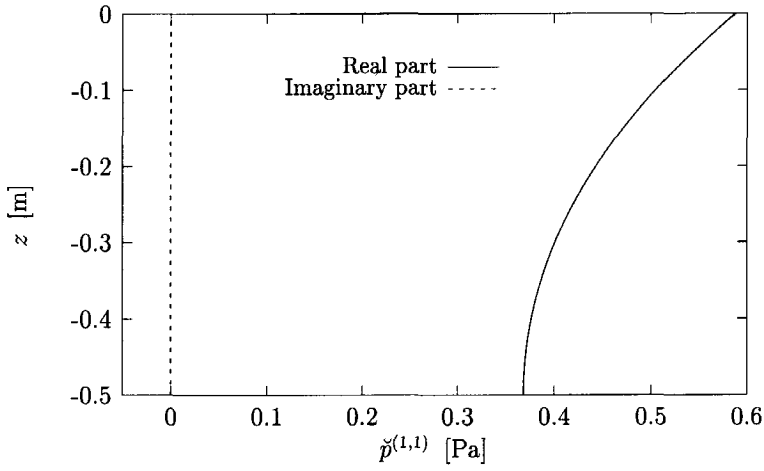


Figure 4.5: (1, 1)-solution for following waves: pressure.

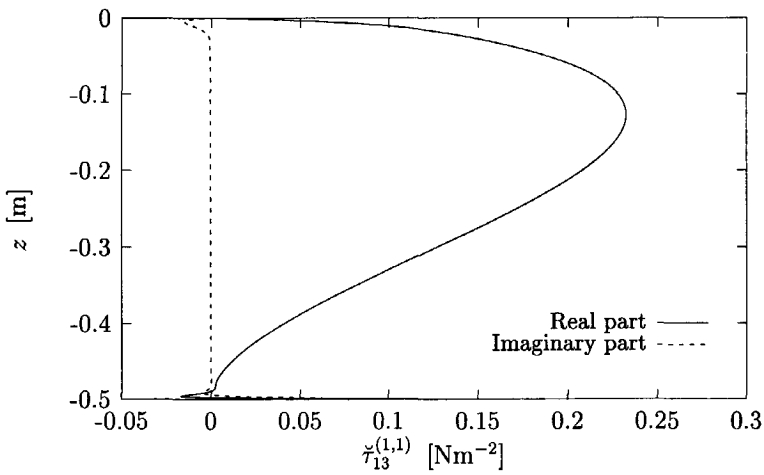


Figure 4.6: (1, 1)-solution for following waves: shear stress.

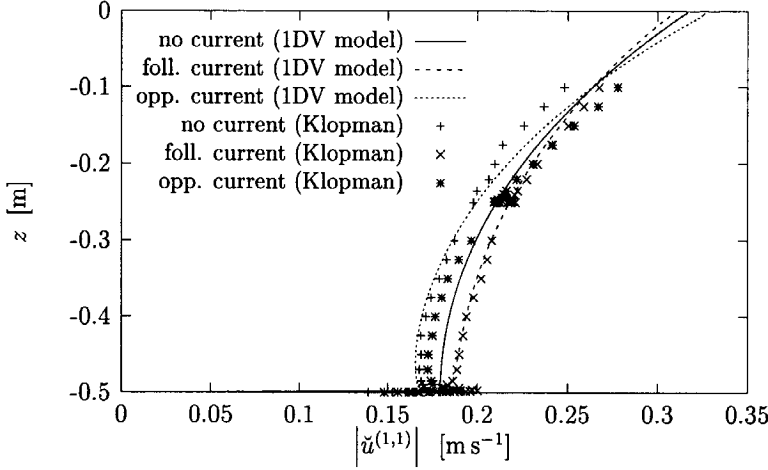


Figure 4.7: GLM results (present model) and experimental results (Klopman, 1994) first-order Eulerian horizontal velocity amplitude profile.

The effect of wave decay has been taken into account. The predicted complex-valued wave number equals  $k = 2.11 + i1.74 \cdot 10^{-3} \text{ rad s}^{-1}$ . Unfortunately, the wave-decay was not reported by Klopman. Hence, validation is not possible. For the situation of waves without an initial current the eddy-viscosity profile is assumed to be constant over depth,  $\nu = 10^{-5} \text{ m}^2 \text{ s}^{-1}$ . This constant is chosen larger than the kinematic viscosity because of the intermediate bed roughness. For this situation and the situation of an opposing current the computed wave number is  $k = 2.35 + i1.66 \cdot 10^{-3} \text{ rad s}^{-1}$  resp.  $k = 2.69 + i4.04 \cdot 10^{-3} \text{ rad s}^{-1}$ . The fact that the wave attenuation is significantly larger for an adverse current agrees with conclusions on wave decay by Kemp & Simons (1983) and Simons et al. (1988) who compared all three situations in their experimental research on wave decay.

In figure 4.7 the absolute value of the complex-valued amplitude functions of the first harmonic Eulerian horizontal velocity  $\tilde{u}^{(1,1)}$  are given for the cases of no current, a following current and an opposing current and they are compared with the values measured by Klopman (1994) in the test series WMN, CMP resp. CMN. The interaction with a following current results in a decrease of the vertical gradient of the amplitude of the horizontal velocity component, while the interaction with an opposing current is shown to increase this vertical gradient. This is in accordance with the change of magnitude of the wave number, which increases for waves opposing the current and decreases in the opposite situation.

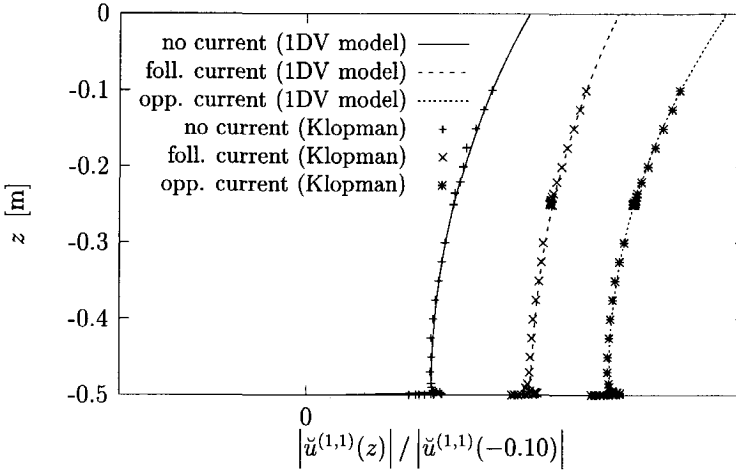


Figure 4.8: GLM results (present model) and experimental results (Klopman, 1994) first-order Eulerian horizontal velocity amplitude profile normalized to their values at  $z = -10$  cm.

The model results do not correspond exactly with the measurements, although a qualitative agreement can be observed. In the wave tank the measured signal includes the reflected wave. In the 1DV model reflection is not taken into account and the incoming wave height and wave period are taken as input parameters. Klopman (1994, table 1) noticed that the reflection coefficient was about 7 à 8 % or less for all tests. By giving the profiles of the normalized velocities  $|\tilde{u}^{(1,1)}(z)| / |\tilde{u}^{(1,1)}(\Delta)|$  with  $\Delta = -10$  cm in figure 4.8 the form of the profiles of the measured and computed velocity amplitudes are shown to coincide.

#### Changes in mean velocity profile: (2,0)-solution

Determination of the second-order mean motion requires evaluation of the wave-induced driving forces. The wave-induced stress  $\langle u^\ell w^\ell \rangle$  and the Stokes correction of the shear stress  $\bar{\tau}_{13}^S$  are the main contributions in the driving force for the horizontal mean motion. In figure 4.9 their distribution is given for waves on a following current. The strong gradients near the free surface are remarkable. These are caused by the strong variations of the first harmonic velocities and shear stress in the free-surface boundary layer.

The modifications of the mean horizontal velocity profile are shown in figure 4.10. Here the Eulerian-mean velocity profiles in case of waves following and opposing the current can be compared to the current profile in the situation



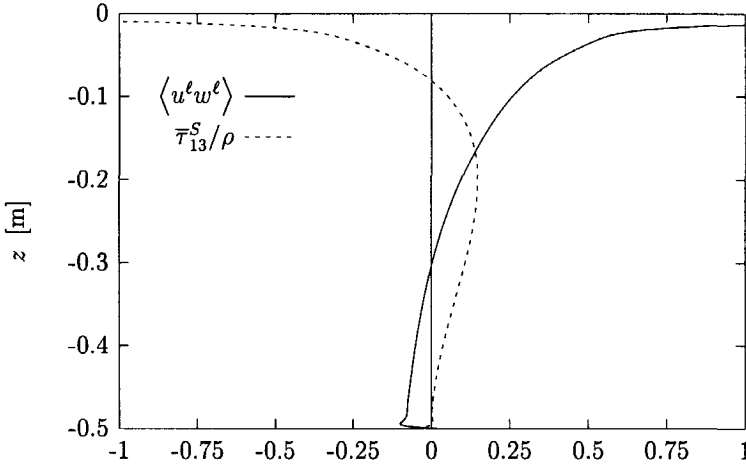


Figure 4.9: Vertical distributions of wave-induced stress and the Stokes correction of shear stress for the situation of waves propagating in current direction (unity is  $\text{cm}^2 \text{s}^{-2}$ ).

without waves. By comparing the model results with the experimental data of Klopman (1994) not only a qualitative agreement can be observed, but the computed velocity profiles show quantitative correspondence as well. The changes of the current velocity profiles due to the presence of following or opposing waves are significant. The waves propagating in the current direction cause a reduction of the mean velocity shear, or vertical gradient of the mean horizontal velocity, whereas waves opposing the current increase the velocity shear. This kind of behavior has also been reported by Bakker & Van Doorn (1978) and Kemp & Simons (1982, 1983).

In the boundary layer at the free surface, where no experimental data are available due to the Eulerian measuring procedure, a rather sharp gradient of the horizontal velocity can be observed as a result of the sharp gradients in the wave-induced driving force.

#### 4.4.3 Conclusions from numerical experiments

Results from the test problems are satisfactory. The wave-induced horizontal drift profiles, which have been obtained for the situation without initial current, agree with Longuet-Higgins' conduction solution. However, these results do not agree with experimental results of Mei et al. (1972) in all situations that

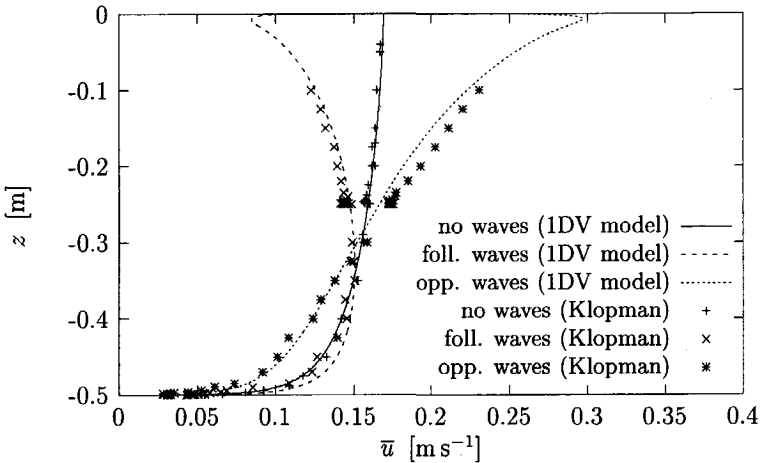


Figure 4.10: GLM results (present model) and experimental results (Klopman, 1994) for Eulerian-mean horizontal velocity profile.

were considered. There might be several reasons for this. As in the analysis of Longuet-Higgins, correlations between mean quantities are neglected in the present model, if no initial current exists. Mei (1989, §9.5) showed that neglecting nonlinear convective terms might be dangerous, especially if the wave amplitude is of the same magnitude as the boundary layer thickness, which is true for this problem. The present WKBJ expansion, which only takes into account the first harmonic at first order, is only valid for currents that are not weak compared to the wave motion. In fact, if there is no initial current higher harmonics should be taken into account. Since these higher harmonics have been neglected the applied WKBJ method might lead to wrong solutions for boundary layer streaming problems. These higher harmonics might have a greater impact on the solution, as the velocities in the boundary layers at the free surface and the bottom are larger. These velocities are large in magnitude for small and large values of  $\text{Re}(kh)$ , probably so large that the analysis in the present model does not hold anymore.

The changes of the vertical gradient of the horizontal velocity amplitude profile, caused by a following or opposing current, are in good qualitative agreement with the experimental results. The form of the predicted velocity profiles correspond to the measured profiles. The observed profile shift has been considered to be caused by reflection in the wave tank.

The changes of the vertical gradient of the mean horizontal velocity, induced

by the modified wave field propagating in the current direction or opposite to this direction, match both qualitatively and quantitatively with the experimental data. For these problems it is not useful to go to higher order in the WKBJ expansion. The model verification of the boundary layer streaming problem showed that inclusion of higher harmonics might be necessary. Since these higher harmonics have been neglected in the present WKBJ expansion, the model results will not necessarily be improved by going to higher order of approximation in the GLM equations or higher order of accuracy in the WKBJ expansion.

## 4.5 Qualitative explanation for profile changes

In the previous section the velocity profile changes observed in the laboratory experiments have been predicted reasonably accurately with the 1DV model. In this section a qualitative explanation is given for the changes in the vertical profile of the Eulerian mean velocity.

In a situation without waves the vertical variation of the shear stress is in balance with the horizontal gradient of the pressure. Hence, the shear stress varies linearly over depth, vanishing at the free surface. Together with a parabolic eddy viscosity, this leads to a logarithmic velocity distribution.

Decay of waves in the propagation direction, as in a flume, causes a downward transport of forward momentum in the surface layers, equivalent to a shear stress. This is most obvious for breaking waves. For waves following the current, this wave-induced shear stress has the same sign as the shear stress related to the current, say positive (dotted line in figure 4.11), whereas for waves opposing the current it has the opposite sign (not shown).

The total shear stress of the combined motion must still be linearly varying in the vertical, vanishing at the free surface, to maintain equilibrium with the mean pressure gradient (solid line in figure 4.11). Since for following waves the wave contribution to the shear stress in the surface layers is positive, the shear stress related to the current (dashed line in figure 4.11) must become negative in that region, as shown in figure 4.11. This causes a backward bending of the mean horizontal velocity profile in the upper layers for following waves, and a forward bending in case of opposing waves, as observed.

In the following the qualitative outline above is made more precise, although strong assumptions are made. The momentum equations (3.28) are simplified by neglecting horizontal variations ( $\partial/\partial x_\beta = 0$ ), except for the horizontal GLM pressure gradient, which is assumed to depend on the horizontal gradient of the GLM free-surface elevation,  $\partial\bar{p}^L/\partial x = \rho g \partial\bar{\zeta}^L/\partial x$ . Following Nielsen & You (1996)  $\tau_{\text{tot}}$  represents the total shearing force per unit area of a cross section or the total transfer of  $x$ -momentum in the  $z$ -direction. If only the dominant terms

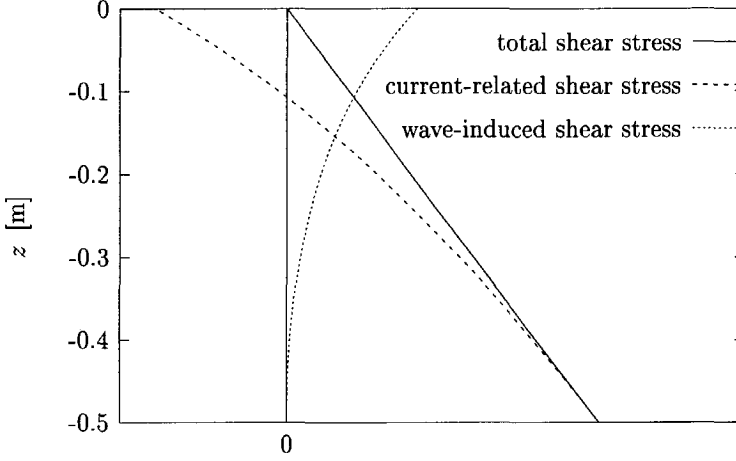


Figure 4.11: Typical distributions for the total shear stress and its wave-induced and current-related part for the case of following waves.

are taken into account,

$$\bar{\tau}_{\text{tot}} = \bar{\tau}_{13}^L - \bar{\tau}_{13}^S - \rho \langle u^\ell w^\ell \rangle, \quad (4.40)$$

with  $\bar{\tau}_{13}^L = \nu \partial \bar{u}^L / \partial z$ . The total normal stress  $\sigma_{\text{tot}}$  or horizontal transfer of  $x$ -momentum is given by

$$\bar{\sigma}_{\text{tot}} = -\bar{p}^L + \bar{p}^S - \rho \bar{u}^L \bar{u}^L - \rho \langle u^\ell u^\ell \rangle. \quad (4.41)$$

In a two-dimensional steady flow these two satisfy the following force balance,

$$\frac{\partial \bar{\tau}_{\text{tot}}}{\partial z} + \frac{\partial \bar{\sigma}_{\text{tot}}}{\partial x} = 0. \quad (4.42)$$

Further simplifications are made to  $\bar{\sigma}_{\text{tot}}$ . The effect of the current on the wave motion is neglected. Consequently, the Lagrangian and Eulerian orbital velocities are equal, at least to leading order,  $\mathbf{u}^\ell = \mathbf{u}'$ . The Stokes correction of the pressure can be evaluated up to second order as  $\bar{p}^S = \langle w'w' \rangle$ . The 2DV balance (4.42) then reduces to

$$\frac{\partial}{\partial z} \left( \frac{\bar{\tau}_{13}^L}{\rho} - \frac{\bar{\tau}_{13}^S}{\rho} - \langle u'w' \rangle \right) = g \frac{\partial \bar{\zeta}^L}{\partial x} + \frac{\partial}{\partial x} (\langle u'u' \rangle - \langle w'w' \rangle). \quad (4.43)$$

The wave-induced stresses in (4.43) are approximated by assuming linear wave theory. First of all the wave-induced shear stress  $\langle u'w' \rangle$  is considered. Several sources of nonzero wave-induced shear stresses  $\langle u'w' \rangle$  for flow over a horizontal bed have been described in literature. Firstly, the oscillatory boundary layer streaming (Longuet-Higgins 1953) is a consequence of the  $\langle u'w' \rangle$  distribution, which is in turn produced by the vorticity generation and diffusion in the bottom boundary layer.

Secondly, a nonlinear vorticity transfer from the current to the wave motion takes place (Peregrine 1976), which directly influences  $\langle u'w' \rangle$ . As long as  $\partial^2 \bar{u}^L / \partial z^2 = 0$  the wave motion will remain irrotational. Moreover, Rivero & Sánchez-Arcilla (1995) showed that the wave vorticity, and thus  $\langle u'w' \rangle$ , will be stronger for larger curvature of the current. For the logarithmic-distributed currents considered in this study, the strongest current curvature is located in the lower part of the vertical.

These two sources for nonzero  $\langle u'w' \rangle$  mainly influence the mean horizontal velocity profile from below. The vorticity is generated in the lower regions and transferred upward. However, the major velocity changes are observed near the free surface. Therefore, we focus on the influence of wave decay. Wave amplitude gradients are known to generate nonzero wave-induced stresses. Using a perturbation analysis Deigaard & Fredsøe (1989) proved that the horizontal orbital velocity lags behind in phase compared to the free surface elevation. This means that the horizontal and vertical velocity are less than 90 degrees out of phase, causing a positive wave-induced stress. In the present setting this is easily seen from the continuity equation. Under the present assumptions the horizontal orbital velocity reads

$$u' = \frac{\omega a(x)}{\sinh(|k|h)} \cosh(|k|(z+h)) \exp[i(k_r x - \omega t)] , \quad (4.44)$$

with  $a(x) = a_0 \exp[-k_i x]$  and  $k_r, k_i$  the real and imaginary parts of the wave number  $k$ . The vertical velocity component  $w'$  is determined from the continuity equation,

$$\begin{aligned} w' &= - \int_{-h}^z \frac{\partial u'}{\partial x} dz \\ &= - \frac{\omega \sinh(|k|(z+h))}{|k| \sinh(|k|h)} \left( \frac{\partial a}{\partial x} + i k_r a \right) \exp[i(k_r x - \omega t)] \\ &= \frac{\omega a \sinh(|k|(z+h))}{|k| \sinh(|k|h)} k_r \left( -i + \frac{k_i}{k_r} \right) \exp[i(k_r x - \omega t)] . \end{aligned} \quad (4.45)$$

The phase shift between  $u'$  and  $w'$  is determined by the complex factor  $-i + k_i/k_r$

and is thus slightly less than 90 degrees. Combining (4.44) and (4.45) yields,

$$\langle u'w' \rangle = \frac{-\omega^2 a \sinh(2|k|(z+h))}{4|k| \sinh^2(|k|h)} \frac{\partial a}{\partial x}. \quad (4.46)$$

This expression coincides with relation (67) given by You (1997). In the present analysis only this contribution to  $\langle u'w' \rangle$  is taken into account.

The second wave-induced stress term, being the latter term in the right-hand side of (4.43), is evaluated as

$$\frac{\partial}{\partial x} (\langle u'u' \rangle - \langle w'w' \rangle) = \frac{\omega^2 a}{\sinh^2(|k|h)} \frac{\partial a}{\partial x}, \quad (4.47)$$

which is constant over depth.

In the following the influence of  $\bar{\tau}_{13}^S$  is neglected. Integration of (4.43) from the bed to some level  $z$  then yields

$$\bar{\tau}_{13}^L + \bar{\tau}_w = \tau_b \left( \frac{-z}{h} \right). \quad (4.48)$$

Here  $\tau_b = -\rho g h \partial \zeta^L / \partial x$  is the bed shear stress and the contribution of the waves to the shear stress is given by

$$\begin{aligned} \bar{\tau}_w &= -\rho \langle u'w' \rangle - \rho(z+h) \frac{\partial}{\partial x} (\langle u'u' \rangle - \langle w'w' \rangle) \\ &= \frac{\rho \omega^2 a}{4|k| \sinh^2(|k|h)} \frac{\partial a}{\partial x} [\sinh(2|k|(z+h)) - 4|k|(z+h)]. \end{aligned} \quad (4.49)$$

The latter expression is obtained by substitution of (4.46) and (4.47). For the conditions of Klopman's (1994) following wave experiments  $\bar{\tau}_w$  is plotted in figure 4.12. Clearly, the current contribution to the shear stress  $\bar{\tau}_{13}^L$  varies linearly over depth in the situation without waves, because then  $\bar{\tau}_w = 0$  (dashed line in figure 4.12).

We first assume that waves and current are propagating in the same positive  $x$ -direction. The vertical profile of the total shear stress  $\tau_{\text{tot}} = \bar{\tau}_{13}^L + \bar{\tau}_w$  is linear with a bed shear stress  $\tau_b(-z/h)$  being larger than in the situation without waves. This explains the difference between the two linear profiles in figure 4.12. The shear stress  $\bar{\tau}_{13}^L$  is smaller than the total shear stress, because the wave-induced shear stress is positive. Clearly, the current shear stress becomes negative in the upper part of the vertical. Consequently, the horizontal velocity  $\bar{u}^L$  decreases in this region.

For waves opposing a current the wave-induced stresses are opposite, and the bed shear stress is reduced. Compared to the situation without waves, the shear

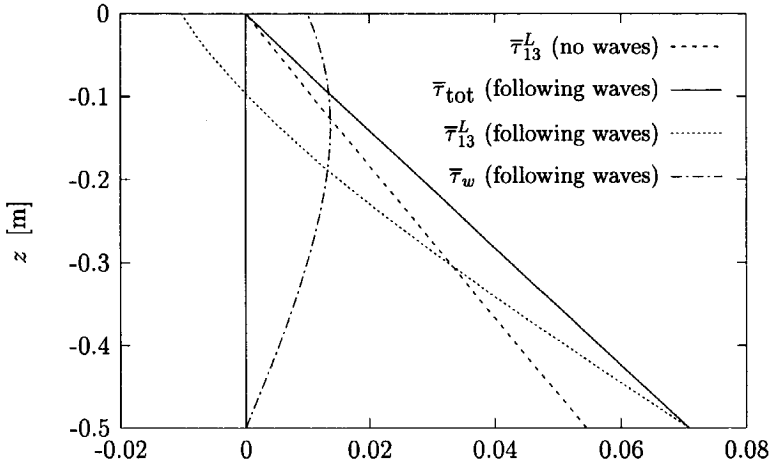


Figure 4.12: Total shear stress distributions and their wave-induced and current-related contribution for the situation without waves and following waves under the conditions in Klopman's (1994) experiments (unity is  $\text{N}/\text{m}^2$ ).

stress increases in the upper part. Consequently, the vertical gradient of the horizontal velocity increases.

The more quantitative explanation given here is based on strong assumptions. The influences of the current vorticity and the boundary layer streaming have not been taken into account. The wave-induced stresses are evaluated from linear wave theory, neglecting the influence of an ambient current. Furthermore, the Stokes correction of the shear stress has been neglected. The Stokes correction of the shear stress can be interpreted as a wave-induced disbalance term of the shear stress. Since the forward excursion of a water particle is larger than its backward excursion, the water particle does not describe a closed orbit. Consequently, a drift velocity  $\bar{\mathbf{u}}^S$  is generated. A sufficient condition for  $\bar{\mathbf{u}}^S$  to exist is that the orbital velocity  $\mathbf{u}^L$  is nonuniform over depth. Analogous, the Stokes correction of the shear stress  $\bar{\tau}_{13}^S$  is significant in regions where the fluctuating part of the shear stress  $\tau_{13}^L$  is changing rapidly over depth. Obviously, this is in the regions near the bed and the free surface. For laminar situations the Stokes correction of the shear stress is negligible, whereas in the turbulent regime the vertical variation of  $\tau_{13}^L$  is significant. Figure 4.9 shows that for the situation under consideration  $\bar{\tau}_{13}^S$  and  $\langle u'w' \rangle$  are of comparable magnitude.

The Eulerian-mean velocity is obtained by subtracting the Stokes drift from the GLM velocity. The horizontal component of the Stokes drift is positive over

the entire depth in the direction in which the waves are propagating. Compared to the GLM velocity the Eulerian-mean horizontal velocity then reduces for following waves and increases for opposing waves.

Summarizing, the cause of the change in the Eulerian-mean horizontal velocity profiles is twofold. Since the mass transport is defined in terms of the GLM velocity, one part of the reduction can directly be ascribed to the Stokes drift. Secondly, vorticity generation and wave decay produce a nonzero wave-induced shear stress, a wave-induced normal stress and a wave-induced disbalance in the shear stress. The current shear stress must balance for these wave-induced contributions to the shear stress, resulting in a vertical transfer of horizontal momentum. Because the mass transport is equal in the situation with and without waves, the depth-integrated GLM correction of the horizontal velocity vanishes. Therefore, the changes due to the wave-induced contribution to the shear stress and the Stokes correction of the shear stress only cause a redistribution of horizontal momentum over depth.



# Chapter 5

## 2DV lateral model

### 5.1 Secondary circulations

In modelling the wave-channel problems, variations in cross-direction have not been taken into account in the 1DV model. Due to the finite channel width secondary circulations will arise. For the situation without waves these are ascribed to asymmetries in the turbulent stresses. This was e.g. confirmed by Knight & Patel (1985). For various aspect ratios, i.e. width to depth ratios, they observed secondary circulation cells. For an overview on turbulence-driven three dimensional flow structures in general, and secondary currents in non-circular open or closed channels in particular, one is referred to Nezu & Nakagawa (1993, chapter 5).

These circulation cells have also been observed in laboratory flume experiments for the combined motion of wave and current, see e.g. Nepf & Monismith (1991), and more recently Nepf et al. (1995), Klopman (1997) and Melville et al. (1998). The secondary circulations have been related to Langmuir circulations. As already mentioned in subsection 2.1.2 the Craik-Leibovich (CL) theory provides an explanation for this phenomenon. In the following we briefly set out the CL theory, and how in this theory the generation of Langmuir circulations is explained.

Leibovich (1980) showed that under mild conditions, the GLM equations (3.12) reduce to, as they are called nowadays, the CL equations in Eulerian coordinates. These equations can be written as

$$\frac{\partial \bar{u}_i}{\partial t} + \bar{u}_j \frac{\partial \bar{u}_i}{\partial x_j} + \frac{\partial}{\partial x_i} \left( gz + \frac{\bar{p}}{\rho} + \left\langle \frac{1}{2} u'_j u'_j \right\rangle \right) = T_i + \bar{X}_i, \quad (5.1)$$

where  $\bar{u}$  and  $u'$  are the (Eulerian) mean velocity and the orbital velocity,  $T$  denotes the CL vortex force and  $X$  is a vector representing viscous or turbulence effects. The mild conditions for which the approximation is valid stress that the

waves are dominated by their irrotational part. This can be shown by comparing the pseudomomentum and the Stokes drift, which also learns that an additional restriction has to be imposed on the mean velocity. If the mean shear rate and the mean velocity curvature are weak, the pseudomomentum may be approximated by the Stokes drift, which then appears in the CL vortex force  $\mathbf{T} = \bar{\mathbf{u}}^S \times \bar{\boldsymbol{\Omega}}$  with  $\bar{\boldsymbol{\Omega}} = \nabla \times \bar{\mathbf{u}}$  the mean vorticity. Craik (1982b) gave an approximation of  $\mathbf{T}$  which is valid for a flume,

$$\mathbf{T} \approx \mathbf{T}_0 = \left( 0, \bar{u}^S \frac{\partial \bar{u}}{\partial y}, \bar{u}^S \frac{\partial \bar{u}}{\partial z} \right)^T. \quad (5.2)$$

with  $y$  the spanwise and  $z$  the vertical direction. The effect of the waves is thus reflected by the Stokes drift.

Leibovich (1980) included viscosity in his original derivation and arrived at

$$\bar{X}_i = \nu_0 \frac{\partial^2 \bar{u}_i}{\partial x_j \partial x_j}. \quad (5.3)$$

However, the derivation crucially depends on the assumption of a constant eddy viscosity. Inclusion of viscosity is necessary for the following reason. The essential point in the CL theory is that a combination of a shear flow and a Stokes drift of the wave field is unstable to disturbances in lateral direction. Viscosity is needed to obtain shear.

Leibovich (1983) reviewed the two classes of mechanisms CL1 and CL2, which originally applied for laterally unbounded water bodies. In the CL1 model, which was proposed by Craik & Leibovich (1976), the vorticity component  $\Omega_1$  in longitudinal direction can be generated by a Stokes drift that varies in lateral direction. However, for a laboratory channel there is no significant amplitude variation in lateral direction. Neither can the waves propagate consistently in a flume in a direction deviating from the mean flow direction.

The CL2 mechanism was originally suggested by Craik (1977) and further developed by Leibovich (1977) and is based on an instability mechanism. The vorticity component  $\Omega_1$  may be generated by the combination of a laterally uniform Stokes drift and a pre-existing vertical vorticity  $\Omega_3$ . Here only the principal result in the latter paper is mentioned. The system is stable if

$$M(z) = \frac{\partial \bar{u}}{\partial z} \frac{\partial \bar{u}^S}{\partial z} < 0 \quad (5.4)$$

over the entire depth, and is unstable otherwise. For an extensive description of the CL2 mechanism one is referred to the original description of Leibovich (1977) or his review paper (1983).

Despite numerous field observations and increasingly sophisticated numerical solutions of the governing model equations (see Melville et al. (1998) for a list of

references) the number of successfully generated and measured Langmuir circulations in laboratories is limited. Faller & Caponi (1978) and Melville et al. (1998) studied the evolution of wind-driven Langmuir circulations as an instability of a wind-driven surface shear layer. The CL2 forcing mechanism was demonstrated by Nepf & Monismith (1991) and Klopman (1997) by combining regular non-breaking waves and a current in a narrow flume with an aspect ratio  $2L/h \approx 2$ . A pair of streamwise vortices was produced from the permanent vertical vorticity in the side-wall boundary layers.

The observations of Klopman (1997) for waves opposing an ambient current are in contrast with the CL2 mechanism. Although (5.4) has been fulfilled and instabilities were not expected according to the CL2 mechanism, streamwise vortices were present. Nepf et al. (1995) conducted a set of experiments in a 1.2 m wide flume with a still-water depth of 10 cm. They considered both breaking and nonbreaking waves propagating in the current direction. Dependent on the distance from the wave maker they observed two or more vertical streaks of downwelling in the cross section under consideration for the situation of breaking waves. This indicates the presence of two or more vortex pairs. This behavior was not observed for nonbreaking waves. Apparently a strong wind-induced shear or wave-instability is required to obtain more than one pair of streamwise vortices. Otherwise only the vortices in the boundary layers can provide the instabilities which lead to the evolution of one pair of vortices.

In order to obtain an explanation for the observed wave-induced changes in the mean horizontal velocity profile in a flume, Radder (1994) considered the addition of the CL vortex force to the Reynolds-averaged momentum equations. For waves following the current the vertical component of  $\mathbf{T}_0$  is positive and secondary flows consisting of counter-rotating vortices with their axis in streamwise direction are induced, with upwelling along the side walls and downwelling in the center of the flume. Low forward momentum from the bed and the side walls is transferred along the upper part towards the center of the flume. Consequently, the mean longitudinal horizontal velocity in the upper regions is expected to decrease. This is confirmed by Leibovich & Paolucci (1980, fig. 3 and 16). For the situation of waves opposing the current, the turbulent mixing is reduced and the mean flow becomes more stable. As a result the mean velocity shear is expected to increase as observed in several experimental studies.

The explanation for the changes of the mean horizontal velocity profile given above is based on the existence of secondary circulation cells. This mechanism contradicts the 1DV explanation of chapter 4 in which lateral uniformity has been assumed. In the 1DV model the driving force for the mean motion is dominated by its longitudinal component. In the CL theory the latter component is neglected, according to (5.2), whereas the lateral and vertical components are responsible for the wave-induced circulations in the cross-sectional plane. In the

following a 2DV lateral model will be developed in which all three components of the wave-induced driving force are included. In this way the effect of the secondary circulations on the mean longitudinal velocity can be compared with the direct influence of the longitudinal component of the driving force.

## 5.2 Formulation of 2DV model in GLM setting

Following the idea of Radder (1994), Dingemans et al. (1996) developed a 2DV non-hydrostatic numerical flow model in order to reproduce the vertical velocity profiles of the horizontal current measured in the laboratory experiments of Klopman (1994). A detailed description of this model is given in the report of Van Kester et al. (1996). They observed in their simulations that secondary circulations induced by the CL vortex force caused changes in the vertical structure of the mean horizontal flow. However, due to poor estimates of the Stokes drift and the CL vortex force in the boundary layers, quantitative agreement with Klopman's experimental results was not obtained for situations of waves following or opposing a current. It is remarked that the conditions for the validity of the CL equations are not satisfied in the regions where the mean flow has relatively strong shear. Corrections of the CL vortex force are required here.

In the following, a 2DV model is obtained by simplifying the three-dimensional GLM equations, derived in chapter 3. This simplification is based on the neglect of longitudinal variation of all GLM quantities, except the hydrostatic part of the pressure. This results in 2DV equations for the GLM flow. The form of these equations is almost similar to the CL equations used in the 2DV model of Dingemans et al. (1996).

Apart from the fact that the quantities in the GLM model are not Eulerian, the major difference concerns the wave-induced driving force. The CL vortex force  $T_0$  is implemented in Dingemans et al. (1996) as a force acting in the cross-sectional plane. However, in the GLM approach the wave-induced driving force is still three dimensional. Consequently, the velocity distribution is not only influenced by the changes of the motion in the cross section. On the other hand, circulation patterns in the cross-sectional plane, as observed in the numerical simulations reported by Dingemans et al. (1996), are still expected to be predicted.

The 2DV model is developed for the same flow regime as has been considered in chapter 4. However, side wall effects have been included now. The amplitude functions of the orbital quantities and the mean quantities are allowed to vary over the entire cross section under consideration.

The development of the 2DV model consists of three analytical phases. Firstly, the 2DV-GLM equations have been formulated (subsection 5.2.1). Secondly, the

distribution of the oscillatory motion in a cross-sectional plane has been determined (subsection 5.2.2) and thirdly, the wave-induced driving forces have been evaluated (subsection 5.2.3). The 2DV-GLM equations have been implemented in the numerical solver which was also used by Dingemans et al. (1996), (subsection 5.3.2). The model verification is presented in section 5.4.

### 5.2.1 Derivation of the 2DV-GLM equations in a cross-sectional plane

As mentioned above a lateral 2DV model, providing a local solution in a cross-sectional plane, will be obtained by neglecting variations in longitudinal direction of GLM quantities in the general three-dimensional GLM equations (3.7), (3.28). Only the hydrostatic part of the GLM pressure which is related to the GLM surface elevation  $\bar{\zeta}^L$ , is not neglected. The total pressure  $\bar{p}^L$  is decomposed in a hydrostatic and non-hydrostatic part,  $\bar{p}^L = \rho g (\bar{\zeta}^L - z) + \bar{\pi}^L$ .

In this chapter the focus is entirely on wave-current motion in a channel. Therefore, the Latin indices used so far are replaced by indices  $x, y, z$  indicating the relationship with the directions under consideration. As mentioned in section 5.1  $y$  and  $z$  denote the lateral and vertical direction respectively, whereas  $x$  is the direction along the flume. The continuity equation and the three momentum equations read as,

$$\frac{\partial \bar{v}^L}{\partial y} + \frac{\partial \bar{w}^L}{\partial z} = -\bar{D}^L(\log J), \quad (5.5)$$

and

$$\frac{\partial \bar{u}^L}{\partial t} + \bar{v}^L \frac{\partial \bar{u}^L}{\partial y} + \bar{w}^L \frac{\partial \bar{u}^L}{\partial z} = -g \frac{\partial \bar{\zeta}^L}{\partial x} + \frac{1}{\rho} \frac{\partial \bar{\tau}_{xy}^L}{\partial y} + \frac{1}{\rho} \frac{\partial \bar{\tau}_{xz}^L}{\partial z} + \bar{S}_x, \quad (5.6a)$$

$$\frac{\partial \bar{v}^L}{\partial t} + \bar{v}^L \frac{\partial \bar{v}^L}{\partial y} + \bar{w}^L \frac{\partial \bar{v}^L}{\partial z} = -g \frac{\partial \bar{\zeta}^L}{\partial y} - \frac{1}{\rho} \frac{\partial \bar{\pi}^L}{\partial y} + \frac{1}{\rho} \frac{\partial \bar{\tau}_{yy}^L}{\partial y} + \frac{1}{\rho} \frac{\partial \bar{\tau}_{yz}^L}{\partial z} + \bar{S}_y, \quad (5.6b)$$

$$\frac{\partial \bar{w}^L}{\partial t} + \bar{v}^L \frac{\partial \bar{w}^L}{\partial y} + \bar{w}^L \frac{\partial \bar{w}^L}{\partial z} = -\frac{1}{\rho} \frac{\partial \bar{\pi}^L}{\partial z} + \frac{1}{\rho} \frac{\partial \bar{\tau}_{yz}^L}{\partial y} + \frac{1}{\rho} \frac{\partial \bar{\tau}_{zz}^L}{\partial z} + \bar{S}_z. \quad (5.6c)$$

The horizontal gradient of the hydrostatic pressure,  $\partial \bar{\zeta}^L / \partial x$ , is assumed constant over each cross section  $\mathcal{V}(x) = \{(y, z) : -L \leq y \leq L, -h \leq z \leq \bar{\zeta}^L(x, y, t)\}$  at a distance  $x$  from the wave maker and is chosen such that the discharge of the

combined flow equals the discharge  $Q$  of the flow without waves,

$$Q = \int_{-L}^L \int_{-h}^{\bar{\zeta}^L} \bar{u}^L dz dy. \quad (5.7)$$

The GLM free-surface elevation  $\bar{\zeta}^L$  is determined from the continuity equation. Integration of (5.5) over depth and substitution of the boundary conditions for the vertical GLM velocity,

$$\bar{w}^L = \bar{D}^L \bar{\zeta}^L \quad \text{at } z = \bar{\zeta}^L, \quad (5.8a)$$

$$\bar{w}^L = -\bar{D}^L h \equiv 0 \quad \text{at } z = -h, \quad (5.8b)$$

yields

$$\frac{\partial \bar{\zeta}^L}{\partial t} + \frac{\partial}{\partial x} \left( \int_{-h}^{\bar{\zeta}^L} \bar{u}^L dz \right) + \frac{\partial}{\partial y} \left( \int_{-h}^{\bar{\zeta}^L} \bar{v}^L dz \right) = - \int_{-h}^{\bar{\zeta}^L} \bar{D}^L (\log J) dz. \quad (5.9)$$

Since longitudinal variations of GLM quantities are neglected, the second term in (5.9) vanishes.

In the right-hand side of (5.6)  $\bar{\mathcal{S}}^L$  denotes the wave-induced driving force, given by

$$\bar{\mathcal{S}}_x^L = \frac{1}{\rho} \frac{\partial \bar{p}^S}{\partial x} - \frac{1}{\rho} \frac{\partial \bar{\tau}_{xx}^S}{\partial x} - \frac{1}{\rho} \frac{\partial \bar{\tau}_{xy}^S}{\partial y} - \frac{1}{\rho} \frac{\partial \bar{\tau}_{xz}^S}{\partial z} - \frac{\partial r_{xx}}{\partial x} - \frac{\partial r_{xy}}{\partial y} - \frac{\partial r_{xz}}{\partial z}, \quad (5.10a)$$

$$\bar{\mathcal{S}}_y^L = \frac{1}{\rho} \frac{\partial \bar{p}^S}{\partial y} - \frac{1}{\rho} \frac{\partial \bar{\tau}_{yx}^S}{\partial x} - \frac{1}{\rho} \frac{\partial \bar{\tau}_{yy}^S}{\partial y} - \frac{1}{\rho} \frac{\partial \bar{\tau}_{yz}^S}{\partial z} - \frac{\partial r_{yx}}{\partial x} - \frac{\partial r_{yy}}{\partial y} - \frac{\partial r_{yz}}{\partial z}, \quad (5.10b)$$

$$\bar{\mathcal{S}}_z^L = \frac{1}{\rho} \frac{\partial \bar{p}^S}{\partial z} - \frac{1}{\rho} \frac{\partial \bar{\tau}_{zx}^S}{\partial x} - \frac{1}{\rho} \frac{\partial \bar{\tau}_{zy}^S}{\partial y} - \frac{1}{\rho} \frac{\partial \bar{\tau}_{zz}^S}{\partial z} - \frac{\partial r_{zx}}{\partial x} - \frac{\partial r_{zy}}{\partial y} - \frac{\partial r_{zz}}{\partial z}. \quad (5.10c)$$

The tensor  $r_{ij}$  contains the well-known wave-induced stress in terms of Lagrangian quantities and is given by (3.32). In the 1DV model the wave-induced driving force consists of first-order first-harmonic quantities as well as zeroth-order mean quantities. A perturbation series approach has not been used in the 2DV model. In fact, the total mean motion is considered. Therefore,  $\bar{\mathcal{S}}^L$  has to be evaluated at each time step of the numerical integration procedure. For that purpose expressions for the fluctuating quantities are required. These will be determined with the 1DV model. According to the WKBJ perturbation series approach (chapter 4) the fluctuating quantities depend on the initial current instead of the instantaneous current. Hence, the part of the driving force that is expressed completely in terms of fluctuating quantities is influenced by the initial current instead of the total mean motion. This inconsistency in the model is

not expected to have significant consequences. The direct influence of the mean motion within the wave-induced driving force is larger than the indirect effect of the mean motion through the fluctuating quantities.

As for the CL equations the flow should be nonuniform in lateral direction in order to induce a nonzero  $y$ -component of the driving force. Regarding the wave motion this non-uniformity is limited to the side-wall boundary layer. As a consequence, superimposing a wave field, that is nonuniform only near the side-walls, on an initially uniform current will lead to longitudinal vortices evolving from the side wall. Due to the symmetry and the limited flume width and depth the growth of the vortices is limited as well.

From (5.10) it is obvious that the longitudinal component of the driving force is nonzero, in contrast to the corresponding component in the CL vortex force. The 1DV model already proved that  $\bar{S}_x^L$  is significant and will be responsible for some part of the mean velocity profile changes.

### 5.2.2 Side-wall effects on fluctuating quantities

In the 1DV model laterally uniform vertical distributions of oscillatory quantities have been determined. Needless to say, this solution does not reflect the side wall influence. In order to take side wall effects into account a procedure has been adopted that was also used by Mei et al. (1972). They analyzed mass transport caused by progressive waves for a situation of constant viscosity and no initial current.

A cross section  $\mathcal{V}(x)$  of the flume at a distance  $x$  from the wave maker is subdivided into five regions, viz. the inviscid core region and the boundary layers at the bottom, the free surface and the two side walls. This is sketched in figure 5.1. In the 1DV model the surface and bottom boundary layers are already included. Here the approach of the 1DV model is extended, such that lateral variations of the fluctuating quantities, being strongest in the side-wall layers, are included. In the following the analysis of Mei et al. (1972), originally for the bottom boundary, is applied to the side-wall boundary. Viscous effects are neglected outside the side wall boundary layers. Consequently, the lateral variations of the amplitude functions of the fluctuating quantities can be neglected in this region. The flow equations for the fluctuating motion are then reduced to those derived for the 1DV problem. The solution of the latter problem will be denoted by  $\varphi = \varphi_1$ . By neglecting the influence of the mean current and variations of the eddy viscosity  $\nu$  in the side-wall boundary layers, Mei et al. (1972, appendix I) showed that the orbital velocity including the no-slip condition at the side walls satisfies Stokes' shear wave solution,

$$u^\ell = [1 - \exp(\beta Y)] u_1^\ell, \quad (5.11a)$$

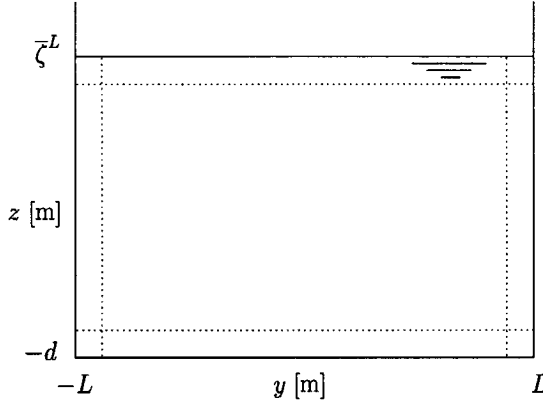


Figure 5.1: Division of a cross section  $\mathcal{V}(x)$  into five regions.

$$v^\ell = v_1^\ell = 0, \quad (5.11b)$$

$$w^\ell = [1 - \exp(\beta Y)] w_1^\ell. \quad (5.11c)$$

with the factor  $\beta = (-i\omega_0/\nu)^{1/2}$  and  $Y$  the distance to the nearest side wall. The complex-valued  $\beta$  is responsible for phase and amplitude changes in the side-wall layer.

To sum up: the 1DV model is used to determine the vertical distribution of the fluctuating quantities. The 2DV profiles are obtained by multiplying the 1DV profile (subscript 1) by a  $y$ -dependent factor, which only affects the fluctuating motion in the side-wall boundary layers. The fluctuating quantities are influenced by a current that is assumed to be uniform in horizontal direction. The effect on the oscillatory motion of the secondary current, i.e. the second-order correction of the longitudinal component of the mean velocity and the secondary circulation, has been neglected.

The distribution of the wave-induced driving forces in the entire cross section can now easily be evaluated by substituting the laterally and vertically varying oscillating quantities in the general expressions for the driving forces.

### 5.2.3 Determination of wave-induced driving forces

For the general three-dimensional situation expressions for the wave-induced driving forces have been derived in chapter 3. These expressions are not only



given in terms of mean and fluctuating quantities as in (3.30)-(3.32) but also in terms of amplitude functions of the latter quantities, see (B.5a)-(B.5c), which have been obtained after application of a WKBJ perturbation series approach.

In subsection 5.2.2 the velocity components have been written as the product of the 1DV solution and a correction term in lateral direction (Stokes' shear wave solution). Under the assumptions stated in subsection 5.2.2 the lateral component of both the disturbed velocity and the displacement vanishes. As a result the second-order approximation of the Stokes correction  $\bar{\varphi}^S$  given by (2.22) can be written as

$$\bar{\varphi}^S = \bar{\varphi}_1^S (1 - \exp(\beta Y)) (1 - \exp(\bar{\beta} Y)) , \quad (5.12)$$

where  $\bar{\beta}$  denotes the complex conjugate of  $\beta$  and  $\bar{\varphi}_1^S$  the Stokes correction of  $\varphi$  determined by the 1DV model. Hence, the dependence of  $x$  and  $z$ -coordinates is separated from the dependence of the  $y$ -direction. A separation of variables of the latter form is only possible for quantities whose oscillating part shows a boundary layer behavior as for the velocity components in (5.11). Relation (5.12) holds in particular for the Stokes drift  $\bar{u}^S$  and the shear stress components  $\bar{\tau}_{ij}^S$  that do not point in the lateral direction ( $i, j \neq 2$ ). Furthermore, the radiation stress terms  $r_{ij}$  can be expressed in the form of (5.12) as well. The only terms in  $\bar{S}^L$  that require special attention are  $\bar{\tau}_{xy}^S$  and  $\bar{\tau}_{zy}^S$ . Under the assumption that the influence of the current and the lateral variations in the eddy-viscosity distribution can be neglected, as has been done in subsection 5.2.2, the oscillating part of the shear stress reads

$$\tau_{xy}^\ell = \nu \frac{\partial u^\ell}{\partial y} = -\nu u_1^\ell \beta \exp(\beta Y) \frac{dY}{dy} . \quad (5.13)$$

A similar expression is obtained for  $\tau_{zy}^\ell$  by replacing  $u^\ell$  by  $w^\ell$  in (5.13). Furthermore  $\tau_{yy}^\ell = 0$ . In terms of 1DV first-order first-harmonic amplitude functions the Stokes correction of the shear stress component  $\bar{\tau}_{xy}^S$  is expressed as

$$\begin{aligned} \bar{\tau}_{xy}^S = & \left( -ik\hat{\xi}^{(1,1)}\nu\hat{u}^{(1,-1)} + \hat{\eta}^{(1,1)}\frac{\partial(\nu\hat{u}^{(1,-1)})}{\partial z} \right) \left( -\bar{\beta}\exp(\bar{\beta}Y)\frac{dY}{dy} \right) (1 - \exp(\beta Y)) E\bar{E} \\ & + \left( ik\hat{\xi}^{(1,-1)}\nu\hat{u}^{(1,1)} + \hat{\eta}^{(1,-1)}\frac{\partial(\nu\hat{u}^{(1,1)})}{\partial z} \right) \left( -\beta\exp(\beta Y)\frac{dY}{dy} \right) (1 - \exp(\bar{\beta}Y)) E\bar{E} , \end{aligned} \quad (5.14)$$

with  $E$  given by (4.12). A similar expression can be obtained for  $\bar{\tau}_{zy}^S$ . A separation as found in (5.12) is not possible here. The components of the wave-induced

driving force can now be expressed in quantities that are computed for the greater part by the 1DV model.

The correction term in the continuity equation (5.5) is approximated up to second order by

$$-\log J = \frac{1}{2} \frac{\partial^2 \bar{\xi}_i \bar{\xi}_j}{\partial x_i \partial x_j} + O(|\xi|^3), \quad (5.15)$$

see e.g. Dingemans (1997, p.241). Alternatively, by applying (3.27) the continuity equation can also be written as

$$\frac{\partial \bar{u}_i^L}{\partial x_i} = C, \quad C = \frac{\partial \bar{u}_i^S}{\partial x_i} + O(|\xi|^3). \quad (5.16)$$

Because the lateral component of the Stokes drift vanishes,  $C$  can be derived directly from the 1DV model,

$$C = C_1 (1 - \exp(\beta Y)) (1 - \exp(\bar{\beta} Y)). \quad (5.17)$$

The correction of the depth-integrated continuity equation (5.9) is equal to  $C$  integrated over depth.

At several stages further modifications have to be made. The shear stresses are given by the strain rate relations, following Boussinesq's hypothesis. The corresponding GLM shear stresses can be defined accordingly, however with an extra wave-induced correction. In tensor notation this reads

$$\bar{\tau}_{ij}^L = \nu \left( \frac{\partial \bar{u}_i^L}{\partial x_j} + \frac{\partial \bar{u}_j^L}{\partial x_i} - T_{ij} \right), \quad (5.18)$$

according to (3.34). Here,

$$T_{ij} = \left\langle \frac{\partial \xi_k}{\partial x_j} \frac{\partial u_i^t}{\partial x_k} \right\rangle + \left\langle \frac{\partial \xi_k}{\partial x_i} \frac{\partial u_j^t}{\partial x_k} \right\rangle - \left\langle \frac{\partial \xi_k}{\partial x_j} \frac{\partial \xi_m}{\partial x_k} \right\rangle \frac{\partial \bar{u}_i^L}{\partial x_m} - \left\langle \frac{\partial \xi_k}{\partial x_i} \frac{\partial \xi_m}{\partial x_k} \right\rangle \frac{\partial \bar{u}_j^L}{\partial x_m} + O(|\xi|^3). \quad (5.19)$$

The wave-induced corrections  $T_{ij}$  are determined with the 1DV model and corrected for variations in the lateral direction. Since the lateral components of the displacement and the disturbed velocity equal zero, the modifications in lateral direction are easily obtained

$$T_{ij} = T_{ij,1} (1 - \exp(\beta Y)) (1 - \exp(\bar{\beta} Y)). \quad (5.20)$$

Obviously, the variations in lateral direction are only significant in the side-wall boundary layers. For each column in the cross section under consideration the 1DV quantities are modified with an expression which either decays or increases exponentially to unity away from the side walls.

## 5.3 Numerical solution method

Because the form of the CL equations is similar to the form of the GLM equations, the 2DV model of Dingemans et al. (1996) has been used to solve the 2DV-GLM equations numerically. Only the minor corrections listed in the previous subsection have to be carried out. The numerical treatment of the CL-based model is given by Van Kester et al. (1996), rather than Dingemans et al. (1996). In Van Kester et al. (1996) several solution techniques were investigated to solve the 2DV flow equations. The pressure correction method of Casulli (1995), which is described in subsection 5.3.1, was concluded to be the best for problems dealing with the combined motion of waves and currents. After all, the superposition of waves on a current introduces a significant deviation from the hydrostatic pressure.

### 5.3.1 Pressure correction method

Casulli & Stelling (1998) applied the pressure correction method in their construction of a computational framework that allows numerical integration of the full Reynolds-averaged Navier-Stokes equations for simulating large-scale non-hydrostatic flows. In this fractional step method the hydrostatic and the hydrodynamic component of the pressure are considered separately. For the numerical implementation and properties of the fractional step method introduced by Casulli (1995) one is referred to Casulli & Stelling (1998).

The solution procedure consists of two stages. In the first step the hydrodynamic part of the pressure is neglected. In the correction step the intermediate velocity computed in the first step is corrected by adding the hydrodynamic pressure terms. Because the driving force  $\bar{S}^L$  is responsible for the existence of the hydrodynamic pressure  $\bar{\pi}^L$ ,  $\bar{S}^L$  should be taken into account in the second step. However this would lead to complications in the numerical treatment of the second stage, because the divergence of the wave-induced driving force would have to be evaluated. Therefore  $\bar{S}^L$  is incorporated in the first stage. This choice is justified because the splitting of the equations in two stages is consistent. Use of an infinitely small time step would result in identical solutions irrespective whether  $\bar{S}^L$  were incorporated in the first or second stage. Concluding, the computation is split in the following two parts:

#### Stage 1

The depth-integrated continuity equation (5.9) and the momentum equations (5.6) are considered with  $\bar{\pi}^L \equiv 0$ . This differs from the usual approach in a shallow water model where the vertical velocity is obtained from the continuity equation. Consequently, the velocity field not necessarily satisfies the continuity

equation (5.5) after the first stage. The resulting shallow-water equations are integrated following the integration schemes of Delft Hydraulics' models TRISULA and TRIWAC, for a complete time step. For stability reasons the vertical advection and a part of the vertical shear stress terms are treated implicitly.

### Stage 2

The momentum equations are considered without the convective terms and only the hydrodynamic pressure is taken into account,

$$\frac{\partial \bar{u}_i^L}{\partial t} + \frac{1}{\rho} \frac{\partial \bar{\pi}^L}{\partial x_i} = 0. \quad (5.21)$$

By taking the divergence of (5.21) and applying the continuity equation as a side condition a Poisson equation for the hydrodynamic pressure is obtained. The conditions of zero normal flow at the bottom and side walls and a vanishing hydrodynamic pressure at the free surface provide a unique solution. A second-order discretization on a rectangular grid leads to a system of equations, with a symmetric positive-definite matrix, that is solved with the preconditioned Conjugate Gradient method. The second stage is completed after substitution of  $\bar{\pi}^L$  in (5.21), resulting in a new estimate for the velocity components.

### 5.3.2 Implementation of 2DV-GLM equations in existing numerical flow model

Certain aspects considering the implementation of the GLM equations in the 2DV numerical model are highlighted in this subsection. Some attention has been paid to the implementation of the wave-induced terms. Computations by the numerical solver are carried out on a grid for which the vertical resolution is different than the grid used for the 1DV model. Therefore interpolation techniques are required. A rational function interpolation through at least three and at most six points based on an algorithm in Stoer & Bulirsch (1980, section 2.2) has been implemented. After having evaluated the wave-induced terms in these grid points, they have been incorporated in the continuity equation and the momentum equations.

The implementation of the bottom and side-wall boundary conditions has to be considered as well. Whereas in the 1DV model no-slip conditions have been imposed at the bed, Dingemans et al. (1996) imposed partial-slip conditions at the bottom and the side-wall boundaries, using a logarithmic law-of-the-wall formulation. This approach has been outlined in appendix C. Given a shear velocity at a certain height or distance from the side wall, the friction velocity and related shear stress are determined, following Grant & Madsen's (1979) formulation. This formulation is given in an Eulerian framework. In order to

obtain the GLM shear stress at a closed boundary, the following algorithm has been applied:

1. The GLM velocity at a certain height or distance from the side wall is transformed to its Eulerian equivalent at the same height.
2. The formulation applied by Dingemans et al. (1996), is used to determine the Eulerian shear stress.
3. The Eulerian shear stresses are transformed to GLM shear stresses by adding the Stokes correction of the shear stress under consideration.

Finally, for simulating turbulent flow a turbulence model has been implemented. In a first approach a classical turbulence model has been used. Any of the turbulence models implemented by Van Kester et al. (1996) can be used. For this study a  $k - \varepsilon$  model was chosen. For closure of the turbulence model the production term is computed with Eulerian velocities, which are determined by transforming the GLM velocities. This implies that the  $k - \varepsilon$  model as implemented by Van Kester et al. (1996) needs no further correction. For completeness a description of the turbulence model is given below.

The two-equation  $k - \varepsilon$  turbulence model provides both the mean turbulent kinetic energy, here denoted as  $\bar{q}$ , and mean dissipation  $\bar{\varepsilon}$  by means of a transport equation with flow dependent source and sink terms. Following Rodi (1980) the transport equations for  $\bar{q}$  and  $\bar{\varepsilon}$ , which are nonlinearly coupled by means of the eddy viscosity  $\nu$  and the dissipation terms, are given by

$$\begin{aligned} \frac{\partial \bar{q}}{\partial t} + \bar{v} \frac{\partial \bar{q}}{\partial y} + \bar{w} \frac{\partial \bar{q}}{\partial z} \\ = \frac{\partial}{\partial y} \left( \left( \nu_0 + \frac{\nu}{\sigma_k} \right) \frac{\partial \bar{q}}{\partial y} \right) + \frac{\partial}{\partial z} \left( \left( \nu_0 + \frac{\nu}{\sigma_k} \right) \frac{\partial \bar{q}}{\partial z} \right) + \mathcal{P}_k - \bar{\varepsilon}, \end{aligned} \quad (5.22a)$$

$$\begin{aligned} \frac{\partial \bar{\varepsilon}}{\partial t} + \bar{v} \frac{\partial \bar{\varepsilon}}{\partial y} + \bar{w} \frac{\partial \bar{\varepsilon}}{\partial z} \\ = \frac{\partial}{\partial y} \left( \left( \nu_0 + \frac{\nu}{\sigma_\varepsilon} \right) \frac{\partial \bar{\varepsilon}}{\partial y} \right) + \frac{\partial}{\partial z} \left( \left( \nu_0 + \frac{\nu}{\sigma_\varepsilon} \right) \frac{\partial \bar{\varepsilon}}{\partial z} \right) + c_{1\varepsilon} \frac{\bar{\varepsilon}}{\bar{q}} \mathcal{P}_k - c_{2\varepsilon} \frac{\bar{\varepsilon}^2}{\bar{q}}, \end{aligned} \quad (5.22b)$$

where  $\nu_0$  denotes the kinematic viscosity. The advection and diffusion terms along the flume have been neglected and the eddy viscosity  $\nu$  and the production term  $\mathcal{P}_k$  are given by

$$\nu = c_\mu \frac{\bar{q}^2}{\bar{\varepsilon}}, \quad (5.23)$$

$$\mathcal{P}_k = 2\nu \left[ \left( \frac{\partial \bar{v}}{\partial y} \right)^2 + \left( \frac{\partial \bar{w}}{\partial z} \right)^2 + \frac{1}{2} \left( \frac{\partial \bar{u}}{\partial y} \right)^2 + \frac{1}{2} \left( \frac{\partial \bar{u}}{\partial z} \right)^2 + \frac{1}{2} \left( \frac{\partial \bar{v}}{\partial z} + \frac{\partial \bar{w}}{\partial y} \right)^2 \right]. \quad (5.24)$$

In  $\mathcal{P}_k$  the longitudinal variations of the velocity components have been neglected. The calibration constants in (5.22)–(5.24) are defined according to Rodi (1980) by:  $c_\mu = 0.09$ ,  $c_{1\varepsilon} = 1.44$ ,  $c_{2\varepsilon} = 1.92$ ,  $\sigma_k = 1.0$  and  $\sigma_\varepsilon = 1.3$ . Substituting (4.3) in (4.5) and comparing the result with (5.23) yields  $c_\mu = c_D c'_\mu = (c'_\mu)^4$ .

As in the 1DV model the boundary conditions for the turbulent kinetic energy at the side walls  $y = \pm L$  and the bed  $z = -h$  is derived from a local equilibrium between production and dissipation of turbulent kinetic energy,

$$\bar{q}|_{z=-h} = \frac{|\mathbf{u}_{*b}|^2}{\sqrt{c_\mu}} \quad , \quad \bar{q}|_{y=\pm L} = \frac{|\mathbf{u}_{*s}|^2}{\sqrt{c_\mu}} . \quad (5.25)$$

The shear stress velocities  $\mathbf{u}_{*b}$  at the bed and  $\mathbf{u}_{*s}$  at the side walls are determined from the velocity near the wall using a logarithmic law-of-the-wall formulation (see appendix C). The only dependence of the wave motion is via the shear stress velocities. As in the 1DV model the fluctuating part of the turbulence quantities  $q$  and  $\varepsilon$  has been neglected. However, in that model the eddy viscosity was entirely independent of the wave motion.

Uittenbogaard & Van Kester (1996) developed a boundary condition at the bed and side walls for the dissipation rate which is imposed at a distance  $\Delta$  from the boundary and is independent of the roughness length  $z_0$ ,

$$\frac{\partial \bar{\varepsilon}}{\partial \psi}(\Delta) = -\frac{|\mathbf{u}_*|^3}{\kappa \Delta^2} , \quad (5.26)$$

where  $\psi = y$  or  $\psi = z$  and  $\mathbf{u}_*$  denotes the friction velocity at the bed or the side wall. At the free surface the turbulent kinetic energy and dissipation vanish. In fact this concerns the free surface in an Eulerian setting. Since the fluctuating part of the turbulence quantities is neglected,  $\bar{q}$  and  $\bar{\varepsilon}$  may as well be assumed to vanish at  $z = \bar{\zeta}^L$ ,

$$\bar{q}|_{z=\bar{\zeta}^L} = 0 \quad , \quad \bar{\varepsilon}|_{z=\bar{\zeta}^L} = 0 . \quad (5.27)$$

The time integration of the transport equations (5.22)–(5.24) combined with the boundary conditions (5.25)–(5.27) consists of two stages. In the first stage only horizontal and vertical advective transport is taken into account. The advection terms normal to the boundary are neglected in the computational layer near the bottom and near the side walls. In the second stage the remaining non-advective terms are integrated, of which the production, dissipation and diffusion are assumed to be dominant terms in the transport equation. The vertical transport terms are integrated implicitly.

## 5.4 Verification of 2DV model

The 2DV model has been verified against experimental data obtained by Klopman (1997) in a laboratory flume with a horizontal bed. He measured the two

mean velocity components in streamwise and vertical direction in a cross section. Furthermore, the numerical results obtained with the 1DV model are compared with the 2DV model results obtained in the center of the flume.

#### 5.4.1 Comparison with flume experiments

For situations of following and opposing waves the mean velocities in a cross-sectional plane have been computed and compared with measurements of Klopman (1997). The initial conditions for those experiments are identical to those of Klopman's (1994) measurements concerning regular waves on a turbulent current and these have been mentioned in subsection 4.4.2. Klopman (1997) reported on vertical and longitudinal mean velocities in 30 points in a cross-sectional plane. Due to limitations in the LDV movements only one half of the cross section was considered. In the ideal case of pure symmetric flow this is not a restriction. In 1994 wave heights and velocities were only measured in the center of the flume.

Klopman (1994) determined the mean horizontal velocity in the center of the flume assuming uniformity in lateral direction. Side-wall effects were neglected. This forced Van Kester et al. (1996) to perform a correction procedure in which for the situation without waves the computed vertically averaged horizontal velocity, evaluated in the center of the flume, was taken as a reference for the vertically averaged velocity as resulting from the measurements. They found that the measured velocities had to be enlarged by a factor 1.135. This factor was also applied to the measured horizontal velocity profiles for the situations where waves are present. In order to avoid these problems the model results are only compared here with the experimental results of Klopman (1997). Moreover, it is not useful to compare the model results with one data set for the center points and with the second for all the other points in the cross section.

In the present 2DV model the wave-induced driving forces depend via the orbital quantities on the factor  $\beta = (-i\omega/\nu)^{1/2}$ . In our analysis  $\nu$  was assumed to be independent of the lateral direction. In all experiments we have taken  $\nu = 10^{-5} \text{ m}^2 \text{ s}^{-1}$ , representing a turbulent oscillatory motion. This choice for  $\nu$  leads to a factor  $\beta$  for which  $\text{Re}(\beta) = -(\omega/2\nu)^{1/2} \approx -467 \text{ m}^{-1}$ . Consequently, the thickness of the side-wall boundary layer is of the order 0.5 cm. For the spatial discretization a computational grid of 100 points in lateral direction and 40 points in the vertical has been used. In both directions the grid refinement procedure of Vinokur (1983) was applied, such that 3 to 4 grid points are inside the boundary layers, including the one near the bottom. The time step for the simulations is 0.01 s. The computations have been carried out as if a wave field is superimposed on a turbulent current. In initially still water a turbulent current is simulated. After 200 s a steady turbulent logarithmic shear flow has developed, see figure 5.2. However, the measured (Klopman 1997, figure 3.48) and theoretically expected

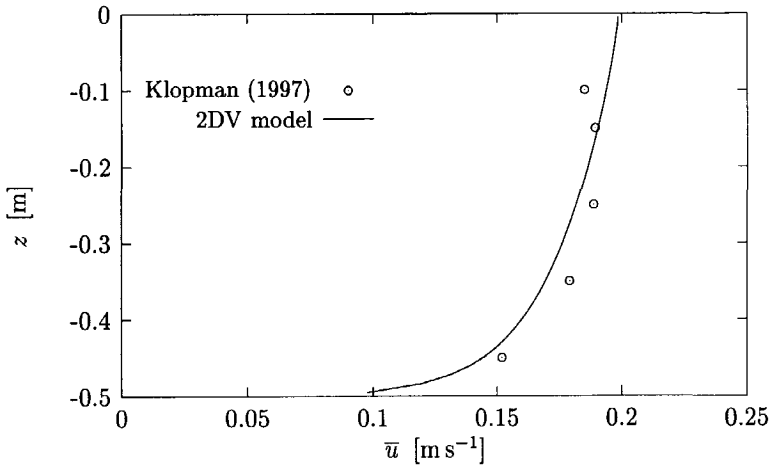


Figure 5.2: Computed and measured vertical current profile in the center of the flume (no waves).

(Nezu & Nakagawa 1993, section 5.3) secondary circulations for the situation without waves have not been predicted, because the concept of isotropic eddy viscosity, such as assumed in the  $k - \varepsilon$  model, is insufficient for predicting the secondary currents in a rectangular channel. These are the result of asymmetry in the turbulent stresses. Moreover, in a historical publication Gibson (1909) inferred that secondary currents cause the mean horizontal velocity profile in the center of the flume to deviate from a logarithmic velocity profile.

In figure 5.3 the nonuniformity in lateral direction of the horizontal velocity in streamwise direction has been confirmed. Although at 25 cm above the bed the horizontal velocity has been underpredicted (see also figure 5.2) the predicted lateral shear  $\partial \bar{u} / \partial y$  agrees with the measured shear. After 200 s ( $t = 0$ ) the wave influence on the mean motion is taken into account by activating the wave-induced driving force.

Since velocity measurements have been carried out at fixed locations and are thus Eulerian, the GLM velocity field  $\bar{\mathbf{u}}^L$  has to be transformed to its corresponding Eulerian field,  $\bar{\mathbf{u}} = \bar{\mathbf{u}}^L - \bar{\mathbf{u}}^S$ . The lateral and vertical components of the Stokes drift  $\bar{\mathbf{u}}^S$  have been neglected.

In figure 5.4 and 5.5 the results for the mean velocity distribution in a cross section at  $x = 22.5$  m from the wave maker and the mean vertical velocity profile at 5 cm, 20 cm and 48.5 cm (near the center of the flume) distance from the side wall are shown for the situation of waves propagating in the current direction. These profiles represent the steady solution obtained at  $t = 600$  s. For clarity in



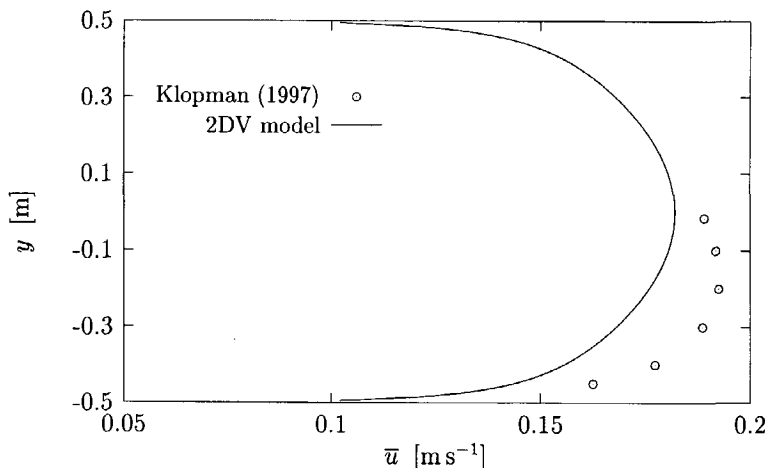


Figure 5.3: Computed and measured horizontal current profiles at 25 cm above the bed (no waves).

the plots, the velocity components have been interpolated to points which form a regular grid (figure 5.4).

The measured mean vertical velocities given in figure 5.5 already indicate that the position of the cell center is not in the middle of the half of the cross section under consideration. Closer inspection of the data in Klopman's (1997) report shows that the cell centers are displaced towards the free surface and close to the center of the flume. Figure 5.4 shows that the 2DV model predicts two counter-rotating vortices. The vertical positions of the circulation cell centers coincide with Klopman's. This can also be concluded from figure 5.5, because the form of the vertical distribution of the computed and measured mean vertical velocity agree. However, the horizontal location of the cell centers is in the middle of each half of the cross section. Nevertheless, qualitative agreement between the computed and measured cross-sectional velocities has been obtained. Under the same conditions Dingemans et al. (1996, figure 3) obtained secondary circulations of which the cell centers are located 5 cm above the middle of both halves of the cross section.

Figure 5.5 shows that the quantitative agreement between the computed and measured velocities in the cross-sectional plane is far from perfect. The downwelling in the center of the flume is overpredicted by a factor 2 and reaches a maximum of  $9 \text{ mm s}^{-1}$  at 13 cm below the water surface.

The influence of the wave motion on the mean motion is significant. For various points of the time mean horizontal velocity profiles in the flume center

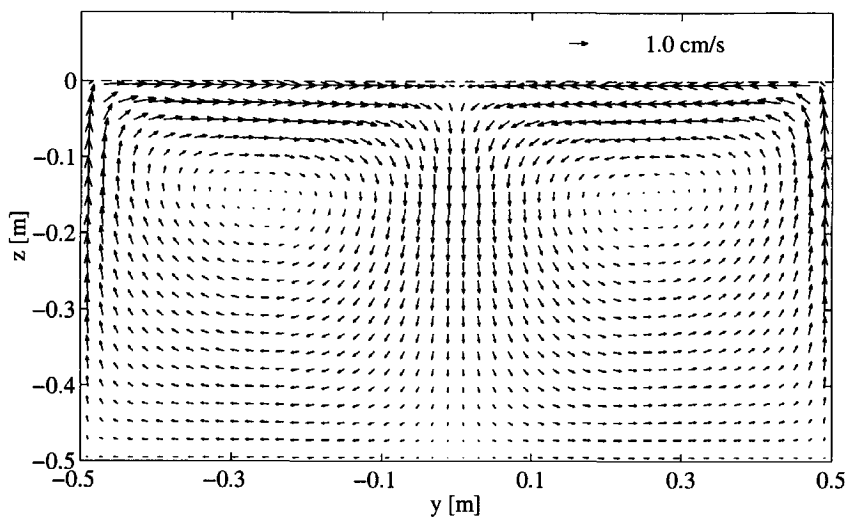


Figure 5.4: Computed mean velocity distribution in cross section for waves following the current.

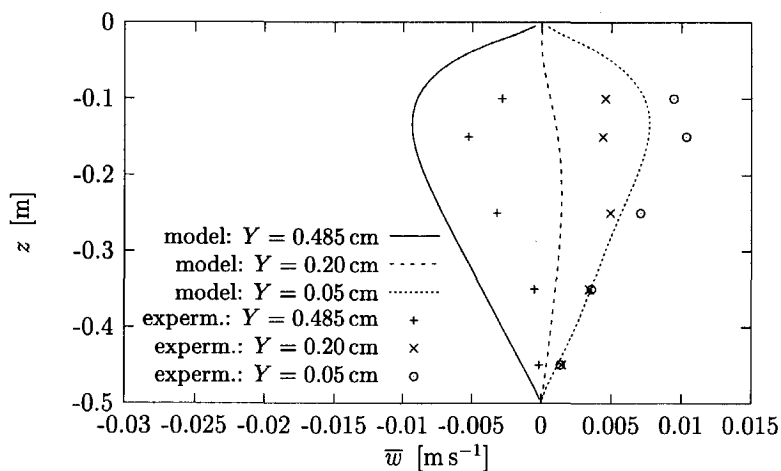


Figure 5.5: Computed and measured (Klopman, 1997) mean vertical velocity profiles at different distances  $Y$  from the side wall (following waves).

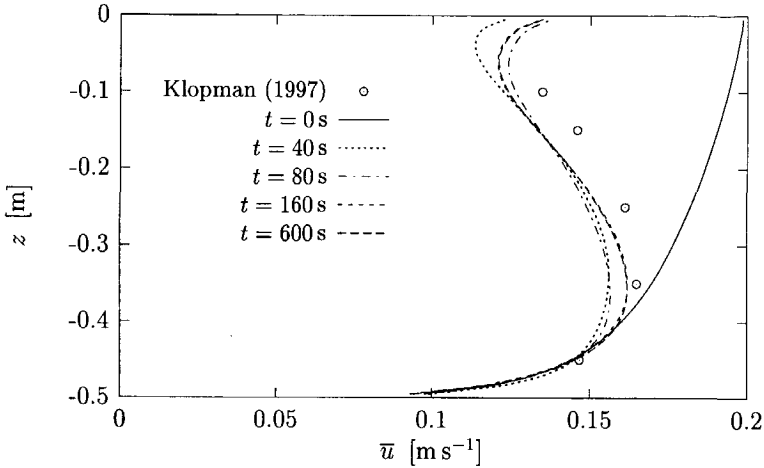


Figure 5.6: Computed and measured vertical profiles of the mean horizontal streamwise velocity in the center of the flume at various points of time (following waves).

are given in figure 5.6. Comparison of the velocity profiles for  $t = 0$  (current alone) and  $t > 0$  exhibits a significant reduction of the mean horizontal velocity towards the free surface. The reduction is even stronger than was measured by Klopman (1997) and predicted by the 1DV model (see figure 4.10) and the model of Dingemans et al. (1996). Near the free surface the velocity is underpredicted by approximately  $1 \text{ cm s}^{-1}$ .

For waves propagating against the current the steady secondary flow is presented in figure 5.7. The vortices rotate opposite to those for the case of following waves. The cell centers are now displaced slightly downward towards the side walls. According to figure 5.8 the measured circulation cells are located in the upper half of the flow, close to the free surface. Despite the fact that the order of magnitude of the lateral and vertical velocity components is predicted correctly, quantitative agreement between these measured and computed velocity components has not been obtained. The 2DV model predicted an upwelling in the center of the flume of at most  $3.3 \text{ mm s}^{-1}$ . This maximum is reached at 22 cm above the bed. The maximal upwelling measured in the center of the flume is at least  $3.5 \text{ mm s}^{-1}$  and is attained at approximately 10 cm below the free surface.

Although the secondary circulations are not predicted correctly, the computed mean horizontal velocity profiles are in good agreement with the measured profiles, as can be seen in figure 5.9. Compared to the situation without waves the mean horizontal velocity reduces near the bed and increases significantly

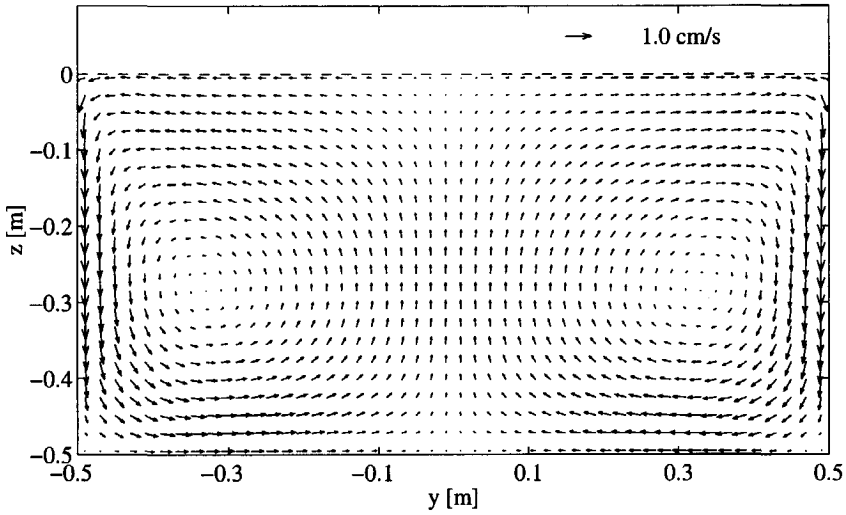


Figure 5.7: Computed mean velocity distribution in cross section for waves opposing the current.

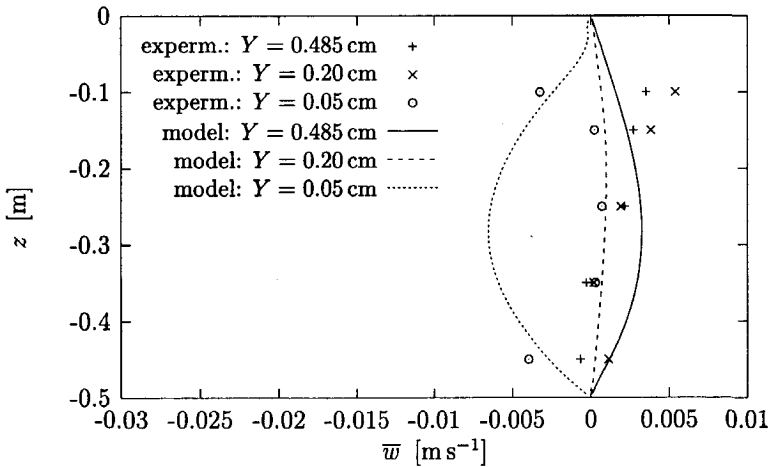


Figure 5.8: Computed and measured (Klopman, 1997) mean vertical velocity profiles at different distances  $Y$  from the side wall (opposing waves).

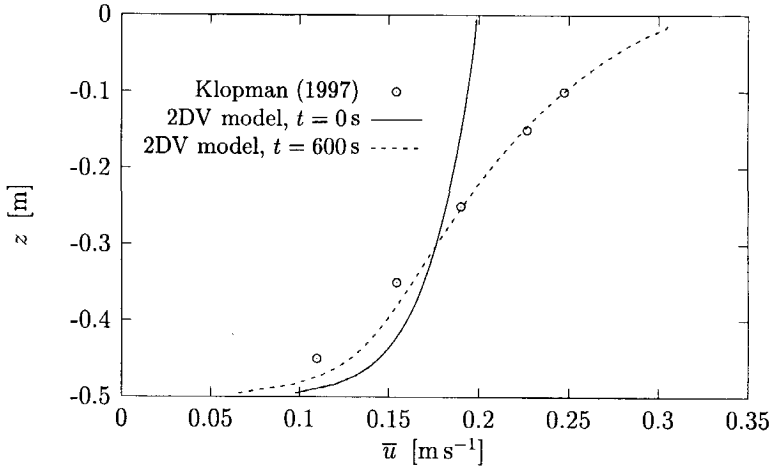


Figure 5.9: Computed and measured vertical profiles of the mean horizontal streamwise velocity in the center of the flume (opposing waves).

towards the free surface. Only near the bed the velocity is overpredicted, by approximately  $1 \text{ cm s}^{-1}$ . The change of  $\partial \bar{u} / \partial z$  just outside the bottom boundary layer is less abrupt than the one that has been measured (see figure 4.10).

#### 5.4.2 Comparison with results 1DV model

To study the effect of the flume width identical situations are considered as in the previous subsection, but now in a 5 m wide flume. The discharge is increased proportionally,  $Q = 0.40 \text{ m}^3 \text{ s}^{-1}$ . In figure 5.10 the computed steady cross-sectional velocity distribution for the situation of waves following the current is given. In view of symmetry only half of the cross section has been plotted. In contrast to the observation of two or more pairs of vortices in the laboratory experiments of Nepf et al. (1995) with breaking waves, only one pair of counter-rotating vortices is predicted. This suggests that the secondary flow in the cross section of the flume is not due to Langmuir circulation and in fact confirms the statements in section 5.1 that a strongly sheared current or instabilities in the wave motion are required for that. Near the side walls the computed vertical velocities in the 5 m wide flume are of the same order of magnitude as those in the 1 m wide flume. However, in the center of the flume the downwelling has decreased significantly and is at most  $1.6 \text{ mm s}^{-1}$ . The cell centers are located approximately 70 cm away from the side wall halfway the water depth. This is relatively farther away from the flume center than in the 1 m wide flume.

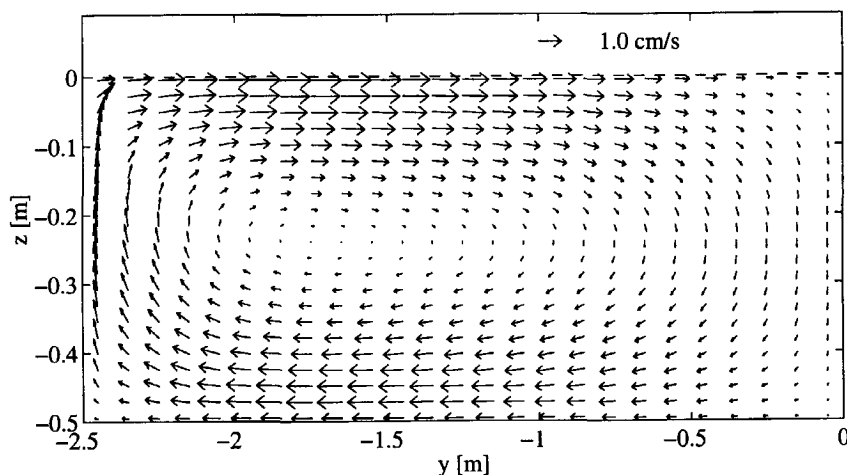


Figure 5.10: Computed mean velocity distribution in the left half of the cross section for waves following the current in a 5 m wide flume.

Our main interest concerns the mean horizontal velocity profile in the center of the flume. The 2DV model result has been compared with the prediction of the 1DV model. Since the velocity distribution is nonuniform in lateral direction, the depth-averaged horizontal GLM velocity computed by the 2DV model is larger than  $0.16 \text{ m s}^{-1}$  in the center of the flume. Therefore, the 1DV model computations have been carried out prescribing a depth-averaged horizontal GLM velocity of  $0.166 \text{ m s}^{-1}$ , being the depth-averaged horizontal GLM velocity in the center flume computed by the 2DV model. The result of the two model computations is shown in figure 5.11. In this figure Klopman's (1997) experimental results from the 1 m wide flume are also plotted. Although a comparison between the measured and computed results is not fully realistic, e.g. the depth-averaged horizontal velocities are different, it exhibits the fact that the reduction of the horizontal velocity towards the free surface is not overpredicted anymore.

Figure 5.12 shows the results for the situation of opposing waves. The secondary circulation consists of two cells for which the centers are located relatively close to the side walls. Once again the vertical velocities near the side walls are comparable to those computed for the 1 m wide flume. The maximal upwelling in the center of the flume is reduced to  $0.3 \text{ mm s}^{-1}$  and can be neglected as such.

The 1DV model has provided the horizontal streamwise velocity with a depth-

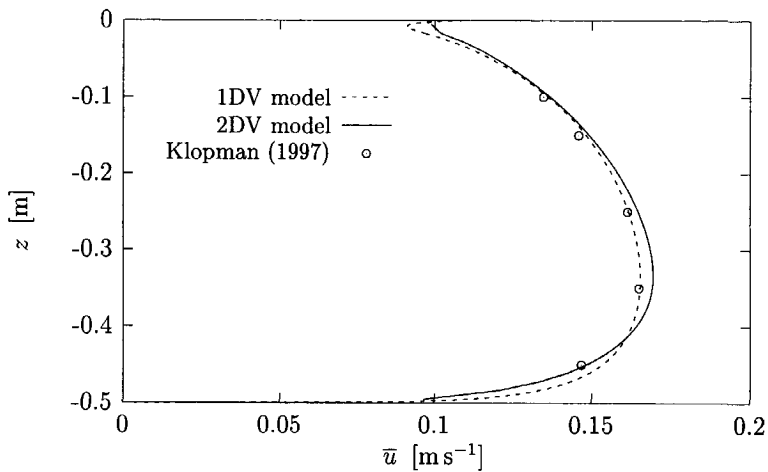


Figure 5.11: Computed mean streamwise horizontal velocity profile in center of a 5 m wide flume for waves following the current.

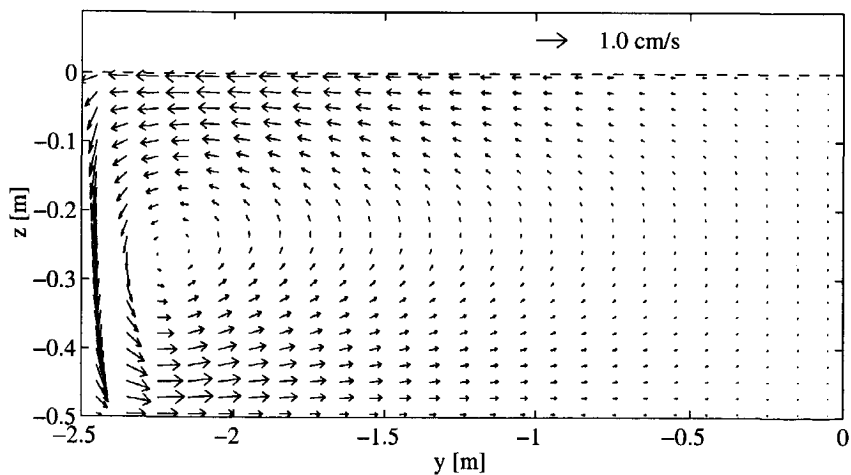


Figure 5.12: Computed mean velocity distribution in a cross section for waves opposing the current in a 5 m wide flume.

averaged value of  $0.181 \text{ m s}^{-1}$ . Comparison with the profile computed by the 2DV model in figure 5.13 shows good agreement between the two profiles. Furthermore, by taking Klopman's (1997) measurements as a reference, comparison of the predicted vertical profiles of the horizontal velocity in the center of the 1 m and 5 m wide flume is possible. The form of both profiles is almost similar. Over the entire depth the horizontal velocity predicted for the 5 m flume is approximately  $0.5 \text{ cm s}^{-1}$  larger than for the 1 m flume.

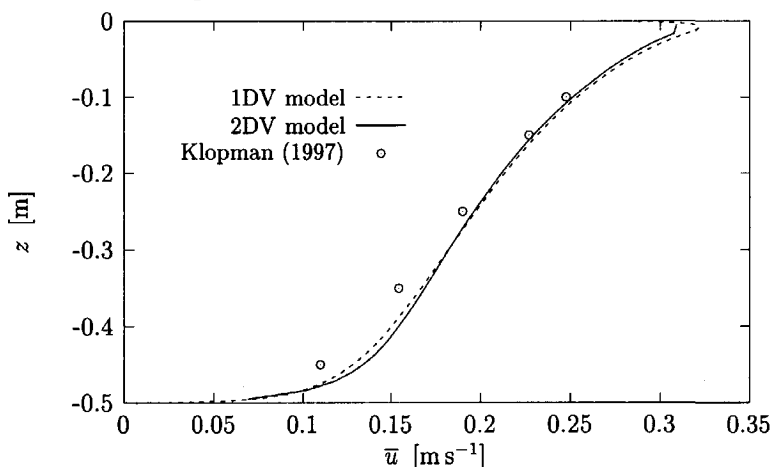


Figure 5.13: Computed mean streamwise horizontal velocity profile in center of a 5 m wide flume for waves opposing the current.

## 5.5 Evaluation of model results

Qualitative agreement between the computed and measured horizontal and vertical profiles of the mean velocity components has been obtained for both situations of waves following and opposing the mean motion. The vertical and lateral components form circulation cells which are rotating in the correct direction. However, quantitative agreement with the measured velocities in the cross sections has not been obtained.

The order of magnitude of the measured circulation velocities is  $1 \text{ cm s}^{-1}$  for both following and opposing waves. For the situation without waves secondary velocities of the same order of magnitude have been measured. Gibson's (1909) explanation for the reduction of the current velocity near the free surface due to secondary circulations also holds for the combined motion of waves on a following current. Low momentum is transported by the secondary motion from the side



wall to the center, and high momentum is moved from the free surface to the bed. The phenomenon that the maximum streamwise velocity does not appear at the free surface, but rather just below it, is often referred as the 'velocity dip', and it is peculiar to currents in open channels.

In the combined motion of waves and currents in a rectangular channel the asymmetry of the turbulent stresses will still appear. In the present 2DV model it has not been taken into account and the circulations are purely caused by the wave-induced driving force. In order to model the secondary circulations properly a turbulence model giving rise to an anisotropic eddy viscosity should be considered.

It is uncertain whether the proposed modification will lead to a correct prediction of the secondary circulations. If the total effect due to the anisotropic eddy viscosity and the wave motion were obtained by a linear combination of these effects, the opposite of the 2DV model predictions should be obtained. For the situation of following waves the two circulation velocities are in the same direction. Inclusion of an anisotropic eddy viscosity in the 2DV model would then result in an even stronger total circulation velocity. On the other hand, there is no evidence that these effects can simply be added and that both effects do not interact. E.g. wave-turbulence interaction has not been taken into account in this study, whereas the asymmetry in the turbulent stresses may very well be influenced by the wave motion. It is out of the scope of this study to investigate wave-turbulence interactions. The aim was to study qualitatively the effect of the secondary circulations on the mean horizontal velocity profile.

Despite the fact that the computations of the secondary circulations have not led to a quantitative agreement with the measured circulations, the computed and measured velocity component in streamwise direction show satisfactory agreement in the center of the flume. For following waves a rather strong overprediction of the downwelling caused an overprediction of the reduction of the horizontal velocity.

In contrast to the 2DV GLM-based model the changes in the horizontal velocity profiles obtained by Dingemans et al. (1996, figure 4) are due to the secondary circulations. For both following and opposing waves the order of magnitude of the circulation velocity is overpredicted by a factor 3 to 4. Despite these strong circulations the obtained reduction of the horizontal velocity in the center of the flume is not as strong as measured for the situation of waves following the current. An overprediction of  $1 \text{ cm s}^{-1}$  to  $2 \text{ cm s}^{-1}$  was obtained. For opposing waves the secondary circulations seem to have hardly any influence, except in the lower part where a reduction is predicted. However, this reduction is not as strong as measured. This change however is partly due to the increase in (apparent) roughness height.

From Dingemans et al.'s (1996) computations and the former GLM results

the conclusion is justified that the secondary circulations have some effect on the ambient current profile. However, the CL vortex force as a sole mechanism for driving the mean motion is insufficient to predict the mean horizontal velocity profiles that have been measured. To achieve this, the driving force requires a significant component in longitudinal direction. To confirm this statement the effect of the side walls, and thus the secondary circulations, has been studied by a simple test. The side walls should have less effect on the mean velocity profile in the center of the flume when a wider flume is considered. The secondary lateral circulations should then decrease in magnitude. Moreover, the 2DV solution should converge to the 1DV solution as  $L \rightarrow \infty$ . Due to some principal differences in the formulation of both models, such as the turbulence model and boundary layer treatment, the results of the 1DV and 2DV computation in a 5 m wide flume are not identical, but the agreement is such that lateral variations seem to have no effect near the flume center.

In so far as comparison between the numerical 2DV model results for a 1 m and a 5 m wide flume is possible, the predicted reduction of the mean horizontal velocity in the center of the flume for the situation of following waves and increase for the opposite case are comparable in magnitude. For the following case the secondary circulation seems to have some influence, whereas it can be neglected for the situation of opposing waves. On the other hand there is a significant difference in the order of magnitude of the circulations near the center. Therefore it is concluded that the effect on the mean horizontal velocity of the longitudinal component of the driving force is dominant over the influence of the cross-sectional part.

## Chapter 6

### Generalization to 3D

For applicability in the coastal regions, the three-dimensional structure of the wave-induced currents has to be taken into account. If e.g. the wave-induced cross-shore sediment transport is considered, descriptions of the near-bed current velocity based on a 2D depth-integrated model will fail. On the other hand 2D-vertical models will not produce satisfactory solutions for lack of longshore information. Improved predictions will be obtained by quasi-3D models. In these models 3D current fields are described by coupling a 1DV and 2D depth-integrated model. So far, only few quasi-3D models are able to describe nearshore currents. The advantage of quasi-3D over fully-3D models is that their computational effort is relatively small. However, time-dependent and detailed spatial information obtained from fully-3D models cannot be provided by quasi-3D models.

The final goal of the present research programme is to develop a GLM-based model for 3D wave-induced currents in coastal areas. In these areas the waves could be either breaking or non-breaking, regular or irregular and the velocity distribution of an ambient current could be arbitrary in both horizontal and vertical direction. In this chapter several points are mentioned that have to be considered attentively to reach the goal just mentioned. In fact, they should be looked upon as recommendations for future study. Furthermore, the proposed ideas are compared with formulations that form the basis of wave-current interaction modelling in existing 3D and quasi-3D models. Some of those are reviewed briefly in the next section.

#### 6.1 Existing quasi-3D and fully-3D models

Ten years ago computers were not able to carry out the computations that are performed nowadays. Therefore the evolution first passed quasi-3D models before moving on to fully-3D. To describe the nearshore circulation several aspects in

the model have to be taken into account.

A wave model is required to determine the associated fluxes of mass, momentum and energy and other wave characteristics to determine the wave-induced driving force for the mean motion. In the surf zone a breaking model has to be implemented as well. Moreover, wave breaking significantly increases the turbulent mixing process. Therefore, its effect on the turbulence quantities have to be reflected. In the following subsections the incorporation of these effects in the various quasi-3D and 3D models is discussed.

### 6.1.1 Quasi-3D models

In general quasi-3D models combine the effect of the vertical structure by means of a 1DV model and a 2DH circulation models. This requires splitting of the velocity field. The models are characterized by their splitting procedure.

De Vriend & Stive (1987) introduced a primary current field, driven by waves and wind. The primary velocity is defined as the product of the depth-averaged horizontal velocity and a shape function describing the variation of the velocity along the vertical, which is independent of the location in the horizontal plane. This result combined with the presence of vertical imbalances, e.g. between momentum fluxes due to convection and hydrostatic pressure, is used to calculate a secondary current field, which in general is vertically nonuniform in both magnitude and orientation. Sanchez et al. (1990, 1992) split the current velocity into a depth-uniform and depth-varying component, the latter yielding a zero mean when integrated from bed to trough level. A similar approach was used in the time-dependent SHORECIRC model, originally presented by Svendsen & Putrevu (1990). A review of the physical concept of this model can be found in Svendsen & Putrevu (1996). Van Dongeren & Svendsen (1997) also treated the numerical solution techniques. The model is based on an analytical solution for the 3D current profiles in combination with a numerical solution of the depth-integrated 2D equations.

The quasi-3D models mentioned here considered the time-dependent, nearly hydrostatic, wave- and turbulence-averaged flow equations. Determination of the vertical structure of the mean flow strongly depends on the type of splitting of the velocity. Each model used a different wave model. However, they all reproduced refraction, shoaling, diffraction and breaking phenomena, including rollers. Consequently, the fluxes of mass, momentum and energy, as well as the wave-induced driving forces can be computed in the locations of interest.

In all models the depth-integrated mass and momentum equations have been exploited to obtain the 2D horizontal distribution of the current. The main part of the driving forces for the current was formed by the gradient of the radiation stresses. De Vriend & Stive (1987) followed Dingemans et al. (1987)

who expressed these gradients in terms of energy dissipation of breaking waves. Sánchez-Arcilla et al. (1992) determined the radiation stresses using the classical expressions of Longuet-Higgins (1970). They calculated the correlation between the horizontal and vertical wave velocity components according to Rivero & Sánchez-Arcilla (1995), whereas other models neglected this term. In the *SHORECIRC* model the radiation stress components are expressed in terms of wave quantities like wave height and wave direction using potential wave theory. The REF/DIF wave model (Kirby & Dalrymple 1994), based on the mild-slope equations, is applied to determine these location-dependent wave quantities. To obtain the driving force, gradients of the radiation stress components and thus of the wave heights and directions have to be determined.

In order to determine the vertical distribution of the flow all models have exploited a three-layer concept. De Vriend & Stive (1987) considered the region below wave trough level for the determination of the secondary current profile. The effect of the surface layer on the layer below was taken into account via an effective shear stress at trough level and via the condition that the net undertow must compensate for the mass flux in the surface layer. The secondary current model induced by nonbreaking waves is very much like Longuet-Higgins' (1953) conduction solution for progressive waves.

For breaking waves the concept is the same as proposed by Stive & Wind (1986), but the elaboration is somewhat different. Mass fluxes consist of contributions due to the progressive character of the breaking waves and to the surface roller (Svendsen 1984b). Notice that the depth-invariant driving force for the primary current not necessarily cause the velocity profile to be uniform over depth. For the situation without waves a logarithmic profile, typical for open channel flow, will be obtained. De Vriend & Stive (1987) inferred that their model required a more detailed investigation of the bottom boundary layer for the current under breaking waves.

Sánchez-Arcilla et al. (1992) matched the bottom boundary layer solution and the middle layer solution. The former is based on Fredsoe's (1984) formulation assuming logarithmic velocity profiles for both waves and currents. The solution in the middle layer is dominated by wave-induced and turbulence-induced effects. The matching conditions indicated continuity of current velocity and shear stress.

In the *SHORECIRC* model (Van Dongeren & Svendsen 1997) the computational domain is defined as the region between the wave boundary layer and the mean water level. In the computations the total mass flux due to waves and current is considered. Only if the depth-integrated current velocity is required, the wave-induced mass flux being nonzero above trough level is considered. Furthermore, the bottom friction is modelled using a weak-current assumption (Liu & Dalrymple 1978), whereas the cross-shore velocity is assumed to be nearly parallel to the short-wave groups. A semi-analytic solution for the velocity distribution

along the vertical is given in terms of short-wave forcing, bottom friction and variables determined from the depth-integrated equations.

All models applied Boussinesq's eddy-viscosity hypothesis and used existing formulations for the eddy-viscosity distribution, which accounted for turbulence induced by purely slope-driven currents, wind-driven currents and breaking waves. In the middle layer and bottom boundary layer De Vriend & Stive (1987) prescribed different but constant eddy-viscosity profiles. Roelvink & Reniers (1994) suggested an improved distribution by prescribing parabolic profiles of the eddy viscosity in both layers. This is more realistic for general 3D flow. Sánchez-Arcilla et al. (1992) also considered a parabolic eddy-viscosity profile as the result of the summation of the current- and breaker-induced eddy viscosity. As in the other models Van Dongeren & Svendsen (1997) allowed the eddy viscosity to vary in horizontal direction and assumed it to be constant over the vertical.

The current-current and current-wave interactions have mostly been neglected in the models described above. Only in the SHORECIRC model it has been accounted for in an intermediate step. Svendsen & Putrevu (1994) recognized that these interactions induce a nonlinear dispersion mechanism, which increases lateral mixing significantly.

### 6.1.2 3D models

The problems that are characteristic for quasi-3D models, like the splitting of the velocity field, do not appear in models concerning the combined flow of waves and currents in all three dimensions. To the author's knowledge the only operational model is the TELEMAC-3D model of Péchon & Teisson (1994). At this moment Delft Hydraulics is also developing a 3D model for describing the motion in the surf-zone (Walstra 1999). The model is based on the 2DV model presented by Walstra et al. (1994) and the mathematical formulation of a 3D hydrostatic current model by De Vriend & Kitou (1990). It has been implemented in the numerical flow solver DELFT3D-Flow (TRISULA).

Péchon & Teisson (1994) considered the time-mean Navier-Stokes equations, containing the radiation stresses. The effect of breaking waves on the radiation stresses was modelled by means of the wave energy dissipation formulation of Dingemans et al. (1987). The waves were assumed to be regular. The contribution of nonbreaking waves was not included. The mixing of momentum induced by turbulent fluctuations was modelled by the eddy viscosity concept. A uniform eddy-viscosity distribution expressed in terms of the dissipation rate of the total energy due to bed friction and breaking was implemented. Furthermore, the roller contribution was expressed by approximating the horizontal velocity profile as suggested by Svendsen (1984a). In contrast to quasi-3D models of De

Vriend & Stive (1987) and Sánchez-Arcilla et al. (1992) the computational domain stretches up to the mean water level. The total flux of momentum due to breaking waves has been specified through the radiation stress and is distributed uniformly from the bed to the wave trough and increases above trough level due to drag from the roller. The shear stress at the free surface has been set to zero. The estimation of the bed shear stress was obtained by a quadratic stress law and the friction coefficient was enhanced by wave effects according to Soulsby et al. (1993).

In the Delft Hydraulics model (Walstra 1999) the depth is divided into a number of layers, indicating the vertical resolution in the numerical solver for hydrostatic flow. The trough-crest region is a separate layer. The time-averaged Reynolds equations are integrated over these layers. This integration procedure leads automatically to the inclusion of wave effects. The mass flux is taken into account implicitly by considering the total mass flux, i.e. the sum of the depth-averaged Eulerian mean flow and the wave-induced mass flux, as a dependent variable. At first the mass flux was conceived as taking place above the computational domain. Recently, the mass flux has been related to a nonuniform vertical distribution as well. As a first guess the distribution of the Stokes drift, derived from potential wave theory, was implemented. The bed shear stress was assumed to depend on the mean motion through the 'Eulerian' part of the velocity (see also Battjes, 1988, p.274). After all, the flow in the bottom boundary layer does not directly depend on the wave-induced mass flux. Due to the layer approach the wave-induced current forcing has a nonuniform vertical distribution. The driving force has been given by gradients of radiation stresses. These have been formulated in terms of wave-energy dissipation rate. The HISWA wave model (Holthuijsen et al. 1989) has been applied to determine the required wave characteristics. The energy dissipation due to breaking waves has been modelled following Battjes & Janssen (1978). Furthermore, a roller concept contributes to the wave-averaged fluxes of mass, momentum and energy. A  $k - \epsilon$  turbulence model has been implemented in order to obtain the eddy-viscosity distribution. To incorporate the effects of breaking waves on the turbulence, the dissipation of wave energy was introduced as production term in the transport equations for both the turbulent kinetic energy and energy dissipation  $\epsilon$ . A similar approach was applied successfully by Wind & Vreugdenhil (1986).

Both models have been validated against real-life situations. Péchon & Teisson (1994) computed cross-shore currents in a flume, 3D circulation along a rectangular beach and currents near a detached breakwater. Although the results are promising, especially with respect to the flume experiments, more research is required on the representation of the wave-induced driving forces. These are overpredicted due to an oversimplified description of the instantaneous wave orbital velocity in the surf zone.

The DELFT3D-Flow model is the most extensive model and uses state-of-the-art wave and turbulence models and other related formulations. Nevertheless, the implementation of the short-wave effects on the 3D mean flow distribution in the DELFT3D-Flow model and the associated validation and verification process are still in a preliminary state. So far the model has only been tested against flume experiments.

## 6.2 Towards a 3D model in GLM formulation

So far the GLM formulation has been applied only in a 1DV and a 2DV perspective for the combined motion of a turbulent current and regular nonbreaking waves propagating in the same or opposite direction. For generalization to a fully-3D model, that is capable of computing nearshore circulation patterns, several aspects have to be considered carefully. First of all a suitable wave model must provide wave characteristics for the evaluation of wave-induced driving forces for the mean motion. For applicability in coastal areas the wave field can no longer be considered regular. The presence of an ambient current under an arbitrary angle should be accounted for. Furthermore, a breaker model must be implemented not only to predict the wave height after breaking, but also to determine the increase of turbulent mixing.

Three important subjects for further research are being discussed in more detail, viz. wave modelling with special attention for breaking waves, a possible generalization of the existing models to a fully-3D GLM model and some additional applications.

### 6.2.1 Modelling of wave motion

Complete 3D wave-induced driving forces have been derived in terms of wave-related quantities in chapter 3. In a 3D description of the total flow, not only quantities such as wave energy and wave height are required, but also the vertical structure of the wave velocity fields in the presence of an ambient current.

Here a quasi-3D approach for the wave motion is proposed. In typical applications, the wave height distribution over a horizontal spatial area has to be found by application of some wave energy model, e.g. the SWAN model (Booij et al., 1999 and Ris et al., 1999). The present study has shown that the vertical structure of the internal velocity field does not simply follow from potential flow theory, but has to take account of the ambient current. In order to find the pertinent vertical structure, resource has to be made to a 2DV model of wave-current interaction. As already mentioned before, the 1DV model developed in this study could be applied in the main-wave direction at each location in the 2DH wave



amplitude field as results from a wave energy model. This also means that the breaking model in the wave energy model is responsible for the amplitude field shoreward of the breaker line.

Instead of applying the 1DV model for a complete spectrum of wave frequencies, vertical distributions obtained with the peak frequency and rms wave height or significant wave height as input parameters might as well be suitable. Before applying the 1DV GLM-based model in the coastal area, one first has to investigate whether the assumptions made in the GLM theory are still valid for the entire region of interest. Strictly, the GLM theory can be applied as long as a displacement vector  $\xi$  can be defined with zero mean. Outside the surf zone, where depth-induced breaking has not taken place, the assumptions for the applicability of the GLM theory are fulfilled. From a conceptual point of view a meaningful relation between the fluctuations such as the displacement vector and the Eulerian point  $x$  only exists if  $|\xi|$  is fairly small. Therefore, the motion under breaking waves, including the onset of breaking, and a turbulent bore, in which the breaking waves transform onshore, have to be regarded critically.

### 6.2.2 Modelling of 3D wave-induced currents

The 3D wave-induced current motion is described by the 3D equations in chapter 3. To close these equations several quantities must be evaluated. First of all the wave-induced driving force must be determined from information provided by some wave model (see subsection 6.2.1). Secondly, a turbulence model must provide the information about the turbulence characteristics in the region of interest. Thirdly, the influence of the waves on the bed shear stress has to be accounted for and finally, the numerical implementation in a 3D solver for either hydrostatic or non-hydrostatic flow has to be carried out. These aspects will be discussed briefly.

In coastal areas the depth is not horizontally uniform. Due to depth-induced breaking, wave energy dissipation is a dominant factor in the surf zone. Therefore, the gradient of the wave radiation stress,  $\partial (\langle u^\ell u^\ell \rangle - \langle w^\ell w^\ell \rangle) / \partial x$ , plays an important role in this area, in contrast to the coastal region outside the surf zone. Furthermore, the role of the wave-induced shear stress  $\langle u^\ell w^\ell \rangle$  should be emphasized. In most nearshore circulation models this term was neglected. For both harmonic and broken waves De Vriend & Kitou (1990) stressed the importance of this term, which was shown to play an essential part in the consistency of the model. This was confirmed by the analysis of the wave-induced driving force in section 4.5.

In the 3D model of P  chon & Teisson (1994) both wave radiation stress and wave-induced shear stress have been taken into account and both are directly related to wave energy dissipation using wave potential theory (Longuet-Higgins

1970). In the DELFT3D-Flow model the wave-induced shear stress has been neglected whereas the wave radiation stress gradient is expressed in terms of the wave dissipation following Dingemans et al. (1987). Stive & Wind (1986) showed that the wave-induced stress terms are hardly varying over depth, as far as they are due to breaking waves. If this would also hold for the wave-induced driving terms in a GLM setting there might be a possibility to express these driving forces in terms of wave characteristics such as wave energy dissipation. However, interaction with an arbitrarily distributed ambient current will cause vertical variations in the wave-induced driving terms.

For the implementation of a turbulence model the effect of waves on turbulence has to be taken into account in the 1DV and the 2DV model. In the region outside the surf zone the nonbreaking waves affect near-bed motion and bed shear stress and to some extent the turbulence above the wave boundary layer. An additional production of turbulence is introduced by breaking waves, which has to be accounted for in the 3D model. This influence extends not only in vertical direction but in horizontal direction as well. In the transition zone, where waves start breaking, there is a transformation of organized motion, through overtopping and roller formation, into turbulence. The  $k - \varepsilon$  turbulence model implemented in the model of Delft Hydraulics (Walstra 1999) seems a reliable option, in particular because the three situations above have been distinguished. Breaking and nonbreaking wave effects are included. This concept has been validated and verified in a 2DV surf-zone model (Walstra et al. 1994).

In the 2DV model given in chapter 5 the bed shear stress was influenced by the wave motion by means of Grant & Madsen's (1979) formulation. Many formulations for the bed shear stresses due to waves and currents have been suggested so far, see e.g. Soulsby et al. (1993), Davies & Villaret (1997). The bed shear stress depends quadratically on the two-dimensional friction velocity, which is determined by the current velocity and the orbital velocity. As shown in appendix C.1 for Grant and Madsen's formulation the angle between both velocity components is important and should therefore be accounted for.

In general, oblique incident waves in the surf zone induce currents with a typical three-dimensional vertical profile. Depending on the bathymetry both longshore and cross-shore velocity components are significant. Whereas longshore uniformity is required in 2DV cross-shore models and a vertical distribution lacks in a 2DH description of the motion, the three-dimensional model will provide wave-induced or wave-affected three-dimensional current velocity profiles.

The basic form of the 3D equations in GLM and Eulerian setting are similar. Therefore, as long as the hydrostatic flow assumption is valid any numerical hydrostatic flow solver can be used to predict the GLM flow. The numerical solver developed by Van Kester et al. (1996), which has been used here to solve the 2DV GLM-based equations, is in fact a 2DV version of the numerical solver

DELFT3D-Flow. The former was extended for allowing the pressure to be non-hydrostatic, whereas the latter only handles hydrostatic flow. In the shallow regions of the coastal area the non-hydrostatic part is often neglected. In some situations the non-hydrostatic part of the pressure might be significant to the prediction of the mean flow field. Then a numerical model for 3D non-hydrostatic flow would be required. The pressure-correction method applied to 3D flow by Casulli & Stelling (1998) might be suitable. However, for large regions of interest the computational time may be enormous.

### 6.2.3 Possible applications of 3D GLM-based model

For validation and verification as well as for possible applications of the 3D model a number of practical situations that could be considered are listed.

The various formulations in the turbulence model and the wave-induced driving forces for breaking and nonbreaking waves must be validated. First of all one could think of the validation of the model under well-controlled circumstances as wave-current channels (2D) or basins (3D). A number of flume experiments have already been mentioned in previous chapters. Among those, boundary layer streaming should be considered, since the situation of waves in a flume without ambient current is in fact a limit situation. A first verification could be carried out by using field observations of a three dimensional circulation along a rectilinear beach. Furthermore, interpretation and validation of the 3D results is possible by deriving 2DV and 2D depth-averaged (2DH) quantities and compare these with corresponding quantities derived from existing 2DV or 2DH models, like those listed in section 1.2. Finally, for the specific situation just mentioned model results might be compared with results obtained with the quasi-3D models listed in subsection 6.1.1 and the 3D models of P  chon & Teisson (1994) and Delft Hydraulics (Walstra 1999). These models have already been tested for some 2D and 3D situations. Performing the same tests would therefore be advisable.

Important phenomena of 3D wave-induced flow in the nearshore region may be analyzed using measurements, physical knowledge and numerical modelling. Dependent on the availability of the field data one could think of rip currents, 3D flow around breakwaters and 3D flow in estuaries. In the end the developed flow model might be coupled to a model for the morphodynamics. At this point the GLM setting is relevant, because Lagrangian velocities might be more useful in describing transport of sediment and suspended material than Eulerian velocities.

Situations occurring outside the coastal area could be considered as well. For the verification of the 1DV and 2DV model, interactions between waves and a horizontally uniform current with a logarithmic velocity distribution have been examined only. Several other features of the mean motion could be considered

as well, such as a strongly sheared wind-driven current. It is a priori not clear what would be the influence of this current on the wave motion, and vice versa, the return influence of the current-affected wave motion on the initial current. Among others the stream function solution of Swan (1992) and his flume data concerning regular (Swan 1990) and irregular waves (Cummins & Swan 1994) may be used for model validation and verification.

A typical product of wave-current interactions in open seas and large lakes are Langmuir circulations. Although they were not observed in the 2DV model results for the flume experiments, they might be predicted by a 3D model. The results can be compared e.g. with observations in the upper ocean by Smith (1992) or Weller & Price (1988).

# Chapter 7

## Conclusions and recommendations

### 7.1 Introduction

The aim of this work was to apply the GLM theory to water wave-current problems and to gain more insight in the mechanism responsible for wave-induced changes in current profiles and the effect of a current on the orbital quantities. Two types of models have been developed describing the combined motion of regular, nonbreaking waves and an ambient current. In the 1DV model, based on the WKBJ perturbation series approach, lateral variations have been neglected. In the 2DV model the side-wall effects have been taken into account. Comparison of the model results enables the quantification of the role of secondary circulations on the current profile changes.

### 7.2 Conclusions

From the present study the following conclusions are drawn, based on:

#### 1DV model

- The WKBJ approach applied in this study is valid for the type of problems that are of interest for this study, viz. regular, nonbreaking waves on a relatively weak current.
- In the limit situation of no ambient current the inclusion of harmonics higher than only the first might be required at first order, in order to be able to determine the correct mass transport velocity profiles.

- GLM-model predictions of the mass transport velocities perfectly agree with Longuet-Higgins' analytical conduction solution. Neglect of nonlinear convective terms seems to be the reason for the mismatch between the computed and measured wave-induced mass transport velocity in very shallow and very deep water.
- For both situations of a following and an adverse current, the vertical distribution of the amplitude functions of the orbital velocity components are in good agreement with the measured orbital velocity profiles of Klopman (1994).
- For waves following an ambient current the observed reduction of the mean horizontal velocity in the upper part of the vertical has been predicted correctly. The same holds for the strong increase of the vertical gradient of the mean horizontal velocity in the entire region above the wave boundary layer for opposing waves. The obtained model results were in good agreement with Klopman's (1994) experimental data.
- Evaluation of the wave-induced driving forces showed that the wave-induced shear stress, due to phase shifting in the bottom boundary layer, vorticity transfer from the current to the wave motion and wave height decay, the wave-induced normal stress and Stokes correction of the shear stress, resulting from the oscillating part of the shear stress, are dominant terms in the wave-induced driving force for the mean motion. Following Nielsen & You (1996) a local force balance proved that the second-order changes in the mean horizontal velocity profile, or more precisely in the current shear stress, are due to a combination of these wave-induced stress terms.
- Application of the time- and wave-independent eddy-viscosity profile, resulting from the strongly simplified  $k - \ell$  turbulence model, as a closure for the first-order first-harmonic problem results in vertical distributions of the wave-induced shear stress and the Stokes correction of the shear stress that are significant over the entire depth. Current-induced turbulence affects the wave motion not only in a small boundary layer near the bed and the free surface, but in the interior region as well.

## 2DV model

- Theoretical and experimental studies have demonstrated the presence of secondary circulations in flows without surface waves in straight laboratory channels. The concept of isotropic eddy viscosity, such as assumed in the  $k - \varepsilon$  turbulence model, can not produce those secondary currents.

- Using a 2D-GLM model, qualitatively correct distributions of the secondary circulations, consisting of two counter-rotating vortices, have been obtained for both situations of waves following and opposing the current. Although the order of magnitude of the maximum velocities agree, the predicted positions of the cell centers do not. The orders of magnitude of the circulations in the situations with and without waves are comparable. Therefore, in the presence of waves the secondary circulations are caused both by the waves and the asymmetry in the Reynolds stresses. However, the latter part has not been taken into account in the model, neither are the effects of wave-turbulence interaction. Beforehand it is not clear whether the asymmetries in the Reynolds stresses are increased or reduced by the presence of the wave motion.
- For following waves a reduction of the mean horizontal velocity in the center of the flume has been predicted, being stronger than measured by Klopman (1997). This is due to an overprediction of the downwelling in the center of the flume. The upwelling in the flume center has not been overpredicted for opposing waves. The mean horizontal velocity profile is in good agreement with the measured profile.
- Comparison between the results of the 2DV model based on the CL vortex force (Van Kester et al. 1996) and the 2DV GLM-based model proves that secondary circulations cannot be ruled out in laboratory experiments such as Kemp & Simons (1982, 1983) and Klopman (1994, 1997). However, the CL theory is insufficient to predict the observed velocity profile changes.
- The CL2 theory states that Langmuir circulation is the result of an instability of the mean flow with a Stokes drift in flow direction. This theory excludes instability when waves are propagating opposite to the mean flow direction. However, both experiments (e.g. Klopman, 1997) and simulations (this thesis and Van Kester et al., 1996) show vortex pairs irrespective of the wave propagation direction. It is concluded that the appearance of secondary circulations is due to the addition of the CL vortex force, or more general the lateral and vertical components of the GLM wave-induced driving force, but not due to the CL1 or CL2 mechanisms. If either one of the theories is used to define Langmuir circulation, then the measured and computed circulations in a laboratory channel can not be called Langmuir circulations.

### General

- From the 1DV and 2DV model results the conclusion is drawn that an explanation for the wave-induced changes in the mean horizontal velocity

profile can be found in the interplay between the wave-induced shear stress and the Stokes correction of the shear stress, both acting in longitudinal direction. These effects are dominant over the transport of longitudinal momentum by the secondary circulations.

## 7.3 Recommendations

### General

- The GLM flow equations in the 1DV and 2DV model are accurate up to second order. For the problems that have been considered in the present study this accuracy is sufficient. If nonlinearity effects are important or if a relatively strong current is considered, higher order approximations are required. The entire derivation has to be carried out once again. Alternatively, the GLM equations derived by Andrews & McIntyre (1978*a*) are exact for inviscid flow. If higher order approximations are required for viscous flow, only the shear stress terms have to be adjusted. However, as explained in section 3.1 this is a rather tedious task. Further research is required to find out which approach is most suitable for higher order approximations of the solutions sought.
- Numerical aspects have not been investigated here. In order to improve the model effectiveness and efficiency from a numerical point of view other and higher order numerical schemes have to be considered. Furthermore, optimization of the grid resolution and time step, for the 2DV model, will lead to improvements in accuracy and/or computational time. In the present 2DV model the wave-induced driving force has been taken into account explicitly in each time step. A more stable solution will be obtained if those terms containing GLM quantities were solved implicitly.
- In order to be valid for strong current applications and boundary layer streaming problems the WKBJ perturbation series should take more harmonics into account. Experimental data are available for validation and verification purposes.
- To obtain more reliable results in the wave boundary layer for e.g. bed shear stress and the velocity profiles, the turbulence model has to be extended with an oscillatory component that depends on the wave motion and/or is time-dependent. The wave-part of the turbulence kinetic energy is expected to be concentrated in the bottom and the free-surface layers and to be small in the interior region. It will be interesting to see its influence on the wave-induced driving force.



## 2DV model

- The turbulence model should be adapted such that asymmetries in the turbulent stresses are accounted for. This is not only to produce secondary currents in a flow without waves, but also to obtain quantitatively better predictions of the secondary circulations in the presence of waves. This is also useful in a 3D model, when this is applied to determine secondary currents in a flume.
- The solution of the wave-related quantities in the side-wall boundary layer, as presented in chapter 5, depends on a constant eddy-viscosity coefficient. It is more realistic to prescribe a distribution of the eddy viscosity that increases linearly from the side wall and is e.g. parabolic in vertical direction. Another option is to apply the 2DV eddy-viscosity profile related to the mean motion. This is comparable to the approach in the 1DV model.
- Presently, the  $k - \varepsilon$  turbulence model has been applied using partial-slip conditions based on shear stress and boundary conditions for log-law boundary layer velocity profiles. Having several grid points in the wave boundary layer, computations have been carried out in the viscous sub-layer as well. The logarithmic law-of-the-wall formulation is not valid in this region. In order to predict the turbulent motion correctly, a different approach must be followed. For this purpose Van Kester et al. (1996) proposed a so-called low Reynolds number  $k - \varepsilon$  turbulence model which allows for solving the velocity profile down to the wall. Then a no-slip condition can be applied at the wall, similar to the 1DV model at the bottom (see chapter 5).
- If one persists in imposing partial-slip conditions, the sensitivity of the bed shear stress formulations for the combined wave-current motion in general and the secondary circulations in particular should be considered carefully. Several boundary layer models have been developed in the past decades and can be implemented to gain more insight in the influence of the friction formulations.
- Unfortunately only few measurements of the cross-sectional velocity distribution of wave-induced currents have been carried out so far. Especially near the side wall there is a lack of experimental data. Also for validation of the computed side-wall shear stresses a larger set of data is desirable.

**3D model**

- In order to develop a complete model in the GLM formulation that describes the three-dimensional character of the combined motion of waves and currents in the coastal area, closure criteria for the fluxes of mass, momentum and energy, as well as the wave and turbulence characteristics have to be validated and verified against laboratory and field data and existing model results. These models may be either 3D, quasi-3D, 2D vertical, 2D horizontal or even 1DV. Recommendations to achieve this goal have been listed in chapter 6.

## References

- Andrews, D.G. & McIntyre, M.E. (1976), Planetary waves in horizontal and vertical shear: The generalized Eliassen-Palm relation and the mean zonal acceleration, *J. Atmos. Sci.* **33**(11), 2031–2048.
- Andrews, D.G. & McIntyre, M.E. (1978*a*), An exact theory of nonlinear waves on a Lagrangian-mean flow, *J. Fluid Mech.* **89**(4), 609–646.
- Andrews, D.G. & McIntyre, M.E. (1978*b*), On wave-action and its relatives, *J. Fluid Mech.* **89**(4), 647–664.
- Bakhmetev, B.A. (1932), *Hydraulics of open channels*, McGraw-Hill.
- Bakker, W.T. & Van Doorn, T. (1978), Near-bottom velocities in waves with a current, in 'Proc. 16th Int. Conf. on Coastal Engng, Hamburg, Germany', ASCE, New York, pp. 1394–1413.
- Battjes, J.A. (1988), Surf-zone dynamics, *Ann. Rev. Fluid Mech.* **20**, 257–293.
- Battjes, J.A. & Janssen, J.P.F.M. (1978), Energy loss and set-up due to breaking of random waves, in 'Proc. 16th Int. Conf. on Coastal Engng, Hamburg, Germany', ASCE, New York, pp. 569–587.
- Battjes, J.A., Sobey, R.J. & Stive, M.J.F. (1990), *Nearshore circulation*, Vol. 9A of *The Sea, Ocean Engng Science*, Wiley, New York, pp. 467–493.
- Booij, N., Ris, R.C. & Holthuijsen, L.H. (1999), A third-generation wave model for coastal regions. Part 1: Model description and validation, *J. Geophys. Res.* **104**(C4), 7649–7666.
- Borgman, L.E. (1990), *Irregular ocean waves: Kinematics and forces*, Vol. 9A of *The Sea, Ocean Engng Science*, Wiley, New York, pp. 121–168.
- Bowen, A.J. (1969), The generation of longshore currents on a plane beach, *J. Marine Res.* **27**, 206–215.

- Bowen, A.J., Inman, D.L. & Simmons, V.P. (1968), Wave 'set-down' and set-up, *J. Geophys. Res.* **73**(8), 2569–2577.
- Bretherton, F.P. (1971), The general linearised theory of wave propagation, *Lectures Appl. Math.* **13**, 61–102. American Math. Soc.
- Bretherton, F.P. & Garrett, C.J.R. (1968), Wavetrains in inhomogeneous moving media, *Proc. Royal Soc. London* **A302**, 529–554.
- Bühler, O. & McIntyre, M.E. (1998), On non-dissipative wave-mean interactions in the atmosphere or oceans, *J. Fluid Mech.* **354**, 301–343.
- Casulli, V. (1995), *Recent developments in semi-implicit numerical models for free-surface hydrodynamics*, Vol. 2 of *Advances in Hydrosience and Engng*, Tsinghua University Press, Beijing, China, pp. 2174–2181.
- Casulli, V. & Stelling, G.S. (1998), Numerical simulation of 3D quasi-hydrostatic, free-surface flows, *J. Hydraulic Engng* **124**(7), 678–686.
- Christoffersen, J.B. & Jonsson, I.G. (1985), Bed friction and dissipation in a combined current and wave motion, *Ocean Engng* **12**(5), 387–423.
- Chu, V.H. & Mei, C.C. (1970), On slowly-varying Stokes waves, *J. Fluid Mech.* **41**(4), 873–887.
- Craik, A.D.D. (1977), The generation of Langmuir circulations by an instability mechanism, *J. Fluid Mech.* **81**(2), 209–223.
- Craik, A.D.D. (1982a), The drift velocity of water waves, *J. Fluid Mech.* **116**, 187–205.
- Craik, A.D.D. (1982b), The generalized Lagrangian-mean equations and hydrodynamic stability, *J. Fluid Mech.* **125**, 27–35.
- Craik, A.D.D. (1982c), Wave-induced longitudinal-vortex instability in shear flows, *J. Fluid Mech.* **125**, 37–52.
- Craik, A.D.D. & Leibovich, S. (1976), A rational model for Langmuir circulations, *J. Fluid Mech.* **73**(3), 401–426.
- Cummins, I. & Swan, C. (1994), Vorticity effects in combined waves and currents, in 'Proc. 24th Int. Conf. on Coastal Engng, Kobe, Japan', ASCE, New York, pp. 113–127.

- Davies, A.G. & Villaret, C. (1997), *Oscillatory flow over rippled beds: Boundary layer structure and wave-induced Eulerian drift*, Gravity waves in water of finite depth, Vol. 10 in series Adv. in Fluid Mech., Computational Mech. Publ., pp. 215–254.
- De Vriend, H.J. & Kitou, N. (1990), Incorporation of wave effects in a 3D hydrostatic mean current model, in 'Proc. 22nd Int. Conf. on Coastal Engng, Delft, The Netherlands', ASCE, New York, pp. 1005–1018.
- De Vriend, H.J. & Stive, M.J.F. (1987), Quasi-3D modeling of nearshore currents, *Coastal Engng* **11**(5/6), 565–601.
- Deigaard, R. & Fredsøe, J. (1989), Shear stress distribution in dissipative water waves, *Coastal Engng* **13**, 357–378.
- Dewar, R.L. (1970), Interaction between hydromagnetic waves and a time-dependent, inhomogeneous medium, *Phys. Fluids* **13**(11), 2710–2720.
- Dingemans, M.W. (1997), *Water wave propagation over uneven bottoms*, World Scientific, Singapore. Part 1 and 2.
- Dingemans, M.W., Radder, A.C. & De Vriend, H.J. (1987), Computation of the driving forces of wave-induced currents, *Coastal Engng* **11**(5/6), 539–563.
- Dingemans, M.W., Van Kester, J.A.Th.M., Radder, A.C. & Uittenbogaard, R.E. (1996), The effect of the CL-vortex force in 3D wave-current interaction, in 'Proc. 25th Int. Conf. on Coastal Engng, Orlando', ASCE, New York, pp. 4821–4832.
- Drazin, P.G. & Reid, W.H. (1981), *Hydrodynamic stability*, Cambridge Univ. Press, Cambridge.
- Ebersole, B.A. & Dalrymple, R.A. (1980), Numerical modelling of nearshore circulation, in 'Proc. 17th Int. Conf. on Coastal Engng, Sydney', ASCE, New York, pp. 2710–2725.
- Eckart, C. (1963), Some transformations of the hydrodynamic equations, *Phys. Fluids* **6**(8), 1037–1041.
- Faller, A.J. & Caponi, E.A. (1978), Laboratory studies of wind-driven Langmuir circulations, *J. Geophys. Res.* **83**, 3617–3633.
- Fenton, J.D. (1985), A fifth-order Stokes' theory for steady waves, *J. Waterway, Port, Coastal and Ocean Engng* **111**(2), 216–234.

- Fredsoe, J. (1984), Turbulent boundary layer in wave-current motion, *J. Hydraulic Engng* **110**(8), 1103–1120.
- Gibson, A.H. (1909), On the depression of the filament of maximum velocity in a stream flowing through an open channel, *Proc. Royal Soc. London* **A82**, 149–159.
- Grant, W.D. & Madsen, O.S. (1979), Combined wave and current interaction with a rough bottom, *J. Geophys. Res.* **84**(C4), 1797–1808.
- Grimshaw, R. (1981), Mean flows generated by a progressing water wave packet, *J. Austral. Math. Soc.* **B22**, 318–347.
- Grimshaw, R. (1984), Wave action and wave-mean flow interaction, with application to stratified shear flows, *Ann. Rev. Fluid Mech.* **16**, 11–44.
- Holthuijsen, L.H., Booij, N. & Herbers, T.H.C. (1989), A prediction model for stationary, short-crested waves in shallow water with ambient currents, *Coastal Engng* **13**(1), 23–54.
- Huang, N.E., Chen, D.T., Tung, C.-C. & Smith, J.R. (1972), Interactions between steady non-uniform currents and gravity waves with applications for current measurements, *J. Phys. Oceanography* **2**, 420–431.
- Iskandarani, M. & Liu, P.L.-F. (1991a), Mass transport in two-dimensional water waves, *J. Fluid Mech.* **231**, 395–415.
- Iskandarani, M. & Liu, P.L.-F. (1991b), Mass transport in three-dimensional water waves, *J. Fluid Mech.* **231**, 417–437.
- Iskandarani, M. & Liu, P.L.-F. (1993), Mass transport in wave tank, *J. Waterway, Port, Coastal and Ocean Engng* **119**(1), 88–104.
- Jonsson, I.G. (1978), *Combination of waves and currents*, Stability of tidal inlets: theory and engineering, Elsevier, Amsterdam, pp. 162–203.
- Jonsson, I.G. (1990), *Wave-current interactions*, Vol. 9A of *The Sea, Ocean Engng Science*, Wiley, New York, pp. 65–120.
- Jonsson, I.G. & Arneborg, L. (1995), Energy properties and shoaling of higher-order Stokes waves on a current, *Ocean Engng* **22**, 819–857.
- Keller, H.B. (1968), *Numerical methods for two-point boundary-value problems*, Blaisdell Publ. Comp., USA.

- Kemp, P.H. & Simons, R.R. (1982), The interaction between waves and a turbulent current: Waves propagating with the current, *J. Fluid Mech.* **116**, 227–250.
- Kemp, P.H. & Simons, R.R. (1983), The interaction of waves and a turbulent current: Waves propagating against the current, *J. Fluid Mech.* **130**, 73–89.
- Kirby, J. T. & Dalrymple, R. A. (1994), Combined Refraction/Diffraction Model REF/DIF 1, Version 2.5. Documentation and User's Manual, Technical Report CACR-94-22, Center for Applied Coastal Research, Department of Civil Engineering, University of Delaware, Newark.
- Klopman, G. (1994), Vertical structure of the flow due to waves and currents: Laser-Doppler flow measurements for waves following or opposing a current, Technical Report H840.32, Part 2, Delft Hydraulics.
- Klopman, G. (1997), Secondary circulation of the flow due to waves and current: Laser-Doppler flow measurements for waves following or opposing a current, Technical Report Z2249, Delft Hydraulics.
- Knight, D.W. & Patel, H.S. (1985), Boundary shear in smooth rectangular ducts, *J. Hydraulic Engng* **111**(1), 29–47.
- Langmuir, I. (1938), Surface motion of water induced by wind, *Science* **87**, 119–123.
- Leibovich, S. (1977), Convective instability of stably stratified water in the ocean, *J. Fluid Mech.* **82**(3), 561–581.
- Leibovich, S. (1980), On wave-current interaction theories of Langmuir circulations, *J. Fluid Mech.* **99**(4), 715–724.
- Leibovich, S. (1983), The form and dynamics of Langmuir circulations, *Ann. Rev. Fluid Mech.* **15**, 391–427.
- Leibovich, S. & Paolucci, S. (1980), The Langmuir circulation instability as a mixing mechanism in the upper ocean, *J. Phys. Oceanography* **10**, 186–207.
- Lighthill, J. (1992), Acoustic streaming in the ear itself, *J. Fluid Mech.* **239**, 551–606.
- Liu, P.L.-F. & Dalrymple, R.A. (1978), Bottom frictional stresses and longshore currents due to waves with large angles of incidence, *J. Marine Res.* **36**, 357–375.

- Liu, P.L.-F. & Dingemans, M.W. (1989), Derivation of the third-order evolution equations for weakly nonlinear water waves propagating over uneven bottoms, *Wave Motion* **11**, 41–64.
- Lo, E.Y. & Mei, C.C. (1985), Long-time evolution of surface waves in coastal waters, Technical Report 303, M.I.T. Rep. Ralph M. Parsons Lab., Dep. of Civil Engng.
- Longuet-Higgins, M.S. (1953), Mass transport in water waves, *Phil. Trans. R. Soc. London* **A245**, 535–581.
- Longuet-Higgins, M.S. (1970), Longshore currents generated by obliquely incident sea waves. Part 1 and 2, *J. Geophys. Res.* **75**, 6778–6801.
- Longuet-Higgins, M.S. & Stewart, R.W. (1960), Changes in the form of short gravity waves on long waves and tidal currents, *J. Fluid Mech.* **8**, 565–583.
- Longuet-Higgins, M.S. & Stewart, R.W. (1961), The changes in amplitude of short gravity waves on steady non-uniform currents, *J. Fluid Mech.* **10**, 529–549.
- Magnaudet, J. (1989), Interactions interfaciales en écoulement à phases séparées, PhD thesis, Institut National Polytechnique de Toulouse.
- McIntyre, M.E. (1980a), An introduction to the generalized Lagrangian-mean description of wave, mean-flow interaction, *Pure Appl. Geophys.* **118**, 152–176.
- McIntyre, M.E. (1980b), Towards a Lagrangian-mean description of stratospheric circulations and chemical transports, *Phil. Trans. R. Soc. London* **A296**, 129–148.
- Mei, C.C. (1989), *The applied dynamics of ocean surface waves*, World Scientific, Singapore. First printing 1983, Wiley.
- Mei, C.C., Liu, P.L.-F. & Carter, T.G. (1972), Mass transport in water waves, Technical Report 146, M.I.T. Rep. Ralph M. Parsons Lab.
- Melville, W.K., Shear, R. & Veron, F. (1998), Laboratory measurements of the generation and evolution of Langmuir circulations, *J. Fluid Mech.* **364**, 31–58.
- Nepf, H.M., Cowen, E.A., Kimmel, S.J. & Monismith, S.G. (1995), Longitudinal vortices beneath breaking waves, *J. Geophys. Res.* **100**(C8), 16211–16221.



- Nepf, H.M. & Monismith, S.G. (1991), Experimental study of wave-induced longitudinal vortices, *J. Hydraulic Engng* **117**(12), 1639–1649.
- Nezu, I. & Nakagawa, H. (1993), *Turbulence in open-channel flow*, IAHR Monograph, Balkema, Rotterdam.
- Nielsen, P. & You, Z-J (1996), Eulerian mean velocities under non-breaking waves on horizontal bottoms, in 'Proc. 25th Int. Conf. on Coastal Engng, Orlando', ASCE, New York, pp. 4066–4078.
- Nordsveen, M. & Bertelsen, A.F. (1997), Wave-induced secondary motions in stratified duct flow, *Int. J. Multiphase Flow* **23**(3), 503–522.
- Olver, F.W.J. (1974), *Asymptotics and special functions*, Academic Press, New York.
- Péchon, P., Rivero, F., Johnson, H., Chesher, T., O'Connor, B., Tanguy, J.-M., Karambas, T., Mory, M. & Hamm, L. (1997), Intercomparison of wave-driven current models, *Coastal Engng* **31**, 199–215.
- Péchon, P. & Teisson, C. (1994), Numerical modelling of three-dimensional wave-driven currents in the surf-zone, in 'Proc. 24th Int. Conf. on Coastal Engng, Kobe, Japan', ASCE, New York, pp. 2503–2512.
- Peregrine, D.H. (1976), Interaction of water waves and currents, *Adv. Appl. Mech.* **16**, 9–117.
- Peregrine, D.H. (1983), Breaking waves on beaches, *Ann. Rev. Fluid Mech.* **15**, 149–178.
- Phillips, O.M. (1977), *The dynamics of the upper ocean*, Cambridge University Press.
- Phillips, W.R.C. (1998), *On the nonlinear instability of strong wavy shear to longitudinal vortices*, Nonlinear Instability, Chaos and Turbulence, Computational Mechanics Publications, UK, pp. 251–273.
- Press, W.H., Teukolsky, S.A., Vetterling, W.T. & Flannery, B.P. (1992), *Numerical recipes in Fortran*, Cambridge University Press. 2<sup>nd</sup> ed.
- Radder, A.C. (1994), A 3-D wave-current interaction theory based on the CL equation, Technical Report RIKZ/OS-94.163x, Rijkswaterstaat, The Netherlands.

- Ris, R.C., Holthuijsen, L.H. & Booij, N. (1999), A third-generation wave model for coastal regions. Part 2: Verification, *J. Geophys. Res.* **104**(C4), 7667–7682.
- Rivero, F.J. & Sánchez-Arcilla, A. (1995), On the vertical distribution of  $\langle \tilde{u}\tilde{u} \rangle$ , *Coastal Engng* **25**, 137–152.
- Rodi, W. (1980), *Turbulence models and their applications in hydraulics. A state of the art review.*, IAHR, Delft.
- Roelvink, J.A. & Reniers, A.J.H.M. (1994), *Upgrading of a quasi-3D hydrodynamic model*, Book of abstracts, Overall workshop Mast G8M, Gregynog.
- Russell, R.C.H. & Osorio, J.D.C. (1957), An experimental investigation of drift profiles in closed channels, in 'Proc. 6th Int. Conf. on Coastal Engng, Miami', pp. 171–193.
- Sánchez-Arcilla, A., Collado, F., Lemos, M. & Rivero, F. (1990), Another quasi-3D model for surf-zone flows, in 'Proc. 22nd Int. Conf. on Coastal Engng, Delft, The Netherlands', ASCE, New York, pp. 316–329.
- Sánchez-Arcilla, A., Collado, F. & Rodriguez, A. (1992), Vertically varying velocity field in Q-3D nearshore circulation, in 'Proc. 23rd Int. Conf. on Coastal Engng, Venice, Italy', ASCE, New York, pp. 2811–2824.
- Simons, R.R., Grass, A.J. & Kyriacou, A. (1988), The influence of currents on wave attenuation, in 'Proc. 21st Int. Conf. on Coastal Engng, Malaga', ASCE, New York, pp. 363–376.
- Sleath, J.F.A. (1990), *Seabed boundary layers*, Vol. 9B of *The Sea, Ocean Engng Science*, Wiley, New York, pp. 693–727.
- Sleath, J.F.A. (1991), Velocities and shear stresses in wave-current flows, *J. Geophys. Res.* **96**(C8), 15237–15244.
- Smith, J.A. (1992), Observed growth of Langmuir circulation, *J. Geophys. Res.* **97**(C4), 5651–5664.
- Soulsby, R.L., Hamm, L., Klopman, G., Myrhaug, D., Simons, R.R. & Thomas, G.P. (1993), Wave-current interaction within and outside the bottom boundary layer, *Coastal Engng* **21**, 41–69.
- Southgate, H.N. (1989), A nearshore profile model of wave and tidal current interaction, *Coastal Engng* **13**, 219–245.

- Soward, A.M. (1972), A kinematic theory of large magnetic Reynolds number dynamos, *Phil. Trans. Roy. Soc. London* **A272**, 431–462.
- Stive, M.J.F. & Wind, H.G. (1986), Cross-shore mean flow in the surf zone, *Coastal Engng* **10**(4), 325–340.
- Stoer, J. & Bulirsch, R. (1980), *Introduction to numerical analysis*, Springer Verlag, New York.
- Stokes, G.G. (1880), On the theory of oscillatory waves, *Mathematical and physical papers* **1**, 197–229. Cambridge Univ. Press. Originally in *Trans. Camb. Phil. Soc.* **8**, 441–455, 1847.
- Supharatid, S., Tanaka, H. & Shuto, N. (1992), Interactions of waves and current (Part I: Experimental investigation), *Coastal Engng in Japan* **35**(2), 187–204.
- Svendsen, I.A. (1984a), Wave height and set-up in a surf zone, *Coastal Engng* **8**(4), 303–329.
- Svendsen, I.A. (1984b), Mass flux and undertow in a surf zone, *Coastal Engng* **8**(4), 347–365.
- Svendsen, I.A. & Putrevu, U. (1990), Nearshore circulation with 3D profiles, in 'Proc. 22nd Int. Conf. on Coastal Engng, Delft, The Netherlands', ASCE, New York, pp. 241–254.
- Svendsen, I.A. & Putrevu, U. (1994), Nearshore mixing and dispersion, *Proc. Royal Soc. London* **A445**, 561–576.
- Svendsen, I.A. & Putrevu, U. (1996), *Surf-zone hydrodynamics*, Advances in Coastal and Ocean Engng, vol. 2, World Scientific, Singapore, pp. 1–78.
- Swan, C. (1990), An experimental study of waves on a strongly sheared current profile, in 'Proc. 22nd Int. Conf. on Coastal Engng, Delft, The Netherlands', ASCE, New York, pp. 489–502.
- Swan, C. (1992), A stream function solution for waves on a strongly sheared current, in 'Proc. 23rd Int. Conf. on Coastal Engng, Venice, Italy', ASCE, New York, pp. 684–697.
- Thomas, G.P. & Klopman, G. (1997), *Wave-current interactions in the nearshore regions*, Gravity waves in water of finite depth, Vol. 10 in series Adv. in Fluid Mech., Computational Mech. Publ., pp. 255–319.

- Thornton, E.B. (1970), Variation of longshore current across the surf zone, in 'Proc. 12th Int. Conf. on Coastal Engng, Washington', ASCE, New York, pp. 291-308.
- Uittenbogaard, R.E. (1992), Wave forces in three dimensions, Technical Report Z553, Delft Hydraulics.
- Uittenbogaard, R.E. & Van Kester, J.A.Th.M. (1996), Modeling seasonal temperature stratification with TRIWAQ: a preparatory study based on one-dimensional computations, Technical Report Z978, Delft Hydraulics.
- Van Dongeren, A.R. & Svendsen, I.A. (1997), Numerical modeling of quasi-3D nearshore hydrodynamics, PhD thesis, Research report No. CACR-97-04, Center for Applied Coastal Research, University of Delaware, Newark. 235 p.
- Van Doorn, T. (1981), Experimental investigation of near bottom velocities in water waves without and with a current, Technical Report M1423, Delft Hydraulics.
- Van Kester, J.A.Th.M., Uittenbogaard, R.E. & Dingemans, M.W. (1996), 3D wave-current interaction, Technical Report Z751, Delft Hydraulics.
- Vinokur, M. (1983), On one-dimensional stretching functions for finite-difference calculations, *J. Comp. Physics* **50**, 215-234.
- Walstra, D.J. (1999), Personal communications.
- Walstra, D.J., Piepers, M., Roelvink, J.A. & Stelling, G.S. (1994), *2DV modelling of surfzone currents*, Book of abstracts, Overall workshop Mast G8M, Gregynog.
- Weller, R.A. & Price, J.F. (1988), Langmuir circulation within the oceanic mixed layer, *Deep-Sea Res.* **35**(5), 717-747.
- Wind, H.G. & Vreugdenhil, C.B. (1986), Rip-current generation near structures, *J. Fluid Mech.* **171**, 459-476.
- Wu, C.-S. & Liu, P.L.-F. (1985), Finite element modeling of nonlinear coastal currents, *J. Waterway, Port, Coastal and Ocean Engng* **111**(2), 417-432.
- You, Z.-J. (1996), The effect of wave-induced stress on current profiles, *Ocean Engng* **23**(7), 619-628.
- You, Z.-J. (1997), On the vertical distribution of  $\overline{uv}$  by F.J. Rivero and A.S. Arcilla: comments, *Coastal Engng* **30**, 305-310.

## Appendix A

### Derivation of wave-action equation

Andrews & McIntyre (1978*b*, appendix A) considered ensemble averaging in their derivation of the wave-action equation. Similar steps like they followed are taken here to arrive at a wave-action equation in case of a slow-modulation average. Important in this analysis is the assumption that for any field  $\varphi$ ,

$$\overline{\frac{\partial \varphi}{\partial t}} = 0. \quad (\text{A.1})$$

This property does not hold for general waves. Only for slowly-varying waves changes in the mean motion may be discarded.

The shifted momentum equations (3.8) are multiplied by  $\partial \xi_j / \partial t$  and averaged. For the first term this gives,

$$\begin{aligned} \overline{\frac{\partial \xi_j}{\partial t} \overline{D^L} u_j^\xi} &= \overline{\frac{\partial \xi_j}{\partial t} \overline{D^L} u_j^\ell} \\ &= \overline{D^L \left( \frac{\partial \xi_j}{\partial t} u_j^\ell \right)} - \overline{u_j^\ell \overline{D^L \left( \frac{\partial \xi_j}{\partial t} \right)}} \\ &= \overline{D^L \left( \frac{\partial \xi_j}{\partial t} u_j^\ell \right)}. \end{aligned} \quad (\text{A.2})$$

Latter equality results directly from (2.5) and the fact that  $\langle \partial(u_j^\ell u_j^\ell) / \partial t \rangle = 0$ , in virtue of (A.1). In manipulating the second term application of (2.15) yields

$$\frac{\partial J}{\partial t} = K_{ij} \frac{\partial^2 \xi_i}{\partial t \partial x_j}. \quad (\text{A.3})$$

Substitution of (A.3) into the expression that is obtained after application of the

chainrule (2.11, second part) then leads to the following relation

$$\begin{aligned} \overline{\frac{1}{\rho} \frac{\partial \xi_j}{\partial t} \left( \frac{\partial p}{\partial x_j} \right)^\xi} &= \frac{1}{\rho} \overline{\frac{\partial \xi_j}{\partial t} \frac{K_{jk}}{J} \frac{\partial p^\xi}{\partial x_k}} \\ &= \frac{1}{\tilde{\rho}} \frac{\partial}{\partial x_k} \left( \overline{\frac{\partial \xi_j}{\partial t} K_{jk} p^\xi} \right) - \frac{1}{\tilde{\rho}} \overline{p^\xi \frac{\partial J}{\partial t}}. \end{aligned} \quad (\text{A.4})$$

The latter term on the right-hand side of (A.4) vanishes due to property (A.1),

$$-\frac{1}{\tilde{\rho}} \overline{p^\xi \frac{\partial J}{\partial t}} = -\frac{1}{\tilde{\rho}} \overline{\frac{\partial}{\partial t} (p^\xi J)} + \frac{1}{\rho J} \overline{\frac{\partial p^\xi}{\partial t} J} = \frac{1}{\rho} \overline{\frac{\partial p^\xi}{\partial t}} = 0. \quad (\text{A.5})$$

As a result of foregoing the wave-action equation is obtained,

$$\overline{D^L \left( \frac{\partial \xi_j}{\partial t} u_j^\ell \right)} + \frac{\partial}{\partial x_k} \left( \overline{p^\xi \frac{\partial \xi_j}{\partial t} K_{jk}} \right) = \overline{\frac{\partial \xi_j}{\partial t} X_j^\ell} + \overline{\frac{\partial \xi_j}{\partial t} F_j^\ell}. \quad (\text{A.6})$$

## Appendix B

### Driving forces at different orders of approximation

The explicit solutions will be presented here up to second order. For the zeroth-order problem ( $n = 0$ ) the forcing terms are given by

$$\hat{F}^{(0,0)} = \hat{H}_i^{(0,0)} = \hat{K}_i^{(0,0)} = \hat{L}^{(0,0)} = \hat{T}_{ij}^{(0,0)} = 0, \quad (\text{B.1a})$$

$$\hat{G}_\alpha^{(0,0)} = \hat{\tau}_{\alpha b}^{(0,0)}/h, \quad (\text{B.1b})$$

$$\hat{G}_3^{(0,0)} = -g. \quad (\text{B.1c})$$

At first order ( $n = 1$ ) all the forcing terms are zero. i.e.

$$\hat{F}^{(1,0)} = \hat{G}_i^{(1,0)} = \hat{H}_i^{(1,0)} = \hat{K}_i^{(1,0)} = \hat{L}^{(1,0)} = \hat{T}_{ij}^{(1,0)} = 0, \quad (\text{B.2})$$

$$\hat{F}^{(1,1)} = \hat{G}_i^{(1,1)} = \hat{D}_i^{(1,1)} = \hat{H}_i^{(1,1)} = \hat{K}_i^{(1,1)} = \hat{L}^{(1,1)} = \hat{T}_{ij}^{(1,1)} = 0. \quad (\text{B.3})$$

The equations for the second-order mean motion ( $n = 2, m = 0$ ) contain forcing terms which are no longer equal to zero, but contain temporal and (horizontal) spatial derivatives of first-order zeroth-harmonic variables ( $n = 1, m = 0$ ) as well as correlations of wave-related variables ( $n = 1, m = \pm 1$ ). The second-order approximation of the Stokes correction of the variable  $\varphi$  will be denoted as  $\tilde{\varphi}^{(2,0)}$ . From relation (2.22) the following expression for  $\tilde{\varphi}^{(2,0)}$  can be derived,

$$\begin{aligned} \tilde{\varphi}^{(2,0)} = & \left[ ik_\beta \hat{\xi}_\beta^{(1,-1)} \left( \hat{\varphi}^{(1,1)} - \hat{\eta}^{(1,1)} \frac{\partial \hat{\varphi}^{(0,0)}}{\partial z} \right) - i\bar{k}_\beta \hat{\xi}_\beta^{(1,1)} \left( \hat{\varphi}^{(1,-1)} - \hat{\eta}^{(1,-1)} \frac{\partial \hat{\varphi}^{(0,0)}}{\partial z} \right) \right. \\ & + \hat{\eta}^{(1,-1)} \frac{\partial}{\partial z} \left( \hat{\varphi}^{(1,1)} - \hat{\eta}^{(1,1)} \frac{\partial \hat{\varphi}^{(0,0)}}{\partial z} \right) + \hat{\eta}^{(1,1)} \frac{\partial}{\partial z} \left( \hat{\varphi}^{(1,-1)} - \hat{\eta}^{(1,-1)} \frac{\partial \hat{\varphi}^{(0,0)}}{\partial z} \right) \\ & \left. + \hat{\eta}^{(1,1)} \hat{\eta}^{(1,-1)} \frac{\partial^2 \hat{\varphi}^{(0,0)}}{\partial z^2} \right] E \bar{E}, \end{aligned} \quad (\text{B.4})$$

with  $\bar{k}_\beta$  the complex conjugate of  $k_\beta$  and  $E = \exp(i(k_\beta x_\beta - \omega t))$ . The forcing functions for  $n = 2, m = 0$  are given by

$$\hat{F}^{(2,0)} = -\frac{\partial \hat{u}_\beta^{(1,0)}}{\partial X_\beta} + i(k_\beta - \bar{k}_\beta) \hat{u}_\beta^{(2,0)} + \frac{\partial \tilde{w}^{(2,0)}}{\partial z}, \quad (\text{B.5a})$$

$$\begin{aligned} \hat{G}_\alpha^{(2,0)} = & -\frac{\partial \hat{u}_\alpha^{(1,0)}}{\partial T} - \hat{u}_\beta^{(0,0)} \frac{\partial \hat{u}_\alpha^{(1,0)}}{\partial X_\beta} - \frac{1}{\rho} \frac{\partial \hat{p}^{(1,0)}}{\partial X_\alpha} + \frac{1}{\rho} \frac{\partial \hat{\tau}_{\alpha\beta}^{(1,0)}}{\partial X_\beta} \\ & + i(k_\alpha - \bar{k}_\alpha) \frac{1}{\rho} \hat{p}^{(2,0)} - i(k_\beta - \bar{k}_\beta) \frac{1}{\rho} \hat{\tau}_{\alpha\beta}^{(2,0)} - \frac{1}{\rho} \frac{\partial \hat{\tau}_{\alpha 3}^{(2,0)}}{\partial z} \\ & + E\bar{E} \left[ (\omega_0 - \bar{\omega}_0) (k_\beta - \bar{k}_\beta) \left( \hat{u}_\alpha^{(1,1)} \hat{\xi}_\beta^{(1,-1)} + \hat{u}_\alpha^{(1,-1)} \hat{\xi}_\beta^{(1,1)} \right) \right] \\ & - E\bar{E} \left[ i(\omega_0 - \bar{\omega}_0) \frac{\partial}{\partial z} \left( \hat{u}_\alpha^{(1,1)} \hat{\eta}^{(1,-1)} + \hat{u}_\alpha^{(1,-1)} \hat{\eta}^{(1,1)} \right) \right] \\ & + E\bar{E} \left[ i(k_\beta - \bar{k}_\beta) \frac{\partial \hat{u}_\beta^{(0,0)}}{\partial z} \left( \hat{u}_\alpha^{(1,1)} \hat{\eta}^{(1,-1)} + \hat{u}_\alpha^{(1,-1)} \hat{\eta}^{(1,1)} \right) \right] \\ & - E\bar{E} \left[ i(k_\beta - \bar{k}_\beta) \left( \hat{u}_\alpha^{(1,1)} \hat{u}_\beta^{(1,-1)} + \hat{u}_\alpha^{(1,-1)} \hat{u}_\beta^{(1,1)} \right) \right] \\ & - E\bar{E} \left[ \frac{\partial}{\partial z} \left( \hat{u}_\alpha^{(1,1)} \hat{w}^{(1,-1)} + \hat{u}_\alpha^{(1,-1)} \hat{w}^{(1,1)} \right) \right], \quad (\text{B.5b}) \end{aligned}$$

$$\begin{aligned} \hat{G}_3^{(2,0)} = & -\frac{\partial \hat{w}^{(1,0)}}{\partial T} - \hat{u}_\beta^{(0,0)} \frac{\partial \hat{w}^{(1,0)}}{\partial X_\beta} - \frac{1}{\rho} \frac{\partial \hat{\tau}_{3\beta}^{(1,0)}}{\partial X_\beta} \\ & + \frac{1}{\rho} \frac{\partial \hat{p}^{(2,0)}}{\partial z} - i(k_\beta - \bar{k}_\beta) \frac{1}{\rho} \hat{\tau}_{3\beta}^{(2,0)} - \frac{1}{\rho} \frac{\partial \hat{\tau}_{33}^{(2,0)}}{\partial z} \\ & + E\bar{E} \left[ (\omega_0 - \bar{\omega}_0) (k_\beta - \bar{k}_\beta) \left( \hat{w}^{(1,1)} \hat{\xi}_\beta^{(1,-1)} + \hat{w}^{(1,-1)} \hat{\xi}_\beta^{(1,1)} \right) \right] \\ & - E\bar{E} \left[ i(\omega_0 - \bar{\omega}_0) \frac{\partial}{\partial z} \left( \hat{w}^{(1,1)} \hat{\eta}^{(1,-1)} + \hat{w}^{(1,-1)} \hat{\eta}^{(1,1)} \right) \right] \\ & + E\bar{E} \left[ i(k_\beta - \bar{k}_\beta) \frac{\partial \hat{u}_\beta^{(0,0)}}{\partial z} \left( \hat{w}^{(1,1)} \hat{\eta}^{(1,-1)} + \hat{w}^{(1,-1)} \hat{\eta}^{(1,1)} \right) \right] \\ & - E\bar{E} \left[ i(k_\beta - \bar{k}_\beta) \left( \hat{w}^{(1,1)} \hat{u}_\beta^{(1,-1)} + \hat{w}^{(1,-1)} \hat{u}_\beta^{(1,1)} \right) \right] \\ & - 2E\bar{E} \left[ \frac{\partial}{\partial z} \left( \hat{w}^{(1,1)} \hat{w}^{(1,-1)} \right) \right], \quad (\text{B.5c}) \end{aligned}$$

$$\hat{H}_i^{(2,0)} = 0, \quad (\text{B.5d})$$

$$\hat{L}^{(2,0)} = \frac{\partial \hat{\zeta}^{(1,0)}}{\partial T} + \hat{u}_\beta^{(0,0)} \Big|_{(z=0)} \frac{\partial \hat{\zeta}^{(1,0)}}{\partial X_\beta}, \quad (\text{B.5e})$$



$$\begin{aligned}
\hat{K}_\alpha^{(2,0)} = & -\hat{\zeta}^{(1,0)} \frac{\partial \hat{\tau}_{\alpha 3}^{(1,0)}}{\partial z} \\
& -E\bar{E} \left[ ik_\alpha \hat{\zeta}^{(1,1)} \hat{p}^{(1,-1)} - i\bar{k}_\alpha \hat{\zeta}^{(-1,1)} \hat{p}^{(1,1)} \right] \\
& +E\bar{E} \left[ ik_\beta \hat{\zeta}^{(1,1)} \hat{\tau}_{\alpha\beta}^{(1,-1)} - i\bar{k}_\beta \hat{\zeta}^{(-1,1)} \hat{\tau}_{\alpha\beta}^{(1,1)} \right], \quad (\text{B.5f})
\end{aligned}$$

$$\begin{aligned}
\hat{K}_3^{(2,0)} = & -\hat{\zeta}^{(1,0)} \left( -\frac{\partial \hat{p}^{(1,0)}}{\partial z} + \frac{\partial \hat{\tau}_{33}^{(1,0)}}{\partial z} \right) \\
& +E\bar{E} \left[ ik_\beta \hat{\zeta}^{(1,1)} \hat{\tau}_{3\beta}^{(1,-1)} - i\bar{k}_\beta \hat{\zeta}^{(-1,1)} \hat{\tau}_{3\beta}^{(1,1)} \right], \quad (\text{B.5g})
\end{aligned}$$

$$\begin{aligned}
\hat{T}_{\alpha\beta}^{(2,0)} = & \hat{\nu}^{(0,0)} \left( \frac{\partial \hat{u}_\alpha^{(1,0)}}{\partial X_\beta} + \frac{\partial \hat{u}_\beta^{(1,0)}}{\partial X_\alpha} \right) \\
& -\hat{\nu}^{(0,0)} E\bar{E} \left[ \bar{k}_\beta k_\gamma \hat{\xi}_\gamma^{(1,-1)} \hat{u}_\alpha^{(1,1)} + k_\beta \bar{k}_\gamma \hat{\xi}_\gamma^{(1,1)} \hat{u}_\alpha^{(1,-1)} \right. \\
& \quad \left. -i\bar{k}_\beta \hat{\eta}^{(1,-1)} \frac{\partial \hat{u}_\alpha^{(1,1)}}{\partial z} + ik_\beta \hat{\eta}^{(1,1)} \frac{\partial \hat{u}_\alpha^{(1,-1)}}{\partial z} \right] \\
& -\hat{\nu}^{(0,0)} E\bar{E} \left[ \bar{k}_\alpha k_\gamma \hat{\xi}_\gamma^{(1,-1)} \hat{u}_\beta^{(1,1)} + k_\alpha \bar{k}_\gamma \hat{\xi}_\gamma^{(1,1)} \hat{u}_\beta^{(1,-1)} \right. \\
& \quad \left. -i\bar{k}_\alpha \hat{\eta}^{(1,-1)} \frac{\partial \hat{u}_\beta^{(1,1)}}{\partial z} + ik_\alpha \hat{\eta}^{(1,1)} \frac{\partial \hat{u}_\beta^{(1,-1)}}{\partial z} \right] \\
& +\hat{\nu}^{(0,0)} E\bar{E} \left[ \bar{k}_\beta k_\gamma \hat{\xi}_\gamma^{(1,-1)} \hat{\eta}^{(1,1)} + k_\beta \bar{k}_\gamma \hat{\xi}_\gamma^{(1,1)} \hat{\eta}^{(1,-1)} \right. \\
& \quad \left. -i\bar{k}_\beta \hat{\eta}^{(1,-1)} \frac{\partial \hat{\eta}^{(1,1)}}{\partial z} + ik_\beta \hat{\eta}^{(1,1)} \frac{\partial \hat{\eta}^{(1,-1)}}{\partial z} \right] \frac{\partial \hat{u}_\alpha^{(0,0)}}{\partial z} \\
& +\hat{\nu}^{(0,0)} E\bar{E} \left[ \bar{k}_\alpha k_\gamma \hat{\xi}_\gamma^{(1,-1)} \hat{\eta}^{(1,1)} + k_\alpha \bar{k}_\gamma \hat{\xi}_\gamma^{(1,1)} \hat{\eta}^{(1,-1)} \right. \\
& \quad \left. -i\bar{k}_\alpha \hat{\eta}^{(1,-1)} \frac{\partial \hat{\eta}^{(1,1)}}{\partial z} + ik_\alpha \hat{\eta}^{(1,1)} \frac{\partial \hat{\eta}^{(1,-1)}}{\partial z} \right] \frac{\partial \hat{u}_\beta^{(0,0)}}{\partial z}, \quad (\text{B.5h})
\end{aligned}$$

$$\begin{aligned}
\hat{T}_{\alpha 3}^{(2,0)} = & \hat{\nu}^{(0,0)} \frac{\partial \hat{w}^{(1,0)}}{\partial X_\alpha} \\
& -\hat{\nu}^{(0,0)} E\bar{E} \left[ ik_\gamma \frac{\partial \hat{\xi}_\gamma^{(1,-1)}}{\partial z} \hat{u}_\alpha^{(1,1)} - i\bar{k}_\gamma \frac{\partial \hat{\xi}_\gamma^{(1,1)}}{\partial z} \hat{u}_\alpha^{(1,-1)} \right. \\
& \quad \left. + \frac{\partial \hat{\eta}^{(1,-1)}}{\partial z} \frac{\partial \hat{u}_\alpha^{(1,1)}}{\partial z} + \frac{\partial \hat{\eta}^{(1,1)}}{\partial z} \frac{\partial \hat{u}_\alpha^{(1,-1)}}{\partial z} \right] \\
& -\hat{\nu}^{(0,0)} E\bar{E} \left[ \bar{k}_\alpha k_\gamma \hat{\xi}_\gamma^{(1,-1)} \hat{w}^{(1,1)} + k_\alpha \bar{k}_\gamma \hat{\xi}_\gamma^{(1,1)} \hat{w}^{(1,-1)} \right]
\end{aligned}$$

$$\begin{aligned}
& -i\bar{k}_\alpha \hat{\eta}^{(1,-1)} \frac{\partial \hat{w}^{(1,1)}}{\partial z} + ik_\alpha \hat{\eta}^{(1,1)} \frac{\partial \hat{w}^{(1,-1)}}{\partial z} \Big] \\
& + \hat{\nu}^{(0,0)} E \bar{E} \left[ ik_\gamma \frac{\partial \hat{\xi}_\gamma^{(1,-1)}}{\partial z} \hat{\eta}^{(1,1)} - i\bar{k}_\gamma \frac{\partial \hat{\xi}_\gamma^{(1,1)}}{\partial z} \hat{\eta}^{(1,-1)} \right. \\
& \left. + 2 \frac{\partial \hat{\eta}^{(1,1)}}{\partial z} \frac{\partial \hat{\eta}^{(1,-1)}}{\partial z} \right] \frac{\partial \hat{u}_\alpha^{(0,0)}}{\partial z} , \tag{B.5i}
\end{aligned}$$

$$\begin{aligned}
\hat{T}_{33}^{(2,0)} = & -2 \hat{\nu}^{(0,0)} E \bar{E} \left[ ik_\gamma \frac{\partial \hat{\xi}_\gamma^{(1,-1)}}{\partial z} \hat{w}^{(1,1)} - i\bar{k}_\gamma \frac{\partial \hat{\xi}_\gamma^{(1,1)}}{\partial z} \hat{w}^{(1,-1)} \right. \\
& \left. + \frac{\partial \hat{\eta}^{(1,-1)}}{\partial z} \frac{\partial \hat{w}^{(1,1)}}{\partial z} + \frac{\partial \hat{\eta}^{(1,1)}}{\partial z} \frac{\partial \hat{w}^{(1,-1)}}{\partial z} \right] . \tag{B.5j}
\end{aligned}$$

# Appendix C

## Boundary layer affected by orbital motion

The influence of the wave motion on the shear stresses in the vicinity of the bed or the side wall has been modelled by means of the formulation of Grant & Madsen (1979). In section C.1 this formulation is briefly revised. The implementation in the 2DV model of Van Kester et al. (1996) has been outlined in section C.2.

### C.1 Grant & Madsen's formulation of the friction velocity

The following outline is given for the bottom boundary layer, but is also applicable to the side-wall boundary by a simple permutation of the coordinates. For the combined wave and current motion Grant & Madsen (1979) defined the instantaneous bed shear stress as

$$\tau_b = \frac{1}{2} \rho f_{cw} (u^2 + v^2) \left[ \frac{u}{|\mathbf{u}_h|}, \frac{v}{|\mathbf{u}_h|} \right]^T, \quad (\text{C.1})$$

with  $|\mathbf{u}_h| = (u^2 + v^2)^{\frac{1}{2}}$  the magnitude of the horizontal velocity of the combined wave-current motion. The magnitude of the maximum bed shear stress can then be expressed as,

$$|\tau_{b,\max}| = \frac{1}{2} \rho f_{cw} \alpha |\hat{\mathbf{u}}_b|^2, \quad (\text{C.2})$$

where

$$\alpha = 1 + \left( \frac{|\bar{\mathbf{u}}_a|}{|\hat{\mathbf{u}}_b|} \right)^2 + 2 \left( \frac{|\bar{\mathbf{u}}_a|}{|\hat{\mathbf{u}}_b|} \right) \cos(\phi_c). \quad (\text{C.3})$$

Here  $\bar{\mathbf{u}}_a$  is the steady current velocity vector evaluated at a height  $a$  above the bed;  $\phi_c$  denotes the angle made by  $\bar{\mathbf{u}}_a$  with the direction of wave propagation;

$\hat{u}_b$  is the maximum near-bottom orbital velocity from linear wave theory. The combined friction velocity is defined as

$$|\mathbf{u}_*| = (|\tau_{b,\max}|/\rho)^{\frac{1}{2}} = \left(\frac{1}{2}f_{cw}\alpha\right)^{\frac{1}{2}} |\hat{u}_b|. \quad (\text{C.4})$$

The turbulent intensities are characterized by the eddy viscosity  $\nu$ . Within the wave boundary layer Grant & Madsen (1979) assume  $\nu$  to be of the form

$$\nu = \kappa |\mathbf{u}_*| z, \quad z_0 \leq z < \delta_w, \quad (\text{C.5})$$

with the wave boundary layer thickness  $\delta_w$  defined as

$$\delta_w = \frac{2\kappa}{\omega} |\mathbf{u}_*|. \quad (\text{C.6})$$

Outside this region the wave-induced turbulence has been assumed to be negligible,

$$\nu = \kappa |\mathbf{u}_{*c}| z, \quad z > \delta_w, \quad (\text{C.7})$$

where the shear velocity  $\mathbf{u}_{*c}$  is based on the time-averaged shear stress,

$$|\mathbf{u}_{*c}| |\mathbf{u}_{*c}| = \bar{\tau}_b / \rho. \quad (\text{C.8})$$

Regarding the current motion, the region close to the boundary has been assumed to be a region of constant stress, i.e. relation (C.4) is valid. Therefore,

$$\kappa |\mathbf{u}_*| z \frac{\partial \bar{u}}{\partial z} = |\mathbf{u}_{*c}| |\mathbf{u}_{*c}|, \quad z_0 \leq z < \delta_w, \quad (\text{C.9a})$$

$$\kappa |\mathbf{u}_{*c}| z \frac{\partial \bar{u}}{\partial z} = |\mathbf{u}_{*c}| |\mathbf{u}_{*c}|, \quad z > \delta_w. \quad (\text{C.9b})$$

The no-slip condition  $\bar{u} = 0$  at  $z = z_0$  implies the following logarithmic distribution for the steady current velocity inside the wave boundary layer,

$$\bar{u} = \frac{|\mathbf{u}_{*c}|}{\kappa} \left( \frac{|\mathbf{u}_{*c}|}{|\mathbf{u}_*|} \right) \log \left( \frac{z}{z_0} \right), \quad z_0 \leq z < \delta_w. \quad (\text{C.10})$$

Equation (C.9b) for the velocity distribution outside the wave boundary layer will also be logarithmic. The two logarithmic distributions are matched at  $z = \delta_w$  by introducing an apparent roughness length  $z_{bc}$ , which reflects the turbulence level that is increased by the presence of the waves. The law of the wall now becomes

$$\bar{u} = 0 \quad \text{at } z = z_{bc}, \quad (\text{C.11})$$

and thus

$$\bar{u} = \frac{|\mathbf{u}_{*c}|}{\kappa} \log \left( \frac{z}{z_{bc}} \right), \quad z > \delta_w. \quad (\text{C.12})$$

Matching relations (C.10) and (C.12) for the magnitude of the current velocity at  $z = \delta_w$  results in the following relation

$$\frac{|\mathbf{u}_*|}{|\mathbf{u}_{*c}|} = \frac{\log(\delta_w/z_0)}{\log(\delta_w/z_{bc})}. \quad (\text{C.13})$$

Re-arrangement of (C.13) yields that  $z_{bc}$  satisfies for  $\delta_w > z_0$ ,

$$\frac{z_{bc}}{z_0} = \left(\frac{\delta_w}{z_0}\right)^\gamma, \quad \gamma = 1 - \frac{|\mathbf{u}_{*c}|}{|\mathbf{u}_*|}. \quad (\text{C.14})$$

The remaining task is to determine the wave-current friction factor  $f_{cw}$  or velocity  $|\mathbf{u}_*|$ . Since  $\tau_{b,\max} = \bar{\tau}_b + \tilde{\tau}_{b,\max}$  with  $\tilde{\tau}_{b,\max}$  the maximum of the oscillating part of the instantaneous bed shear stress, the wave-related friction velocity is defined as

$$\tilde{\tau}_{b,\max}/\rho = |\mathbf{u}_{*w,\max}| |\mathbf{u}_{*w,\max}|. \quad (\text{C.15})$$

Hence  $|\mathbf{u}_*|$  can be expressed as

$$|\mathbf{u}_*| = (|\mathbf{u}_{*c}| |\mathbf{u}_{*c}| + |\mathbf{u}_{*w,\max}| |\mathbf{u}_{*w,\max}|)^{\frac{1}{2}}. \quad (\text{C.16})$$

Given a certain mean velocity field  $\bar{\mathbf{u}}$  the shear velocity  $|\mathbf{u}_{*c}|$  can now be determined in two ways, both giving the same result. Firstly, an expression can be derived directly from (C.12),

$$|\mathbf{u}_{*c}| = \frac{\kappa |\mathbf{u}_c(z_1)|}{\log(z_1/z_{bc})}, \quad z_1 > \delta_w, \quad (\text{C.17})$$

with  $z_{bc}$  determined by (C.14). Secondly, relation (C.10) yields

$$|\mathbf{u}_{*c}| = \frac{B}{\sqrt{2}} \left[ 1 + \left\{ 1 + \left( \frac{2 |\mathbf{u}_{*w,\max}|^2}{B} \right)^{\frac{1}{2}} \right\}^{\frac{1}{2}} \right], \quad B = \frac{\kappa |\mathbf{u}_c(z_1)|}{\log(z_1/z_0)}, \quad z_0 \leq z_1 \leq \delta_w. \quad (\text{C.18})$$

Both relations are given here, since the shear velocity depends on the current velocity. If the current velocity is evaluated in a grid point near the wall that happens to be in the wave boundary layer, then relation (C.18) has to be used instead of (C.17).

## C.2 Inclusion of bottom and side wall friction

The effects of bottom and side wall friction are incorporation via the boundary conditions at the bed and the side walls. The mean shear stresses  $\bar{\tau}_b$  and  $\bar{\tau}_s$  at these boundaries are given by

$$\bar{\tau}_b = \rho \mathbf{u}_{*b} |\mathbf{u}_{*b}|, \quad \bar{\tau}_s = \rho \mathbf{u}_{*s} |\mathbf{u}_{*s}|, \quad (\text{C.19})$$

with  $\mathbf{u}_{*b} = (u_{*b}, v_{*b}, 0)^T$  and  $\mathbf{u}_{*s} = (u_{*s}, 0, w_{*s})^T$  the mean shear velocities. Here only the situation in the bottom boundary layer is considered. Van Kester et al. (1996) followed Grant & Madsen (1979) in defining the mean shear velocities which are effected by wave motion. The general idea is that the wave motion increases the turbulent intensities. Grant & Madsen (1979) modelled this phenomenon by introducing an apparent roughness length  $z_{bc}$  (see (C.14)), which senses the wave boundary layer as a bed with increased roughness,

$$\frac{z_{bc}}{z_0} = \left( \frac{\delta_w}{z_0} \right)^\gamma, \quad \gamma = 1 - \frac{|\mathbf{u}_{*c}|}{\{|\mathbf{u}_{*c}| \mathbf{u}_{*c} + |\mathbf{u}_{*w, \max}| \mathbf{u}_{*w, \max}\}^{\frac{1}{2}}}. \quad (\text{C.20})$$

Here  $\mathbf{u}_{*c}$  and  $\mathbf{u}_{*w, \max}$  are the friction velocities related to the mean and oscillating part of the shear stress, defined by (C.8) and (C.15). The wave friction velocity is determined from

$$\mathbf{u}_{*w, \max} = \left( \frac{1}{2} f_w \right)^{\frac{1}{2}} \hat{\mathbf{u}}_b, \quad (\text{C.21})$$

where  $f_w$  is the wave-related friction coefficient, for which an expression given by Soulsby et al. (1993, p.59) has been applied, and  $\hat{\mathbf{u}}_b$  denotes the near-bottom horizontal orbital velocity magnitude. Van Kester et al. (1996) used potential theory for infinitesimal waves on a uniform current to compute  $\hat{\mathbf{u}}_b$  and thus  $\mathbf{u}_{*w, \max}$ . This approach differs from the one used by Grant & Madsen (1979), who substituted expression (C.5) for the eddy viscosity into the relation between the wave-related shear stress and the orbital velocity. As a result an expression was derived for the wave-induced friction velocity in terms of the Kelvin functions  $Ker$  and  $Kei$ .

The magnitude of the shear velocity  $|\mathbf{u}_{*c}|$  for the mean motion is related to the magnitude of the mean horizontal velocity evaluated at a position  $\Delta$  outside the wave boundary layer,

$$|\mathbf{u}_{*c}| = \frac{\kappa |\bar{\mathbf{u}}(\Delta + z_{bc})|}{\log(1 + \Delta/z_{bc})}, \quad \Delta \geq \delta_w, \quad (\text{C.22})$$

as given by (C.17). If  $\Delta$  were inside the wave boundary layer, relation (C.18) should be applied. Relations (C.20) and (C.22) are implicitly related and have to be solved iteratively. Because the mean bed shear stress must balance the steady current, the direction of the friction velocity  $\mathbf{u}_{*c}$  equals the mean flow direction, thus for each component

$$(\mathbf{u}_{*c})_i = \bar{u}_i \frac{|\bar{\mathbf{u}}_{*c}|}{|\bar{\mathbf{u}}|}. \quad (\text{C.23})$$

The latter approach for incorporation of wave-induced friction is generally applicable both at the bottom and the side wall. However, the solutions for  $z_{bc}$

and  $u_{*c}$  depend on the roughness length  $z_0$ . For a rough bottom this constant is known, but for the hydraulically smooth side walls  $z_0$  is related to the initially unknown wall shear velocity,

$$z_0 = 0.116 \frac{\nu}{|u_{*c}|}, \quad (C.24)$$

with  $\nu$  the kinematic viscosity. Instead of solving (C.20), (C.22) and (C.24) simultaneously, Van Kester et al. (1996) first determined  $z_0$  from (C.22) and (C.24) assuming that  $z_{bc} = z_0$ . After substituting the value  $z_0$  in (C.22) the nonlinear equations (C.20) and (C.22) are solved using Picard iteration.





# List of Figures

2.1	Mean and actual particle trajectories (this figure is identical to figure 3 in Bühler & McIntyre 1998) . . . . .	16
4.1	Second-order drift velocities: (a) $\text{Re}(kh) = 1.02$ , (b) $\text{Re}(kh) = 1.81$ . . . . .	48
4.2	(0, 0)-solution: (a) mean horizontal velocity, (b) eddy viscosity. . .	50
4.3	(1, 1)-solution for following waves: horizontal velocity. . . . .	51
4.4	(1, 1)-solution for following waves: vertical velocity. . . . .	51
4.5	(1, 1)-solution for following waves: pressure. . . . .	52
4.6	(1, 1)-solution for following waves: shear stress. . . . .	52
4.7	GLM results (present model) and experimental results (Klopman, 1994) first-order Eulerian horizontal velocity amplitude profile. . .	53
4.8	GLM results (present model) and experimental results (Klopman, 1994) first-order Eulerian horizontal velocity amplitude profile normalized to their values at $z = -10$ cm. . . . .	54
4.9	Vertical distributions of wave-induced stress and the Stokes correction of shear stress for the situation of waves propagating in current direction (unity is $\text{cm}^2 \text{s}^{-2}$ ). . . . .	55
4.10	GLM results (present model) and experimental results (Klopman, 1994) for Eulerian-mean horizontal velocity profile. . . . .	56
4.11	Typical distributions for the total shear stress and its wave-induced and current-related part for the case of following waves. . . . .	58
4.12	Total shear stress distributions and their wave-induced and current-related contribution for the situation without waves and following waves under the conditions in Klopman's (1994) experiments (unity is $\text{N/m}^2$ ). . . . .	61
5.1	Division of a cross section $\mathcal{V}(x)$ into five regions. . . . .	70
5.2	Computed and measured vertical current profile in the center of the flume (no waves). . . . .	78
5.3	Computed and measured horizontal current profiles at 25 cm above the bed (no waves). . . . .	79

5.4	Computed mean velocity distribution in cross section for waves following the current. . . . .	80
5.5	Computed and measured (Klopman, 1997) mean vertical velocity profiles at different distances $Y$ from the side wall (following waves). . . . .	80
5.6	Computed and measured vertical profiles of the mean horizontal streamwise velocity in the center of the flume at various points of time (following waves). . . . .	81
5.7	Computed mean velocity distribution in cross section for waves opposing the current. . . . .	82
5.8	Computed and measured (Klopman, 1997) mean vertical velocity profiles at different distances $Y$ from the side wall (opposing waves). . . . .	82
5.9	Computed and measured vertical profiles of the mean horizontal streamwise velocity in the center of the flume (opposing waves). . . . .	83
5.10	Computed mean velocity distribution in the left half of the cross section for waves following the current in a 5 m wide flume. . . . .	84
5.11	Computed mean streamwise horizontal velocity profile in center of a 5 m wide flume for waves following the current. . . . .	85
5.12	Computed mean velocity distribution in a cross section for waves opposing the current in a 5 m wide flume. . . . .	85
5.13	Computed mean streamwise horizontal velocity profile in center of a 5 m wide flume for waves opposing the current. . . . .	86

# List of Symbols

## Roman symbols

$a$	wave amplitude
$A$	wave action
$B$	flux of wave action
$c$	absolute phase velocity
$c_{1\varepsilon}, c_{2\varepsilon}, c_\mu$	empirical constants in $k - \varepsilon$ turbulence model
$c_D, c'_\mu$	empirical constants in $k - \ell$ turbulence model
$c_g$	absolute group velocity
$c_{g0}$	intrinsic group velocity
$D$	dissipation of turbulence kinetic energy per unit of mass
$E$	wave-energy density
$f_{cw}$	wave-current friction factor
$f_w$	wave friction factor
$f$	flux of turbulence kinetic energy per unit of mass
$F$	large-scale driving force
$\mathcal{F}$	sink and/or source terms in wave-action equation
$g$	gravitational acceleration
$h$	still-water depth
$i$	$= \sqrt{-1}$ , imaginary unit
$J$	Jacobian of the mapping $\mathbf{x} \rightarrow \mathbf{x} + \boldsymbol{\xi}$
$k$	wave number
$k_i$	imaginary part of wave number
$k_r$	real part of wave number
$\mathbf{k}$	wave number vector $(k_1, k_2)^T$
$K_{ij}$	cofactors of the matrix $\partial \Xi_j / \partial x_i$
$\ell$	mixing length
$L$	half of the channel width
$M$	stability parameter in CL2 theory
$\mathbf{n}$	vector normal to the free surface
$p$	pressure

$p_F$	pressure just above the free surface
$\mathcal{P}, \mathcal{P}_k$	production of turbulence kinetic energy per unit of mass
$\overline{\mathbf{P}}^L$	pseudomomentum per unit of mass
$q$	turbulence kinetic energy per unit mass
$Q$	mass transport per unit channel width
$r_{ij}$	tensor related to radiation stress
$\mathbf{r}$	vector tangential to the free surface, perpendicular to $\mathbf{s}$
$\mathbf{s}$	vector tangential to the free surface, perpendicular to $\mathbf{r}$
$\overline{\mathbf{S}}^L$	wave-induced driving force
$t$	time
$T$	$= \delta t$ , slowly-varying time (WKB), wave period
$\mathbf{T}$	CL-vortex force
$\mathbf{T}_0$	simplified CL-vortex force valid for flumes
$\mathcal{T}$	operator related to Stokes correction
$u$	horizontal velocity in $x$ -direction
$\mathbf{u}$	velocity vector $(u, v, w)^T$
$\overline{\mathbf{u}}_a$	steady current velocity vector at a height $a$ above the bed
$\hat{\mathbf{u}}_b$	maximum near-bottom orbital velocity
$\mathbf{u}_h$	horizontal velocity vector $(u, v)^T$
$U$	depth-averaged mean horizontal velocity in $x$ -direction
$\mathbf{u}_*$	friction velocity due to waves and current, eq. (C.4)
$\mathbf{u}_{*c}$	friction velocity based on time-averaged shear stress, eq. (C.8)
$\mathbf{u}_{*w, \max}$	wave-related friction velocity, eq. (C.15)
$\mathbf{u}_{*b}$	friction velocity at the bed
$\mathbf{u}_{*s}$	friction velocity at the side wall
$v$	horizontal velocity in $y$ -direction
$\mathbf{v}$	reference velocity vector
$\mathcal{V}$	cross-sectional plane
$w$	vertical velocity component
$x$	horizontal coordinate
$\mathbf{x}$	spatial coordinate vector $(x, y, z)^T$
$\mathbf{x}_h$	horizontal spatial coordinate vector $(x, y)^T$
$\mathbf{x}_0$	initial position of a fluid particle
$\mathbf{X}$	vector containing viscous and/or turbulent stresses
$\mathbf{X}_h$	$= \delta \mathbf{x}_h$ , slowly-varying horizontal spatial coordinate
$y$	horizontal coordinate
$Y$	distance to nearest side wall
$z$	vertical coordinate
$z_a$	measure for mixing length near free surface
$z_{bc}$	apparent roughness length

$z_0$  roughness length

## Greek symbols

$\beta$	$= (-i\omega_0/\nu)^{1/2}$
$\delta$	modulation parameter
$\delta_{ij}$	Kronecker's delta
$\delta_w$	wave boundary layer thickness
$\varepsilon$	$= ka$ , nonlinearity parameter (WKBJ), dissipation of turbulence kinetic energy per unit mass
$\zeta$	free-surface elevation
$\eta$	vertical displacement of a fluid particle
$\chi$	ensemble label
$\kappa$	Von Kármán constant ( $\kappa = 0.41$ )
$\nu$	eddy viscosity
$\nu_0$	kinematic viscosity
$\xi$	disturbance displacement of a fluid particle
$\Xi$	instantaneous particle position
$\bar{\pi}^L$	non-hydrostatic part of the pressure $\bar{p}^L$
$\rho$	fluid density
$\bar{\rho}$	$= \rho^\xi J$ , density related to GLM velocity
$\sigma_k, \sigma_\varepsilon$	empirical constants in turbulence models
$\sigma_{\text{tot}}$	total normal stress
$\tau_b$	bottom shear-stress vector
$\tau_{b,\text{max}}$	maximum bed shear stress
$\tau_{ij}$	stress tensor
$\tau_F$	wind shear stress vector just above the free surface
$\tau_s$	wall shear stress vector
$\tau_{\text{tot}}$	total shearing force
$\varphi$	general quantity
$\phi_c$	angle between direction of current and wave propagation
$\omega$	wave frequency
$\omega_0$	intrinsic wave frequency
$\Omega$	vorticity

## Superscripts

$\bar{\varphi}^L$  GLM quantity

$\overline{\varphi}, \langle \varphi \rangle$	Eulerian-mean quantity
$\overline{\varphi}$	complex conjugate
$\varphi^S$	total Stokes correction
$\overline{\varphi}^S$	Stokes correction
$\varphi^{\mathbf{e}}$	quantity evaluated in instantaneous particle position
$\varphi^L$	pure Lagrangian quantity
$\varphi^{\mathbf{e}}$	disturbance-associated quantity
$\varphi'$	Eulerian disturbance-associated quantity
$\hat{\varphi}^{(n,m)}$	amplitude function at $n$ -th order corresponding to $m$ -th harmonic
$\tilde{\varphi}^{(n,0)}$	amplitude function of Stokes correction at $n$ -th order
$\check{\varphi}^{(1,1)}$	Eulerian counterpart of $\hat{\varphi}^{(1,1)}$

## Subscripts

$i, j, k, m$	indices being 1, 2 or 3
$x, y, z$	indices corresponding to streamwise, lateral and vertical direction
$\alpha, \beta, \gamma$	indices being 1 or 2
1	1DV solution

## Additional symbols

$D/Dt$	rate of change following total flow
$\overline{D}^L$	rate of change following GLM flow
Im	imaginary part
$Ker, Kei$	Kelvin functions
Re	real part

## Acknowledgements

This research was supported by the Technology Foundation STW, applied science division of NWO and the technology programme of the Ministry of Economic Affairs under grant DCT22.2854, as well as by the Commission of the European Communities, Directorate General for Science, Research and Development (contract no. MAS3-CT97-0081, MAST-project Surf and Swash Zone Mechanics (SASME)).

With great pleasure I remember the stimulating conversations with the members of the KADWCI group. I kindly appreciate the offered possibility to present my research results within this MAST project on wave-current interaction. In this respect I wish to thank Niall Madden and Gareth Thomas of University College Cork for their cooperation in the study on current-affected orbital motion and Maarten Dingemans for his valuable advice on GLM-related subjects.

Likewise I want to express my gratitude to the SASME group for giving me the opportunity to participate in this MAST project and present the concept and results of the 2DV GLM-based model.

For their valuable comments and suggestions as members of this project's users committee I am indebted to John de Ronde and Anne Radder from the Ministry of Transport and Public Works, Guus Stelling and Rob Uittenbogaard of Delft Hydraulics and Gert Klopman of Albatros Flow Research.

I am most grateful to Delft Hydraulics, who by means of Jan van Kester, Rob Uittenbogaard, Heleen Leepel and Guus Stelling provided me with the source code of the 2DV version of DELFT3D-Flow (TRISULA) for non-hydrostatic flow and gave valuable support whenever necessary.

I gratefully thank Jurjen Battjes. His guidance, insight and positive way of criticizing are highly appreciated. Most of all, I would like to address a special word of thank to my supervisor Gert Klopman for his support and many fruitful discussions. Besides being a great stimulant to this research, he provided me with a numerical solver for the 1DV GLM-based equations and introduced me to the KADWCI group.

During the four years at the Hydromechanics section I have had many fine colleagues, who cannot be mentioned all. A special exception should be made for Simon de Boer and the capable assistants for their help with many computer problems, Lucas Merkelbach for sharing his knowledge of LATEX, Marco Bijvelds

for his support regarding the 2DV code, Ad Reniers and Ap van Dongeren for useful discussions about 3D models and my former room mate Yasser Eldeberky for the pleasant conversations.

Among my personal friends and family I would like to thank those who took interest in my work. Especially, I am grateful to my parents and my wife Bianca for their stimulation and support during this study and throughout earlier years at school and university.



## Curriculum Vitae

Jacco Groeneweg werd op 24 september 1970 geboren te Marknesse in de gemeente Noordoostpolder. Na van 1982 tot 1988 het VWO aan de Rijksscholengemeenschap te Oud-Beijerland te hebben doorlopen, startte hij de studie Wiskunde aan de Rijksuniversiteit te Leiden. Binnen vier jaar studeerde hij af bij de vakgroep Numerieke Wiskunde. Onder begeleiding van prof.dr. M.N. Spijker, dr. J.F.B.M. Kraaijevanger en dr. J.A. van de Griend heeft hij diverse aspecten van de numeriek behandeling van gewone differentiaalvergelijkingen onderzocht.

In de periode van 1992-1994 werkte hij als tweejarig assistent-in-opleiding (TWAIO) bij de vakgroep Numerieke Wiskunde, alwaar het eerste half jaar is gewerkt aan de toepassing van de Newton iteratie methode bij het numeriek oplossen van gewone differentiaalvergelijkingen. De overige tijd was hij gedetacheerd bij het Waterloopkundig Laboratorium in Delft, alwaar hij onder begeleiding van prof.dr.ir. G.S. Stelling en dr. E.D. de Goede domeindecompositie technieken heeft ontwikkeld en geïmplementeerd in het numerieke stromingsmodel TRISULA.

Van 1994 tot 1999 was hij als toegevoegd onderzoeker werkzaam bij de sectie Vloeistofmechanica van de Technische Universiteit Delft. Begeleid door prof.dr.ir. J.A. Battjes en ir. G. Klopman verrichtte hij onderzoek naar de wisselwerking tussen golven en stroming. Dit onderzoek is beschreven in dit proefschrift.

Vanaf 1 april 1999 is hij als onderzoeker werkzaam bij de afdeling MCI (Marine & Coastal Infrastructure) van het Waterloopkundig Laboratorium in Delft.

